MELCOR FEASABILTY ANALYSIS USING CONTAINMENT HEAT REMOVAL SYSTEMS AND PARS TO PREVENT FCV OPENING IN A PWR DURING AN SBO

Gaston Eduardo Pintos
Fernando Robledo Sanz
Francisco Calvino Tavares

JUNE 1, 2018
CONSEJO DE SEGURIDAD NUCLEAR

Table of Contents

List of Tables

Introduction

During severe accident conditions at a nuclear power plant (NPP), it is of utmost importance to maintain the structural integrity of the containment building. The containment building prevents the escape of harmful radiation to the environment in case of a severe accident. Any ruptures that lead to radioactive gas leakage from it pose a potentially serious threat to the well-being of surrounding populations.

The severe accident that occurred in Fukushima- Daichi in March 2011 had a significant impact on the safety of operational light water reactors (LWRs). This accident highlighted the need for implementation of additional safety systems in present LWRs to provide additional protection to the integrity of the containment building against the threat of a severe accident.

As a result, regulatory authorities (including the Consejo de Seguridad Nuclear [CSN]) require the implementation of safety enhancements which must be licensed for NPPs to operate. These severe accidents and containment building severe accident management strategies (SAMG) have increased in importance for the licensing process after Fukushima-Daiichi. Among the many safety enhancements required by the regulatory authorities, two are specifically relevant for this study: the implementation of Passive Auto-catalytic Recombiners (PARs) and Filtered Containment Venting Systems (FCVS) in all the Spanish Nuclear Plants.

Motivation

These new safety requirements led the proposal and execution of a severe accident study using PARs, the FCV and the containment heat removal systems (CHR). This study was inspired and motivated by a previous study performed by the United States Nuclear Regulatory Commission [NRC]. The NUREG/CR-5567 "PWR Dry Containment Characterization Study" is a "review and discussions of early containment failure due to direct containment heating (DCH), in-vessel steam explosions, hydrogen burns and steam spikes, late containment failure due to gradual over-pressurization and basemat melt-through, and containment bypass (interfacing systems LOCA) events are included. An assessment of potential improvements such as RCS depressurization, reactor cavity reflooding, hydrogen control, containment venting and accident management strategy is presented. containment behavior during severe accidents." [NUREG 5567, Yang]

Based on the findings of the report, it was decided to follow a similar path analyzing the evolution of containment conditions using the new safety implementations (PARs and FCVs) and the nuclear power plants containment heat removal systems. Specifically, analyzing how CHR systems could be used to forego opening the CFVS and thus preventing release of gases from inside the containment.

Furthermore, the activation of the different CHR systems lead to scenarios where the hydrogen and carbon monoxide concentrations were high enough to cause a combustion event. This led to the questions of how effective are PARs in removing hydrogen from the containment atmosphere? How does the initiation of fan coolers or the containment spray system affect the containment atmosphere? What would the effects be on the containment building if there is a combustion scenario?

To be able to properly answer these questions, proper knowledge of severe accidents and their phenomenology is required along with a great amount of knowledge of severe accident codes. Severe accident codes are fundamental to perform safety assessments and study of the efficiency of different severe accident management actions. CSN has the nuclear code MELCOR for its independent safety evaluations so it was the code of choice to perform the analysis.

Objectives

Based on the motivation above, 3 main objectives were placed for this project. The first one was to be able to run and execute MELCOR and provide technical assistance to the CSN staff. With time, some of the expertise within the CSN was lost with this code and re-familiarization was necessary to be able to carry on the project. This requires learning how the code worked, its structure, how to utilize the different code packages and their implementation into the input deck as well as executing it and performing troubleshooting operations when needed. It also involved learning and using all the tools required to execute MELCOR and analyze the results.

The second objective was to try and implement improvements in the MELCOR inputs for Spanish nuclear power plants. The form of these improvements could be upgrades in some of the packages to make the code run smoother or more accurate, update the input deck to run with the latest version as MELCOR is currently in version 2.X with the latest build being 2.2.94, and optimize other places.

The third and last objective of this project was to provide insights into heat removal strategies that preclude opening the filtered vent system and utilizing instead containment heat removal systems such as fan coolers and the containment spray along with the implementation of passive autocatalytic recombiners (PARs) in large dry containments. The objective was also expanded to analyze the performance of (PARs) and investigate the amount of hydrogen removed from the containment due to their effect.

Using the NUREG/CR-5567 report as an idea mat and with these 3 objectives, the project was started. The next sections discuss the phenomenology involved during a severe accident and connects it into the MELCOR package or packages that are used to calculate and simulate the scenarios. The MELCOR description is a quick preview of how the code tackles the phenomenology when performing the calculations and simulations.

Severe Accident Phenomenology, Containment Heat Removal Systems and MELCOR Packages

Severe Accident Phenomenology

A severe accident (SA) in a light water reactor is an accident during which the reactor fuel is significantly damaged with partial or full melting of the reactor core. If core degradation cannot be stopped within the reactor pressure vessel (RPV), the extreme conditions lead to RPV failure where molten core contents leak into the cavity inside the containment building. This may ultimately lead to the loss of containment integrity with subsequent release of radioactivity into the environment.

This section follows accident progression and explains the occurring phenomena through the accident transient with an emphasis on combustible gas generation and molten core-concrete interactions. This report will focus mainly on the metallic oxidation during the early in-vessel phase without core reflooding that generates a vast amount of hydrogen during the in-vessel phase which plays a critical role in containment integrity and give a brief overview of the other phenomena involved during a SA.

IN-VESSEL MELT PROGRESSION

In many cases, the reactor core melt progression is characterized by two different phases: An early phase and a late phase. The “early-phase” refers to the damage occurring during the initial fuel and control rod overheating with some melting and relocation of metallic materials. This damage occurs through core heat-up from a lack of cooling, beginning the deformation of fuel rod cladding leading to

ballooning and clad rupture. The oxidation of metallic materials is also present in this phase. The phenomena related to this phase are well understood. However, some other events in this phase require further study such as control rod melting, relocation and interaction with neighboring fuel rod and structures, uncertainties with eutectic interactions, oxide layer failure and degraded core quenching.

The "late phase" is characterized by the melting of ceramic material, molten material relocation to the lower plenum and the phenomena involved in this stage. This stage occurs once the core is in a highly degraded state with most of the cladding in the core melting.

I) Zircalloy Oxidation

Zircalloy oxidation is the main contributor in H_2 production during the in-vessel phase of a severe accident. During a severe accident the oxidation of the Zirconium structures (the cladding of the fuel rods) has a significant consequence for the overall behavior of the LWR core. In general, the exponential increase with temperature of the Zr oxidation rate produces sharp temperature increases in the core as soon as it exceeds 1500 K. As shown in experiments, the initial core heat-up rate (less than 1 K/s due to decay heat) is rapidly increased by an order of magnitude due to the additional heat released by the Zircaloy oxidation reaction. As a result, temperatures of the fuel rods and intact core structures increase rapidly above the melting point of Zircaloy (2100 K).

The oxidation reaction occurs between zircalloy and steam inside the vessel and is denoted below:

$$Zr + 2H_2O \rightarrow ZrO_2 + 2H_2 + 600\ kJ/mol\ Zr \qquad \{1\}$$

The reaction rate is dependent on a couple of factors which include the availability of steam in the core, the diffusion of steam through the hydrogen-rich boundary layer along the cladding (hydrogen blanketing), and the rate of diffusion of oxygen through the external ZrO_2 (Zirconia) crust to get to the underlying zirconium.

The diffusion coefficient K for Zircaloy is generally characterized by an exponential function of temperature and the diffusion-controlled reaction is governed by a parabolic kinetic law given below:

$$\frac{dX^2}{dt} = K \qquad \{2\}$$

Where X is the layer thickness or total oxygen mass gain in both α – Zr(O) and ZrO_2 layers. In addition, the temperature dependent kinetic constant verifies an Arrhenius formulation:

$K = Ae^{-BIRT}$

where T is the wall temperature and R is the perfect gas constant. A and B are constants.

Once zircalloy oxidation has started, several more factors come into play to determine the reaction rate. When temperature exceeds 1500 K, the limiting factor between core temperature and oxidation rate is the oxide thickness (Zirconia). However, as temperatures continues increasing from the heat generated by the oxidation reaction, the diffusion rate incr3eases and completely overwhelms the protective effect of the ZrO_2 layer. As a result, the Zr is completely oxidized in these instances.

At this point where the total hydrogen concentration is increasing, the availability of steam and the diffusion of steam to the surface of Zircaloy are limiters in the oxidation rate and thermal-hydraulic conditions become more important than the temperature itself. As an example, in the upper region of the core, the increased hydrogen concentration and decrease of steam generation rate due to decreased water level limit the maximum oxidation rate.

At a given location of the core, the total amount of oxidation dependent on the amount of Zircaloy present at that location can also be limited by the liquefaction and relocation of Zircaloy. For transient sequences characterized by relatively rapid initial heating rates (above 0.5 ºC/s), the build-up of a protective oxide layer on the outer surface of the Zircaloy cladding is limited resulting in cladding failure and relocation of molten Zircaloy to the lower core region. When this occurs, the oxidation process is terminated at its origin.

Although the relocating Zircaloy continues to oxidize, the enhanced cooling as the melt moves toward colder regions of the core tends to rapidly lower the temperature, in turn terminating the oxidation process as the material moves lower in the core. For transient sequences characterized by slower heating rates, typically lower than 0.3 K/s the formation of a thicker protective oxide layer prevents the relocation of the molten metal and the Zr oxidizes in place. For intermediate initial heating rates, a combination of relocating Zircaloy and complete Zr consumption tends to control the oxidation process.

The total amount of hydrogen released to the RCS and containment building is mainly related to the oxidation of the Zircaloy. Although the oxidation of the core structures (stainless steel, B_4C) can contribute to the total amount of hydrogen generated in the vessel, the early melting of these structures tends to limit their contribution. The oxidation of the fuel can also contribute to the total hydrogen, but is limited by the exposure to steam and the rate of oxidation

The temperature response of the core is directly related to the Zircaloy oxidation process. Although the maximum core temperature is ultimately limited by the melting of the fuel, the peak core temperature is limited by the peak oxidation rate. At rapid heating rates, the peak core temperature occurring during rapid oxidation approaches the melting point of Zircaloy. At slow heating rates, the peak core temperature can be limited by the melting point of the ZrO_2 material. The bundle heating and melting experiments are normally terminated just after the rapid oxidation and melting occurs, and the peak core temperature measured in the experiments is directly related to the peak oxidation rate.

Cladding failure

Cladding failure occurs when increased fuel temperature and formation of fission gases within the pellets increase fuel rod internal pressure causing distortions in the zircalloy cladding. Distortions initiate once temperatures exceed 1000K, commencing the degradation of the material's mechanical properties. In some cases, the pressure inside the fuel rods can exceed the pressure inside the reactor vessel. This overpressure within the fuel rod causes the cladding to swell because of creep processes. This phenomenon, called "ballooning", can cause a mechanical failure in the cladding before it is oxidized. Another major distortion referred to as "flowering" has also been observed. This is the result of the fuel pellets growing in volume, causing additional stresses in the cladding.

Zircaloy melting and fuel dissolution

Once the zircalloy melting point is reached at 2100 K, mechanical integrity of the rods may be lost and fragments may begin to accumulate around the core. The distribution of the degraded materials in the reactor core and their evolution during the course of an accident is determined the mechanical degradation and relocation of core materials within the reactor pressure vessels. These materials come from the fusion-dissolution arising from partially dissolved fuel rods. The fuel rod is said to be partially dissolved because UO_2 high melting temperature of 3100 K maintains the fuel rod as a liquid metal. These factors must be taken into account in the modelling to realistically predict the degraded condition of the core and can then be used to predict which areas are likely to be cooled if water is

injected (reflooding) and which areas cannot be cooled because molten materials have accumulated, thereby preventing water from reaching them.

Corium Formation and Properties

Corium is a mixture formed from molten fuel materials, partially or totally oxidized cladding, non-volatized fission products and various structural materials that flow through the degraded reactor core. The main constituents of in-vessel corium are UO_2, ZrO_2, Zircalloy and steel. The basic properties of corium are:

- Solidus-liquidus temperature: 1500-2850ºC (~1.800 - 3.100 K)
- Density 7 to 10 tons/m^3

Corium is characterized mainly by two parameters: the degree of oxidization of Zr and the U/Zr ratio. Associated to the term corium are an impressive list of physical and thermodynamic properties which play a role in corium progression during a severe accident: liquidus and solidus temperatures, enthalpy, density, viscosity, thermal conductivity, emissivity, surface tension and so on. Additionally, most of these properties vary significantly with the composition and/or temperature of the mixture. Zirconium oxidation will continue in the zircaloy in the corium that has not been completely oxidized, further increasing the in-vessel production of hydrogen and the corium temperature.

Formation of a corium pool and corium flow

A “molten pool” forms if the UO_2 reaches its melting point of 3100 K, slowly relocating to the lower head of the vessel. This molten pool is produced by eutectic liquids. Eutectic liquids begin to form several hundred degrees below the UO_2 melting temperature and as this eutectic mass increases, the molten pool will expand axially and radially in the core until it reaches either the baffle or the core support plate. From there, high corium temperatures will gradually begin melting the lower baffle and core support plate and corium will start flowing into the lower head. When the molten pool is formed this way, it is very difficult to cool due to its low surface/volume ratio and can continue growing by incorporating the rods located around, even if it is reflooded.

Corium flow depends on various factors. An important one is its viscosity, which is a function of its oxidation degree. In the 2100-2900 K temperature range, the viscosity of a U-Zr-O mixture is an increasing function of the oxygen content; therefore, knowing how to calculate the oxidation of such mixtures is thus particularly critical in determining the corium flow. Cooling can have a significant impact in corium flow. Colder areas in the RPV and core can cause the solidification of corium thereby impeding its flow and the flow of coolant which may result in considerable localized reductions in flow cross-sections affecting coolant flow and the cooling of the degraded core.

More research is needed however in corium flow. Currently, the understanding of corium flow is limited. The most recent experiments, PHEBUS, CORA and PBF, had corium run only in one-dimensional (vertically). The results while helpful still contain uncertainties about the behavior and flow of corium during a severe accident.

MELCOR Package: CORE (COR)

The MELCOR Core (COR) package calculates the thermal response of the core and lower plenum internal structures, including the portion of the lower head directly below the core. The package also models the relocation of core and lower plenum structural materials during melting, slumping, and formation of molten pool and debris, including failure of the reactor vessel and ejection of debris into the reactor cavity. Oxidation reactions involving metals used in cladding and other critical core structures are modeled in this package as well.

This section only describes the oxidation models, more specifically MELCOR is capable to predict the hydrogen generation during a severe accident, including:

- Hydrogen generation due to Zr-steam reaction, Fe oxidation, and B_4C oxidation for "ROD-LIKE" geometry.
- Hydrogen generation due to Zr-steam reaction, Fe oxidation, and B_4C oxidation in the "LATE PHASE" configuration.
- Ex-vessel generation due to MCCI and DCH.

The first two bullets will be described with detail below, the ex-vessel generation is analyzed in the molten core concrete interactions section. Hydrogen generation during the DCH is beyond the scope of this report.

Metal oxidation in the MELCOR COR Package

Oxidation of Zircaloy by both steam (H2O) and oxygen (O2) and of steel by H2O is modeled in the COR package. Metal oxidation is calculated using standard parabolic kinetics, with appropriate rate constant expressions for Zircaloy and steel, limited by gaseous diffusion considerations if necessary. Zircaloy oxidation is calculated for cladding, for both canister components, and for control rod guide tubes; steel oxidation is calculated for the other structure (SS or NS) components. Both Zircaloy and steel oxidation are calculated for particulate debris. MELCOR also calculates the oxidation of unquenched Zircaloy and steel surfaces that are below the pool surface.

The effects of steam (or oxygen) starvation and flow blockage are simulated by explicitly considering the direction of flow within the CVH control volumes representing the core fluids and by evaluating the unblocked flow area along the portion of the radial rings located within these CVH volumes. The allocation of steam and oxygen to the rings is based on the fraction of the total unblocked flow area of the CVH volume represented by each ring. Furthermore, oxidizers in each ring are partitioned among the surfaces of each COR cell (see Section 2.5.6) to remove any dependence of oxidation results on the order of surface processing. The partial pressures of steam and oxygen and the amounts available in the control volume interfaced to a COR cell are appropriately decreased, and, in the case of steam, the hydrogen partial pressure and mass are increased. (These local gas concentrations are also used in the convection model to obtain local properties for the heat transfer correlations.)

The reaction equations for Zircaloy are given by

$$Zr + 2H_2O \rightarrow ZrO_2 + 2H_2 + Q_{OX}$$

$$Zr + O_2 \rightarrow ZrO_2 + Q_{OX}$$

In MELCOR, the oxidation of steel is divided into the constituent elements iron (Fe), chromium (Cr), nickel (Ni), and carbon (C) according to the mass fractions optionally specified by the user in Material Properties package input (converted to moles using the atomic weights for each element). The reaction with steam equations for these species are given by

$$Fe + H_2O \rightarrow FeO + H_2 + Q_{OX}$$

$$2Cr + 3\,H_2O \rightarrow Cr_2O_3 + 3\,H_2 + Q_{OX}$$

$$Ni + H_2O \rightarrow NiO + H_2 + Q_{OX}$$

$$C + H_2O \rightarrow CO + H_2 + Q_{OX}$$

The reaction energies, Q_{OX}, are calculated from the enthalpies of the reactants and products. The reaction of steel with O_2 is not calculated currently in the COR package. Instead, the reaction energy is calculated by mass weighting the reaction energies for Fe and Cr (Nickel, Carbon and other components are currently ignored) by the relative masses of the two components in the steel composition. All actual reaction energies during a transient are evaluated at the control volume temperature and for Zircaloy and steel oxidation, the energies are deposited in the component being oxidized.

Given that oxidation forms an oxide layer on the outside of the metal structure, the solid-state diffusion of oxygen through an oxide layer to unoxidized metal is represented by the parabolic rate equation:

$$\frac{d(W^2)}{dt} = K(T)$$

where W is the mass of metal oxidized per unit surface area and K(T) is a rate constant expressed as an exponential function of surface temperature T.

$$(W^{n+1})^2 = (W^n)^2 + K(T^n)\Delta t$$

The equation above is integrated analytically over timestep Δt assuming a constant temperature. The rate constant is given by:

$$K(T) = A \exp\left(\frac{-B}{T}\right)$$

Where A and B are constants according to the reaction type (Zircalloy-H2O, Zircalloy-O2, Steel- H2O). For the Zircaloy-H2O reaction, the rate constant is evaluated using the Urbanic-Heidrich constants. Steel- H2O reactions use constants from White. As for the Zircaloy-O2, the constants are taken from technical literature.

For very low oxidant concentrations, gaseous diffusion may limit the reaction rate. This oxidation rate is given by

$$\frac{dW}{dt} = \frac{MW\ k_c P_{ox}}{n\ R\ T_f}$$

Where MW = molecular weight of metal being oxidized; kc = mass transfer coefficient; Pox = partial pressure of oxidant (H2O or O2); n = number of moles of oxidant (H_2O or O_2) consumed per mole of metal; R = universal gas constant; T_f = gas film temperature, (T + T_{gas}) / 2.

For the oxidation of Zircaloy in environments containing both H_2O and O_2, the maximum oxidation rate calculated for the two gases is used. There are two options for partitioning the oxidant consumption between the oxygen and steam. The default option is recommended and does not permit the consumption of steam until all the available oxygen has been consumed. This option is equivalent to assuming that all hydrogen produced by steam oxidation is instantaneously converted back to steam by combustion with the available oxygen.

II) Molten Core-Concrete Interactions

This section is aimed at providing a basic understanding on the core-concrete interaction. This report assumes that the reactor pressure vessel (RPV) neither fails catastrophically, e.g. due to a steam explosion, nor high pressure melt ejection. In addition, the amount of water within the cavity is small so that it can be considered a dry cavity. Based on these conditions, the high temperature corium melts through the RPV and falls into the reactor cavity initiating the molten core-concrete interaction (MCCI) phenomena. In MCCI, the hot corium starts eroding the concrete in the cavity. Heat transfer

occurs mostly through convective and radiative mechanisms. The formation of gases is based on the composition of the concrete used in the cavity.

Concrete composition description

The composition of the concrete used in the cavity is important in determining how the corium reacts with the concrete. Concrete is a complex mixture of mostly cement, water, aggregates and additives (in a small amount). Cement, usually in powder form, acts as the binding agent when mixed with water and aggregates. Water is needed to chemically react with the cement (hydration) and provide workability to the concrete.

Typical concrete is made of two different types of aggregate substances: a coarse aggregate (usually gravel) and a fine aggregate or sand. Sand or fine aggregate is generally defined as particles with a size lower than 4.75 mm. Coarse aggregate particles are above 9 mm and seldom beyond 25-40 m. Concrete is usually reinforced by steel rebars. Depending on the design, steel rebars can account for 6-16% in mass of the structural concrete. Steel rebars are a supplementary source of metal in the long-term molten core concrete interaction (Journeau & Piluso, 2002).

The properties of concrete vary slightly depending on its composition. Generally, concrete density is generally around 2,000 - 2,500 kg/m^3, specific heat typically lies between 900 J/kg*K (at room temperature) and 1,100 J/kg*K above 400° C. The thermal conductivity of concrete is low (0.96 kJ/kg*K) and significantly decreases with temperature.

Concrete is an inhomogeneous material which undergoes changes in composition as it is heated and its response of concrete to high heat fluxes is complex. Several authors have described the reactions that occur with an increase of temperature in concrete. Below, the most relevant chemical processes during the concrete heat-up are shown (Journeau & Piluso, 2002).

- 30 - 105 ºC: Evaporable water and part of bound water escape.
- 120 ºC: Evaporable water is completely eliminated
- 180 - 300 ºC: Loss of bound water from the first stage of decomposition of CaO-SiO2-H2O and carbo-aluminate hydrates
- 300+ ºC: Increase in porosity and microcracking.
- 374 ºC: Critical point of water above which no free water is possible.
- 573 ºC: α → β transformation of quartz aggregates.
- 700 - 900 ºC: Decarbonation of calcium carbonate in cement paste and carbonate aggregates.
- 720 ºC: Second stage of decomposition of CaO -SiO2-H2O.
- 1,100 to 1,250 ºC: Start of concrete melting.

The table below shows the solidus and liquidus temperatures for the different concrete types. (Roche & al., 1993)

Table 1- Solidus and Liquidus Temperature for Concrete Types

		Siliceous	Lime-siliceous	Calcareous
Solidus temperature (ºC)		1,130	1,120	1,220
Liquidus temperature (ºC)		1,250	1,295	2,305

The decomposition enthalpy to bring concrete from room temperature to total melting is generally between 1.8 MJ kg^{-1} to 2.5 MJ kg^{-1}. When applying corium concrete heat transfer models based on a global heat transfer coefficient, the relevant temperature at which the concrete ablates, the so-called

ablation temperature, needs to be specified. The ablation temperature is not a thermodynamic quantity, at least not a known thermodynamic quantity (Epstein, 1997). In the Sandia MCCI test program, a concrete ablation front was identified at the 1,600 K isotherm as determined by the thermocouples cast into the concrete base mat. In the Argonne ACE test program, a thermocouple reading of 1,673 K was assumed to indicate the passing of the concrete ablation front. For the theoretical calculations shown (Epstein, 1997), an ablation temperature of 1,600 K was chosen. A general procedure that can be applied to various concretes (Nie, 2005) proposed to use the temperature at which the volumetric liquid fraction in the concrete slag has reached 50%.

Concrete ablation

The attack of concrete by core debris is largely thermal in a LWR (Bradley & al., 1993). Heat is generated in the core debris from radionuclide decay and from chemical reactions. Energy is lost from the top through radiative heat transfer and through conduction on surfaces adjacent to the concrete. In either case, if the heat source is sufficiently large, the situation rapidly approaches a quasi-stationary state where the losses from the core debris balance the internal sources.

The first instant of MCCI is controlled by the melt overheat which increase concrete temperature, leading to the release of steam and carbon dioxide and the initial melting of concrete begins. As concrete decomposition bubbles enter the corium pool, the materials are agitated and when possible, oxidize the metal components in the sequence Zr, Cr, Fe (Powers & al., 1986). The oxidation causes the further release of hydrogen into the containment atmosphere.

The line of contact between corium and the concrete is the ablation line. At this line the heat transfer is through convection as the erosion of the concrete due to the high temperatures releases different gas mixtures. The gases created and released are carbon monoxide, carbon dioxide, hydrogen and water vapor.

The ablation rate is the ratio of the heat flux to the enthalpy needed to heat and melt a unit volume of concrete and shown in the equation below:

$$\nu = \frac{\phi}{\rho\,(H_{concrete\ melting} - H_0)}$$

Where:

- v is the ablation rate
- ϕ is the heat flux
- ρ the solid concrete density
- $H_{concrete\ melting}$ is the enthalpy at the “concrete melting” temperature
- H_0 is the concrete enthalpy at room temperature

Note that the ablation rate highlights that core-concrete interaction is governed by the heat flux, and not by an imposed temperature (Seghal & al., 2012).

The heat transfer mechanisms are strongly dependent on the (varying) compositions of the corium and concrete. The heat flux through a given interface is given by

$$\emptyset_i = h_i\,(T_{cool} - T_i)$$

Where:

- h_i is the convective heat transfer coefficient (mixed convection due to the sparging gases)
- T_i is the interface temperature for the considered boundary

Several heat transfer coefficient correlations have been developed for the heat transfer to the pool walls as well as for heat transfer between two immiscible liquid layers

Homogeneous vs Stratified Pool Melt

The stratification of metal and oxide melts under melts under gas bubbling is a complex phenomenon. This phenomenon is influenced by differences in density, viscosity, by the size distribution of metal droplets and by the convection processes in the melt induced by the gas released from concrete. The assumption in this project is that of a homogenous pool melt since experimental evidence shows that the various oxidic species in the melt are highly miscible according to (Bradley & al., 1993). The same holds true for metallic components. In absence of bubbling flow, it should be expected that core debris will stratify into distinct layers based on the relative densities of the materials within. The stratification of corium is shown in the figures of the next section.

MELCOR Package: Cavity (CAV)

The MELCOR Cavity (CAV) package models the interactions between core debris and concrete. The physical system considered by the CAV package consists of an axisymmetric concrete cavity containing debris in one or more layers. The package calculates heat transfer rates from the debris to the concrete and to the top surface of the debris, as well as the heat transfer between layers. MELCOR adapted the CONCOR-Mod 3 code for CAV package calculations applying some changes to improve interaction between the codes.

The CAV package considers all debris, metallic and oxidic, to be mixed into a single layer of homogeneous melt pool. However, the user may choose modelling that considers multiple layers in a molten pool. Figure CAV1 below provides a good picture of the usual lumped-parametric codes to the molten core concrete interaction phenomenology and shows the stratification of the layers mentioned previously.

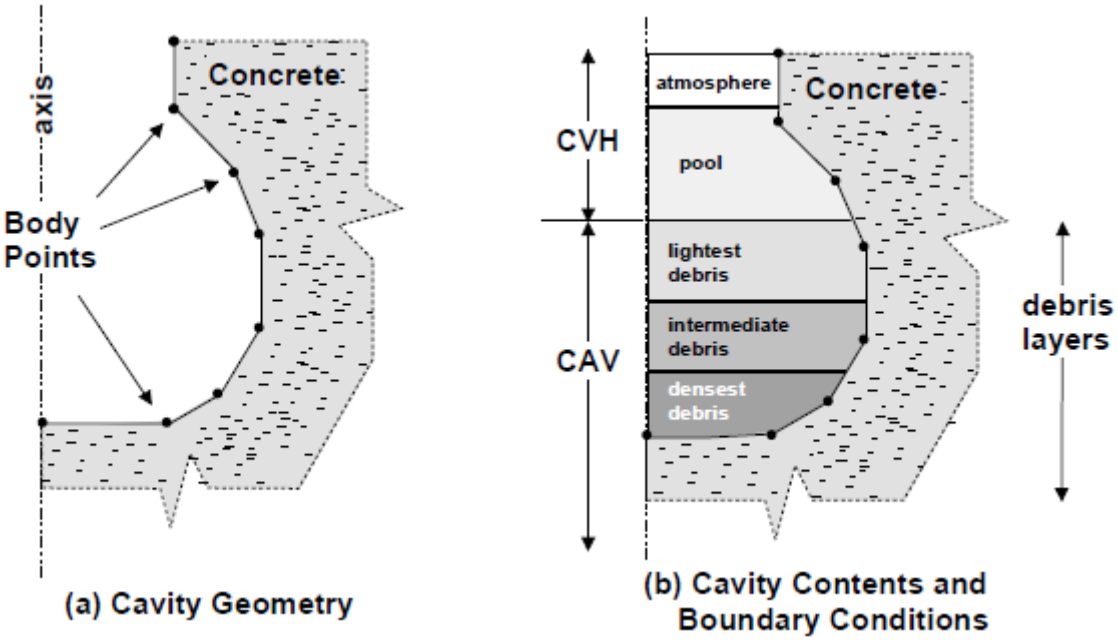

Figure 1 - Visualization of Physical System considered in CAV Package

Given the high heat fluxes expected during core-concrete interactions, a steady state ablation process is assumed in MELCOR and the ablation enthalpy which dominates the process for concrete is calculated internally, consisting of both sensible and chemical energies. The ablation temperature of concrete is not precisely defined because ablated material may not be completely molten. In MELCOR, a melting range is defined by the concrete liquidus and solidus temperatures, with the ablation

temperature ordinarily chosen by the user to lie between them. The choice affects the calculated heat of ablation. If the concrete contains reinforcing steel, the energy necessary to raise it to the concrete ablation temperatures is included in the concrete ablation enthalpy.

The steady-state model calculates the generation of decomposition gases. In MELCOR, both the reactions of metals with gases from the concrete and the condensed phase reactions between oxides and metals are modeled. The chemical equilibrium solver minimizes the Gibbs free energy function subject to constraints on mass conservation and on non-negativity of concentrations.

As for the bulk pool, the convective bulk pool heat transfer model in CORCON-Mod3 has evolved from those used in previous versions of the code. For the bottom interface of the melt pool, where gas bubbles may be injected from the incoming concrete, the heat transfer coefficient for a liquid layer is calculated using the Kutateladze correlation. For liquid layers within the melt pool, Greene's correlation is used to calculate the heat transfer coefficient in each layer, except for the uppermost melt layer, for which the Kutateladze correlation is simply multiplied by an area enhancement factor derived by Farmer. Heat loss from the pool surface includes convective heat transfer to the atmosphere and radiative heat transfer to the surroundings and thermal radiation is the dominant mechanism.

MELCOR contains a wide range of thermodynamics and thermochemical properties which are used for material properties. The thermodynamic properties calculated are density, specific heat, enthalpy, and chemical potential. Mixture densities are computed from the molar volumes of the individual species. These properties are treated as functions of composition and of temperature.

III) Gas Combustion: Hydrogen and Carbon Monoxide

The generation of combustible gases from cladding oxidation and MCCI interactions can severely threaten the integrity of the containment building. An ignition event that combusts these gases can create big pressure spikes and temperature increases. This can push the containment building beyond its designed limits and damage safety equipment and other instrumentation that may help measure conditions. Hydrogen distribution, combustion types, and mitigation strategies are described below.

Combustible gases distribution

During the oxidation of zirconium inside the RPV, hydrogen can be released into the containment through engineered pathways and breaks in the reactor cooling system (RCS). In MCCI, hydrogen as well as carbon monoxide produced will freely travel through the containment atmosphere. However, the transport of these flammable gases inside the containment building is mostly driven by convection loops generated by the releases of hot steam/gas mixtures and/or steam condensation on cold walls and structures. Depending on the level of mixing in the containment atmosphere, hydrogen can be well-mixed or stratified. If considerable hydrogen stratification exists, local concentration of hydrogen and other flammable gases could become a serious safety concern. These local pockets of highly flammable gas may lead to different combustion modes resulting in very high-pressure peaks posing a containment integrity threat.

The distribution of flammable gases and local concentrations can also be affected by the operation of safety systems such as spray systems and fan coolers. For instance, spray systems and fan coolers are designed to limit the containment pressure and to provide heat removal through water injection and steam condensation These safety systems can homogenize the flammable gases distribution in the containment due to enhanced mixing from newly created convection loops, arising from temperature differences, but can negatively impact the containment atmosphere by lowering the vapor concentration. A high vapor ratio in the containment maintains the atmosphere inert thereby preventing the combustion of hydrogen and carbon monoxide gases.

Combustion

The chemical formulas for the combustion of hydrogen and carbon monoxide are shown:

$$2H_2 + O2 \rightarrow 2H_2O + 483.2\ KJ/(gm\text{-}mole)$$

$$2CO + O_2 \rightarrow 2CO_2 + 566\ KJ$$

The combustion of these gases results in the release of high amounts of thermal energy. The main safety concern over H_2 and CO combustion in the primary containment is that the high pressure generated by the burning of these gases might cause a containment breach. A second concern is that the resulting high temperature or pressure might damage important safety-related equipment. This latter concern is ignored in this report.

Combustion conditions require molar fractions of the gases in the atmosphere to be above and below certain values. These are:

- $H_2 + CO > 9\%$
- $O_2 > 5\%$
- $H_2O < 55\%$

These values are based on standard combustion experiments which have defined the flammability limits. Combustion will begin if the gases involved are within the flammability limits and an initiating event takes place, ignition.

There is a “lower flammability limit” (that is, a necessary minimum concentration of burnable gas) as well as a “high flammability limit” (that is, a maximum concentration of burnable gas, as the mixture should also contain a sufficient amount of oxidant). Flammability limits of a gas mixture depends on its temperature and pressure and composition. For hydrogen, the point representing the mixture composition (hydrogen, air, steam) on the Shapiro diagram (see Figure 2) is generally used to determine whether the mixture is flammable. In this diagram, the combustible regions (yellow – non-complete combustion, light orange – complete combustion) and the detonable region (dark orange) are delimited by the exterior and interior curves, respectively. The detonation limit is not an intrinsic property: it is geometry dependent.

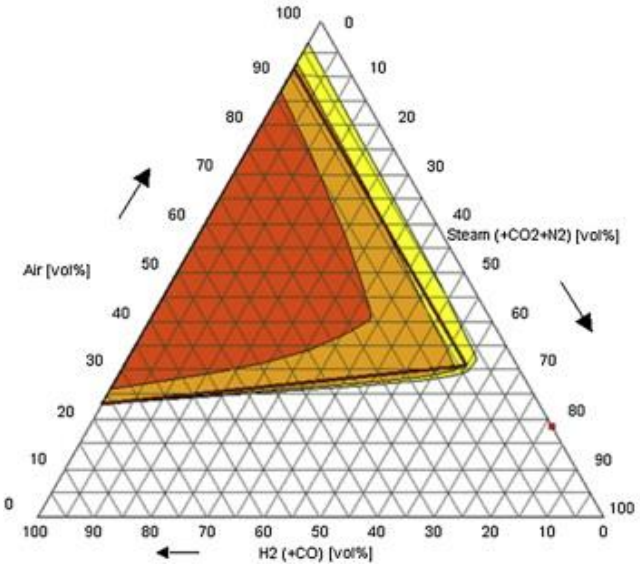

Figure 2 - Shapiro Diagram of Hydrogen Flammability

The combustion regimes are briefly explained below.

Deflagrations: Deflagrations are combustion waves in which unburned gases are heated by thermal conduction to temperatures high enough for chemical reaction to occur. Deflagrations normally travel sub-sonically and result in quasi-static (nearly steady state) loads on containment. Deflagrations may be "slow" (laminar) or "fast" (mostly turbulent). Only laminar deflagrations are considered in this project.

Detonations: Detonations are combustion waves in which heating of the unburned gases is due to compression from shock waves. Detonation waves travel supersonically and produce dynamic or impulsive loads on containment in addition to quasi-static loads. Detonation is the most devastating mode of gas combustion and produces much higher pressure increase than a deflagration. As a result, in nuclear safety, hydrogen detonation is a phenomenon that must absolutely be prevented.

Deflagration to Detonation Transition(DDT): DDT may occur between spaces depending on volume geometry and combustible gas concentration. If flames accelerate during hydrogen deflagration and sufficient space and time for acceleration are available, then combustion may very well evolve into detonation. The mechanism of transition to detonation is still not fully understood. Presently, apart from some criteria, there is no theory (in the strict sense of the term) that can predict conditions for deflagration to detonation transition.

Diffusion flames*:* If oxygen and ignition sources are present in the vicinity of the hydrogen release (e.g., near the pipe break where the hydrogen generated in the reactor core flows out), then hydrogen will ignite and could burn as a standing flame at the release location. Standing diffusion flames can exert thermal loads on the containment via different heat transfer mechanisms:

- Direct contact with structures.
- Heat transfer via radiation (mainly infrared radiation on steam).
- Convection of hot combustion products followed by gas/structure heat transfer.
- Flame acceleration

These combustion modes are not considered in this project. For a flammable hydrogen-air-steam mixture, deflagration may be initiated by an energy source of a few milliJoules (i.e., actuator switching, hot points developing, hot gases released from the reactor coolant system or use of igniters). In contrast, a much more powerful energy source (>100 kJ) is required to trigger a stable detonation.

Mitigation

Since the TMI accident many severe accident management (SAM) strategies has been developed to preclude the containment failure by combustible gas combustion within the reactor building. One of these strategies is the implementation of passive autocatalytic recombiners (PARs). PARs remove hydrogen from the reactor containment by an exothermal reaction of hydrogen oxidation by the oxygen presented in the containment atmosphere with the use of metals as catalysts generating steam and heat. This method is entirely passive so they can work under a SBO scenario. These devices need a minimum of 1-2 % of hydrogen as well to start operating.

MELCOR Packages: Burn (BUR)

The Burn (BUR) package models the combustion of gases in control volumes. The models consider the effects of burning on a global basis without modeling the actual reaction kinetics or tracking the actual flame front propagation. The BUR package models are based on the deflagration models in the HECTR 1.5 code. Detonations are merely flagged and not modeled. a

Deflagrations are ignited if the mole fraction composition in a control volume satisfies a form of LeChatelier's formula shown below:

$$X_{H2} + X_{CO}\left(\frac{L_{H2,ign}}{L_{CO,ign}}\right) \geq L_{H2,ign}$$

where: XH2 = hydrogen mole fraction in the control volume; XCO = carbon monoxide mole fraction in the volume; LH2,ign =XH2IGN (hydrogen mole fraction), if there are no igniters in the volume and DCH is not occurring, LCO,ign = XCOIGN (CO mole fraction) if there are no igniters in the volume and DCH is not occurring.

Tests for sufficient H2 and O2 are performed, as well as an inerting test for the presence of excessive diluents (H2O and CO2). Deflagrations are propagated into adjoining control volumes if additional tests for the H2 and CO mole fractions in those volumes are satisfied and if the flow path is open to gas flow.

The combustion rate is determined by the flame speed, the volume characteristic dimension, and the combustion completeness. The flame speed and combustion completeness can each be input as constant values, or they may be calculated from user-defined control functions or the default empirical correlations.

Containment Heat Removal and Engineering Safety Systems

Severe accident scenarios resulting in severe fuel failure leading to RPV failure can lead to dangerous conditions inside the containment building. The pressure increase caused by the heating of the atmosphere from the decay heat of fission products can threaten the structures integrity creating cracks to a full collapse of the building. This would lead to extreme environmental consequences. Therefore, safety systems are needed to remove heat from the containment atmosphere. This section provides information on the systems used to maintain the safety of the containment building.

Containment Heat Removal System – Containment Spray

The containment spray system is a critical safety system in NPPs that removes heat from the containment atmosphere through sprays at the top of the containment building. The spray system works by spraying cold water which is being pumped from the reactor water storage tank (RWST) at low pressures. The cold-water droplets absorb heat, lowering the vapor concentration inside and temperature, effectively also lowering the pressure. Once the RWST is emptied, water may be taken from the containment building sumps and recirculated through pumps to continue the injection of water into the containment building. A drawback of this method is that the water being sprayed increases in temperature over times since it is absorbing heat from the containment atmosphere. This results in a continually diminishing heat transfer rate between the water sprayed and the atmosphere until the temperature of the water sprayed will be equal to that of the atmosphere. To continue providing cooling, some NPP have heat exchangers that cool the water taken from the sumps to continue injecting cold water into the atmosphere.

MELCOR PACKAGE – Containment Spray (SPR)

The Containment Sprays (SPR) package models the heat and mass transfer between spray droplets and the containment building atmosphere. The modeling in the SPR package was taken virtually intact from the HECTR 1.5 code, following the recommendations of the MELCOR phenomena assessment on modeling containment spray systems. The model assumes, among other things, that spray droplets are spherical and isothermal and that they fall through containment atmospheres at their terminal velocity with no horizontal velocity components.

An arbitrary number of spray sources may be placed at various heights in any containment control volume. The source of water for each spray may be associated with the pool in any CVH control volume or it may be left unspecified. For each spray source, except for sources associated with rain from the HS film-tracking model, the user must specify an initial droplet temperature and flow rate, each of which may be controlled by a control function. The user may turn the sprays on and off with a separate control function for each spray source. A droplet size distribution also may be input for each spray source.

The user can describe how droplets falling from one control volume are to be carried over to lower volumes. A control volume may be designated as the containment spray sump. Droplets leaving designated control volumes and not carried over to other volumes will be placed in the pool of the sump. Droplets reaching the bottom of a control volume and not being carried over to other volumes or placed in the sump are put into the pool of the control volume.

Containment Heat Removal System – Fan Coolers

Another important system are the fan coolers. Fan coolers are large heat exchangers used to remove heat from the containment building. Such coolers circulate hot containment atmosphere gases over cooling coils through which secondary water coolant at low temperatures is circulated. This results in the removal of heat by convection and condensation heat transfer.

MELCOR PACKAGE – Fan Cooler (FCL)

The Fan Cooler (FCL) package constitutes a sub-package within the ESF package and calculates the heat and mass transfer resulting from operation of the fan coolers. Two models are available in MELCOR for simulating fan coolers, the simple MARCH model based on the fan cooler model in the MARCH 2.0 code and a more rigorous mechanistic model based on the CONTAIN mechanistic fan cooler model. The user may select between these two models and vary cooler design parameters through the MELGEN input.

Containment Heat Removal Systems – Filtered Containment Venting System

The FCVS is a system used to prevent damage to the containment building from over-pressurization. When pressure inside the containment building reaches dangerous levels, the FCVS allows for the release of the over-pressure through a scrubber normally containing water, stones and chemicals, where most of the fission products are contained. This reduces the radioactive release to the environment with up to 99%. FCVS have a set-point to open based on the structural integrity curve of the containment building.

There is no MELCOR package to model FCVS. They are modeled using control functions that will open according to pressure set points.

Engineering Safety Systems – Particle Auto-catalytic Recombiner (PARS)

Particle recombiners are also starting to be implemented in containment buildings after the Fukishima-Daiichi accident. Hydrogen generation during severe accident condition creates very dangerous conditions which can lead to damage to the containment building from the combustion of combustible gases.

PARS are considered “passive” because of the self-starting and self-feeding nature and require no external energy. A passive autocatalytic recombiner comes into action spontaneously as soon as the hydrogen concentrations begins to increase in the reactor building atmosphere. In practice, catalytic recombiner starts up with hydrogen concentration equal to 1-2 %. A passive autocatalytic recombiner consists of a vertical channel (stack) equipped with a catalyst bed in the lower part. In case of an accident, the catalyst bed is in contact with the gas mixture of the containment. Hydrogen molecules coming into contact with the catalyst surface -platinum or palladium- and react with oxygen in air. The heat of the reaction at the catalyst surface induces convective flow, without mechanical assistance or outside power. The heat release of the reaction in the lower part of the recombiner causes a buoyancy accelerating the inflow rate and thereby feeding the catalyst with a large amount of hydrogen bearing gases ensuring high efficiency of recombination. Natural air circulation starts linked to the passive autocatalytic recombiner in the partly confined control volume around it. The natural convective flow currents promote mixing of combustible gases in the containment, and avoid probable hydrogen over-concentrations (« hydrogen pockets »). The natural air circulation assures a continuous air supply to the catalytic recombiner.

MELCOR PACKAGE – Passive Autocatalytic Recombiner (PAR)

The Passive Autocatalytic Recombiner (PAR) package constitutes a sub package within the ESF package and calculates the rate of hydrogen removal generated by PAR type hydrogen removal systems. The default MELCOR model is based on the Fischer model, which is a parametric model developed for a particular type of PAR unit. The user input provides correlation coefficients for the general mathematical form of the model. These coefficients are used by the code to calculate the total gas flow rate through a PAR unit. From the PAR gas flow rate together with user provided PAR efficiencies, transient relaxation times, delay times, and the internally calculated hydrogen mole fractions, a per-PAR-unit hydrogen reaction rate is calculated. This rate is then multiplied by the current timestep and

the user provided number of active PAR units to determine the change in hydrogen, oxygen, and steam masses. These differential masses are then passed to CVH as sources/sinks.

It is noted that one particular PAR design has been developed, studied, tested, and reported on in the technical literature. The NIS Company in Hanau, Germany developed this type of PAR. The design consists of parallel plate cartridges containing palladium-coated aluminum micro-pellets. It has been tested in a series of experiments performed at the Sandia National Laboratories for the NRC and thus, the NIS PAR is the default model in MELCOR. In case that it is desired to study a different design concept, more general input options are available. This provides the user with the option to specify a control function with which the PAR flow rate can be calculated as a function of one or more system variables. In addition, an option is provided that allows the user to specify the PAR efficiency through the use of a control function.

Plant Description and Modeling

Power Plant Description

The reactor that is modeled in this project is a 3-loop Westinghouse PWR equipped with a large dry cavity. The table below is a summary of the reactor and plants properties and characteristics.

Table 2 – Plant and Reactor Properties

PLANT PROPERTIES	
REACTOR TYPE	PWR
THERMAL POWER	2,686 MW
FUEL TYPE	Enriched UO_2
OPERATING PRESSURE	157.2 bar
HOT LEG TEMPERATURE	327.3 °C
COLD LEG TEMPERATURE	288.7 °C
RWST VOLUME	1,381 m^3
REACTOR CORE AND VESSEL MASS	
FUEL	82.2 Tons
ZIRCALLOY	17.8 Tons
STAINLESS STEEL	35 Tons
AG-IN-CD (CONTROL RODS)	2.34 Tons

The composition of the concrete in the cavity is described in the table below. It is composed mostly of limestone concrete. The description below also accounts for iron bars in the concrete.

Table 3 – Concrete Composition of Cavity

Concrete Composition	Mass fraction (-)
SiO2	0.4270
TiO2	0.0017
MnO	0.0003
MgO	0.0209
CaO	0.2487
K2O	0.0073
Fe2O3	0.0045
Al2O3	0.0293
Cr2O3	0.0001
CO2	0.0991
Na2O	0.0087
H2O	0.0808
Fe	0.0715

The containment building of this NPP is a reinforced concrete structure with a containment design pressure of 4.5 bars-abs. Pressures higher than 4.5 bars (absolute) start increasing the probability of containment failure. A containment fragility curve is shown in the figure below with relevant values shown in the table 4. The mean value for the distribution function is 8.51 bars-abs and the STD is 0.6 bars.

Table 4 - Containment Fragility Curve Values

PRESSURE (BARS-ABS)	CUMULATIVE PROBABILITY
4.5	1.1 E-11
7.1	0.01
7.75	0.10
8.5	0.49
10	0.99

The containment fragility curve shown below was created out of an average from other curves.

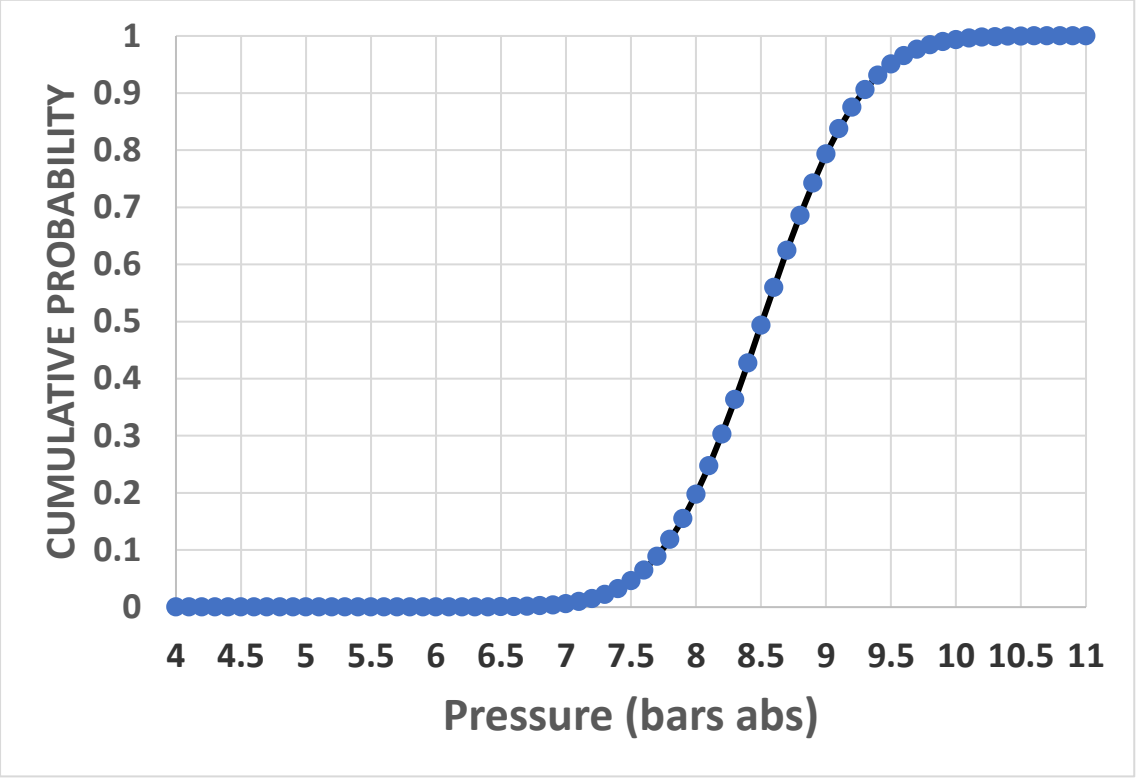

Figure 3 - Containment Fragility Curve

The plant's Emergency Core Cooling system (ECCS) is comprised by Low and high-pressure injection systems [LPIS/HPIS] and accumulators. LPIS and HPIS pump water from the RWST into the reactor coolant system during accidents, and switch to recirculation with a heat exchanger cooling from the containment sump once the RWST is empty. However, both LPIS and HPIS are not activated since it is a SBO scenario.

The containment heat removal system of the NPP consists of the containment spray system and fan coolers. Fan coolers are set to be automatically activated when containment pressure reaches 1.285 bar-abs and the containment spray system is automatically activated. The containment spray system can operate in both injection mode (i.e., by drawing water from the Refueling Water Storage Tank [RWST]) and recirculation mode (i.e., by drawing water from the containment sump). However, the containment sprays cannot provide long-term containment cooling in recirculation mode due to the lack of heat exchangers. It should be noted that the containment heat removal systems will only be manually activated in this job, i.e. as an accident management measure.

Model Description

The model for this project was created to be executed in MELCOR. The model was created using SNAP (Symbolic Nuclear Analysis Package) which is a tool that can create visual models of the reactor or power plant which can then be imported into the input files required for execution for any number of nuclear code. The model created was for MELCOR 2.X version and the input decks were executed on the MELCOR 2.1.6342 version.

The input deck used for this simulation was obtained from CIEMAT with some minor modifications and improvements made. These changes include the creation of control functions that actuate the spray and fan cooler systems at desired times after the initiation of the accident. The burn package had some additional options enabled for fine-tuning of the combustion events to modify flammability limits and combustion completeness.

The plant model for this project consisted of 2 parts: Control volumes making up the primary side of the reactor vessel and hot/cold loops and a second set of control volumes representing the reactor containment building. In the primary side, the RPV was modeled using the COR package to track fuel degradation and CVH for thermal hydraulic calculations. The core model consisted of 10 axial and 3 radial meshes for the active fuel region additional meshes were added to account for the lower plenum and upper and lower core baffles. 5 control volumes were created representing the RPV: a channel, bypass, downcomer, lower plenum, upper plenum. 11 additional volumes were created to represent the steam generators, cold and hot legs, pressurizer, and accumulators.

The reactor containment building houses the primary side. It has a total free volume of 62054 m^3. The containment building was nodalized into 10 volumes. There are 3 major compartments and 7 minor compartments. The minor compartments created represent the major components of the NPP. These include 3 steam generators, a pressurizer, the cavity, a lower compartment and a chamber. The major compartments represent 90% of the total free volume of the containment building. These are the upper compartment, the dome and the annulus. The table below shows the volume of each node and the percentage it occupies of the total.

Table 5 - Volume of Containment Compartments

COMPARTMENT	VOLUME (M^3)	VOLUME FRACTION (%)
CAVITY	447.0	0.72
LOWER COMPARTMENT	2146.6	3.46
UPPER COMPARTMENT	40738.3	65.65
DOME	9258.3	14.92
STEAM GENERATOR A COMPARTMENT	1141.0	1.84
STEAM GENERATOR B COMPARTMENT	1145.5	1.84
STEAM GENERATOR C COMPARTMENT	597.0	0.96
PRESSURIZER	328.3	0.53
ANNULUS	5861.6	9.45
CHAMBER	390.5	0.63
TOTAL	**62054.1**	**100.0%**

Figure 4 below shows all the flow path connections. The upper compartment has direct connections to the cavity, the annulus, the dome, the pressurizer, and the steam generators. Meanwhile, the lower compartment connects with the annulus, steam generators, pressurizer and the cavity. The chamber connects the cavity and the annulus. It's role in the plant cannot be disclosed due to confidential nature.

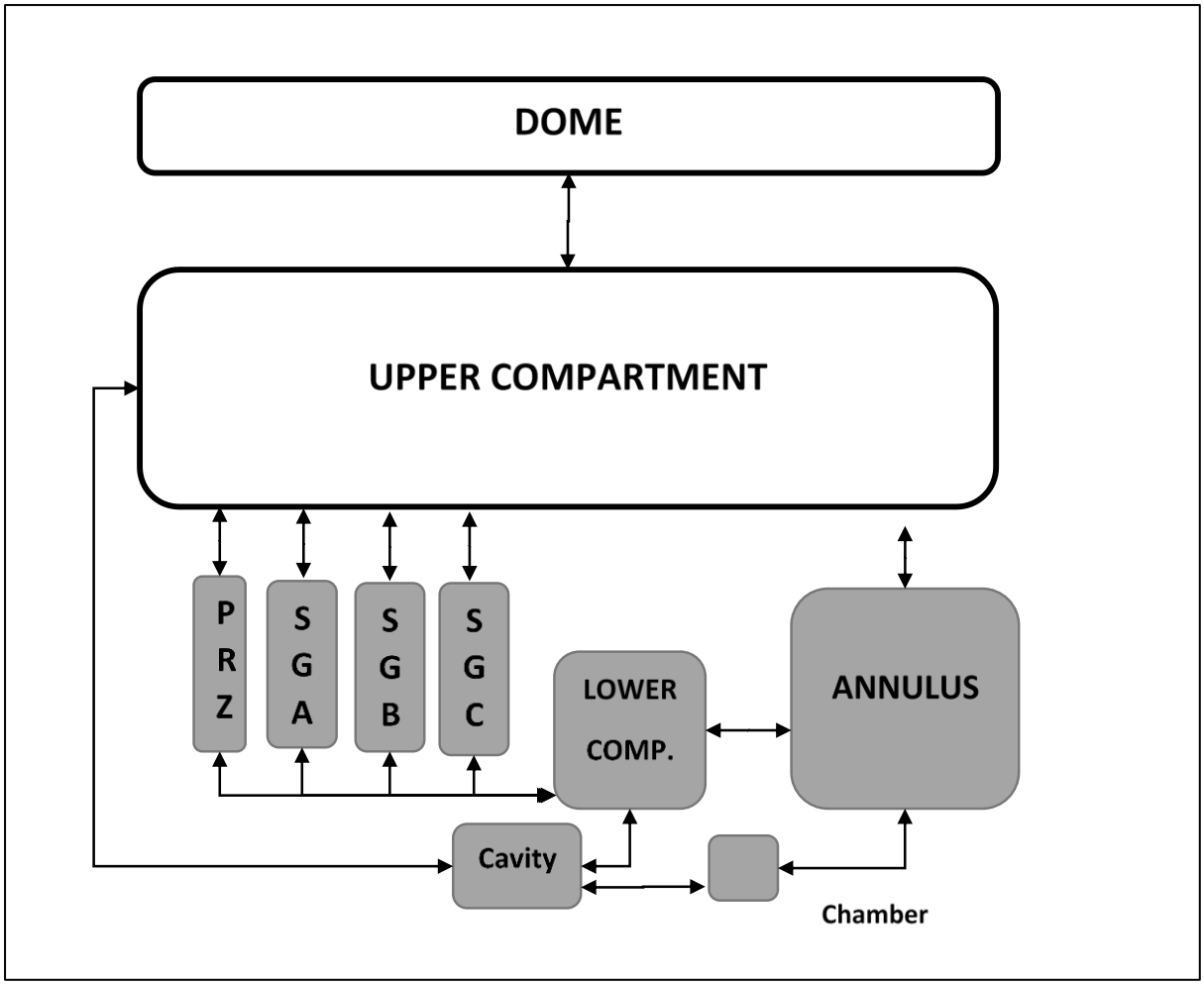

Figure 4 - Visual Representation of Containment Nodalization

The PARs modeled in this simulation are the NIS-88 developed by Siempelkamp. They are effective for removing hydrogen and CO from containment. Their removal rates are dependent on atmospheric composition and conditions (pressure and temperature). Their efficiency, removal rates, and enthalpy increase from the reactions were implemented in MELCOR using control functions. The number of PARs in each compartment were input as sources in the CVH for each compartment and is shown in table 2 below.

Table 6 - Number of PARs in Containment

COMPARTMENT	# OF PARS
CAVITY	0
LOWER COMPARTMENT	1
UPPER COMPARTMENT	8
DOME	7
STEAM GENERATOR A COMPARTMENT	1
STEAM GENERATOR B COMPARTMENT	1
STEAM GENERATOR C COMPARTMENT	1
PRESSURIZER	1
ANNULUS	1
CHAMBER	1
TOTAL	22

The containment spray and fan cooler systems were modeled according to plant specifications with control functions created for manual control of the system's activation. The table below shows the properties for the CHR systems.

Table 7 - Containment Heat Removal System Properties

CHR SYSTEM -CONTAINMENT SPRAY PROPERTIES	
HEIGHT	57.53 m
SPRAY TEMPERATURE	295.0 K
NOMINAL FLOW RATE	0.1244 GPM
DROP DIAMETER	7.07E-4 m
SOURCE	RWST
RECIRCULATION SOURCE	SUMPS
CHR SYSTEM - FAN COOLER PROPERTIES	
GAS VOLUMETRIC FLOW RATE	42.66 m^3/s
INLET GAS TEMPERATURE	322.0 K
COOLANT MASS FLOW RATE	251.0 kg/s
COOLANT INLET TEMPERATURE	313.0 K
FAN COOLER CAPACITY	15.0 MW
STEAM MOLE FRACTION	0.55

MELCOR Calculation Results

Major Accident Events

The accident begins at t=0 seconds in the MELCOR simulation, with a loss of power that causes the stop of the RCS pump and feedwater. The reactor scrams immediately after and decay heat starts to increase the temperature of the fuel rods. Table 8 is the timetable for the major events during the accident.

Table 8 - Major Events Timetable

EVENT	TIME (HRS)	TIME (MIN)
STATION BLACK OUT	0	0
REACTOR SCRAM	0	0
CORE UNCOVERING	1.9 – 3.1	113-186
IN-VESSEL H2 PRODUCTION	2.35	143
CORE DRYOUT	3.1	186
RPV RUPTURE	3.9	233
CONTAINMENT FAILURE	38.8	2,328

Pressure increases from the heating of water inside the RPV from the decay heat of the fuel rods to 16.1 MPa where the PRZ relief valve opens to depressurize the primary side. When it reaches this valve set point at 66 minutes, it begins to cycle to continue relieving pressure in the RPV as shown by figure 5.

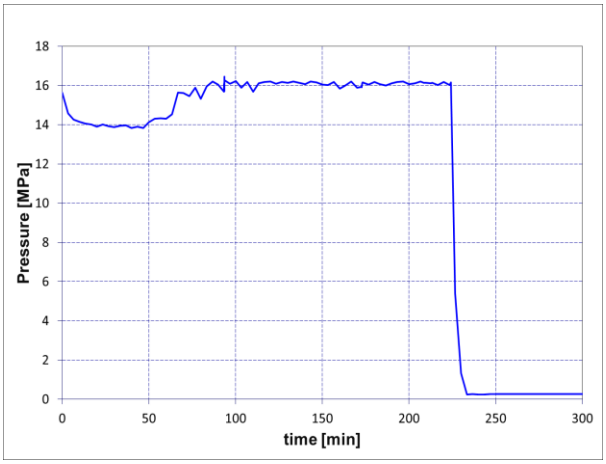

Figure 5 - RPV Pressure

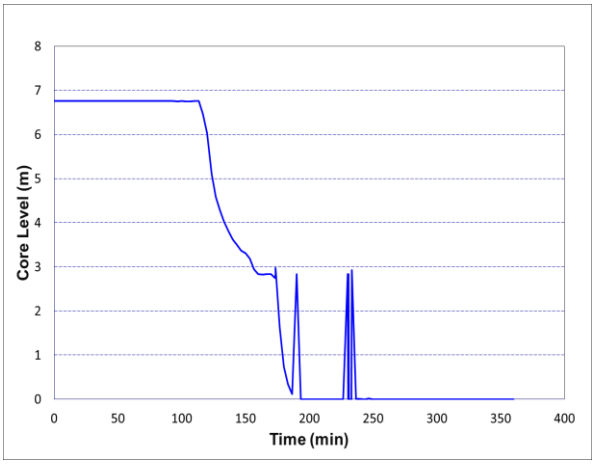

Figure 6 - Reactor Core Water Level

After 1.9 hours, core uncovering begins and clad temperature begin to increase. Core dry-out occurs after 186 minutes as seen in figure 6 where the core water level reaches 0. The maximum cladding temperature is 2342.1 °C at 166 minutes as shown in figure 8.

Hydrogen production from the oxidation of the Zirconium cladding begins at 143 minutes. Note that clad temperature and hydrogen production from the oxidation of the cladding have a close relationship as more hydrogen is produced as clad temperature increases past 1000 K. This can be seen by looking side to side to figures 8 and 9. Furthermore, 371.2 kg of H_2 are produced from the oxidation of Zircalloy, and 73.5 kg of H_2 produced from the oxidation of stainless steel (SS). Total In-vessel hydrogen production during the accident is 444.7 kg.

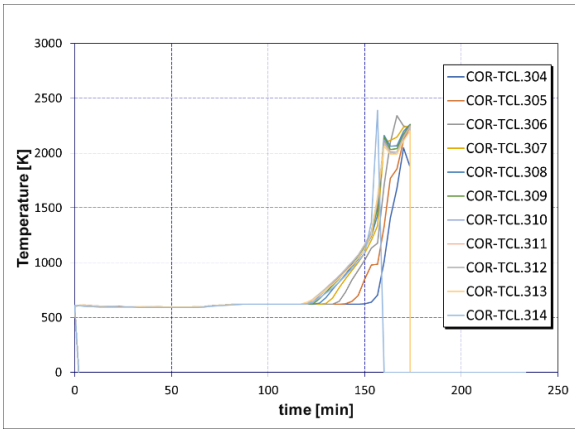

Figure 7 - Clad Temperature

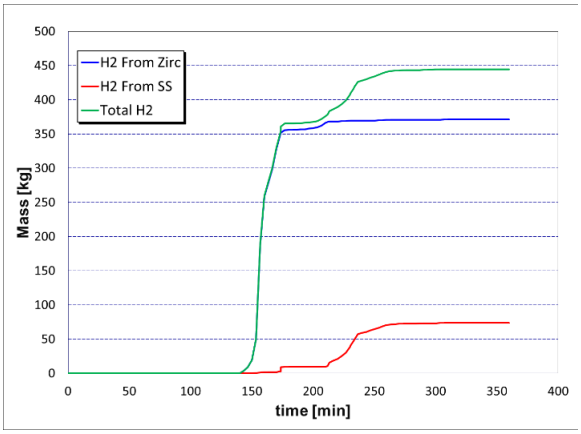

Figure 8 - In-Vessel Hydrogen Production

The rupture of the RPV occurs after 3.9 hours. Figure 3 shows the plummeting of RPV pressure and the ejection of corium at the same (Figure 10). Containment pressure then rapidly begins to increase as seen in figure 11 at the time of RPV rupture.

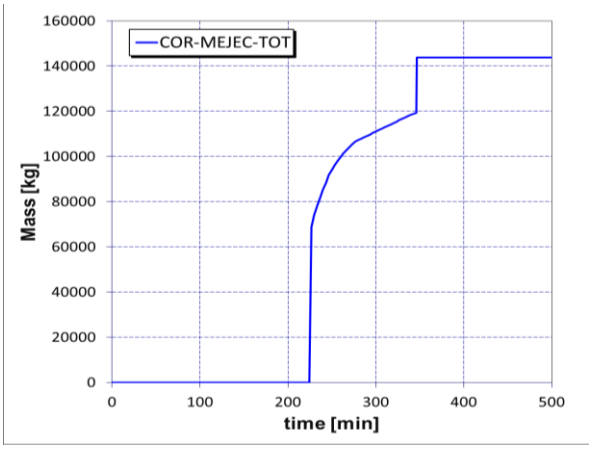

Figure 9 - Mass Ejection from RPV

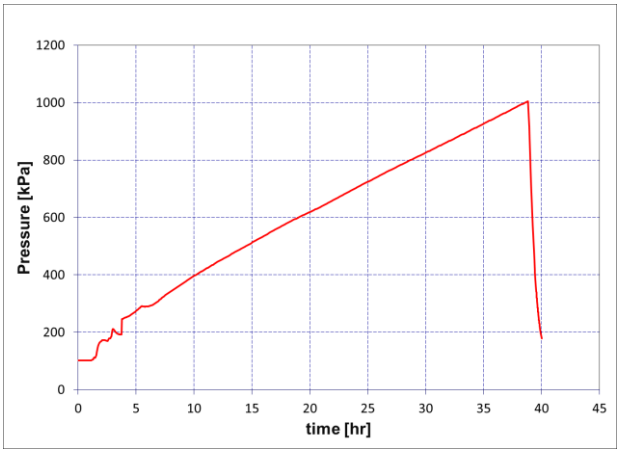

Figure 10 - Containment Pressure

Once the corium enters the cavity, MCCI begin to occur liquifying the concrete and beginning the generation of gases. The high heat starts to break down the structure and the generation of CO begins. The oxidation of Zircalloy continues due to the release of steam from the breakdown of the concrete. Figure 9 below shows the mass of gases generated during this process.

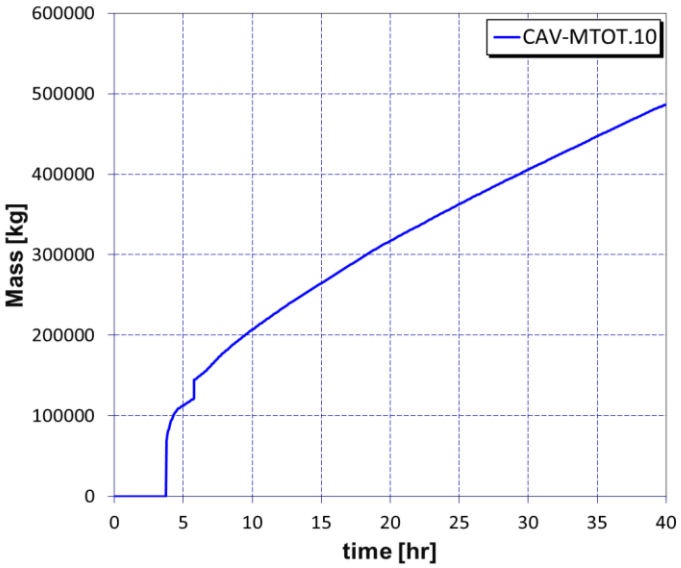

Figure 11 - Molten Mass in Cavity

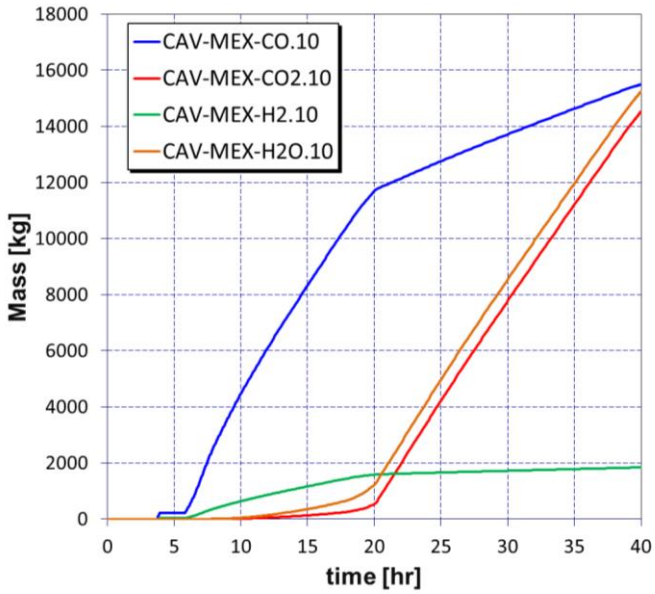

Figure 12 - Gas Generated in Cavity

Table 9 below gives the total amount of gases created in-vessel and ex-vessel.

Table 9 - Mass of Gasses Created

GAS GENERATED	IN-VESSEL (KG)	EX-VESSEL (KG)	TOTAL (KG)
H_2	444.7	1747.7	2192.4
CO	0	14320.3	14320.3
CO_2	0	16864.7	16864.7
H_2O (VAPOR)	0	16558.0	16558.0

Finally, containment failure occurs after 38.8 hours as containment pressure reaches 10 MPa (Figure 11) as seen by the sharp decrease in the containment pressure.

Fan Cooler Study

The activation of fan coolers helps to maintain containment integrity by lowering pressure through the cooling of the atmosphere. This however can have an adverse effect as vapor is effectively condensed which can cause the de-inertization of the atmosphere causing hydrogen deflagrations. For this case-study, the fan coolers were activated at the 7, 8, 9, and 10 hours after the beginning of the accident. Burn package was not activated for these simulations but PARS were applied to the compartments as mentioned in the model description.

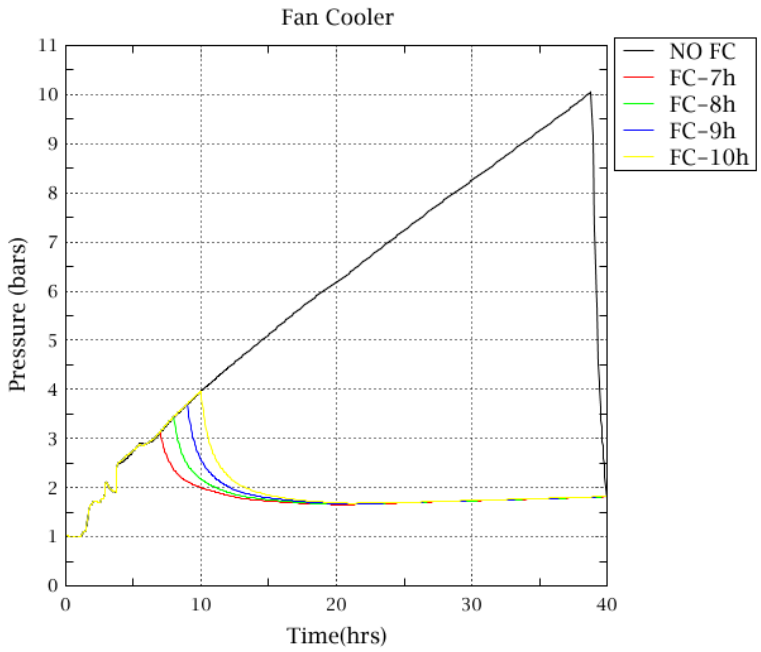

Figure 13 - Containment Pressure at Fan Cooler activation

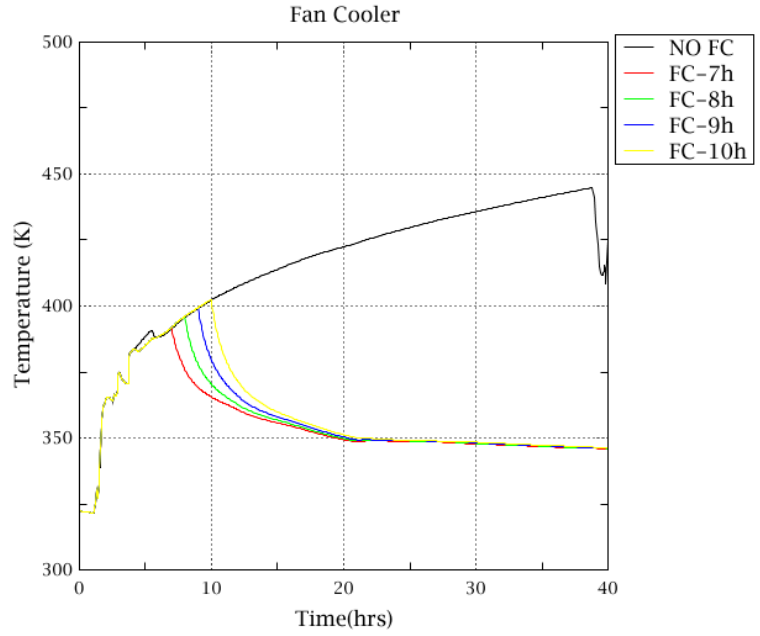

Figure 14 - Containment Temperature at Fan Cooler Activation

As seen by fan activation times in figure 14, containment pressures drop quickly once the fan coolers are activated. Earlier activation time avoids higher increases in pressure as can also be seen in the

figure. After 7 hours, independent of fan cooler activation time, the pressure bottoms out and remains effectively constant, only less than 0.1 bars over the next 20 hours. The pressure does not pose a threat for containment integrity safety with a final pressure below the 2 bars mark with the activation of fan coolers.

The temperature inside the containment follows mostly the same trend as the fan cooler as shown in the figure 15. The temperature drop begins once the fan cooler is activated since air is being cooled through the fan coolers heat exchanger. One difference however is that atmospheric temperature continues to decrease very slightly after 20 hours unlike the pressure. This is due to the decrease of vapor in the atmosphere.

It is also of high importance to examine the molar mass concentrations in the containment compartments to determine the probability of deflagrations which may damage the containment building. Each case is analyzed below.

Fan Cooler activation at 7 hours

The figures below show the molar mass fractions of oxygen, vapor, carbon monoxide and hydrogen when fan coolers are activated at 7 hours for the cavity, annulus, and lower and upper compartments. In all 4 figures, the vapor fraction decreases once fan coolers are turned on. The annulus has a gradual decline to just below 40% when the fan coolers are turned on, the cavity ends with a molar fraction of vapor of 32% and it is just 20% in the lower and upper compartments. Oxygen mass fraction after 10 hours remain above 5% for all figures but go below 5% 2-3 hours after which cancels the risk for hydrogen deflagrations. However, because the vapor molar mass fraction drops so drastically with the initiation of the fan coolers and the oxygen molar mass fraction remains above 5%, there is a small window where deflagrations are possible creating a risk for the containment building.

In the cavity, lower and upper compartments, between 12 and 15 hours there is a probability that hydrogen combustion will occur given that the H_2+CO molar fractions is about 9% and the oxygen fraction remains above 5% with vapor molar mass fraction decreasing drastically from 50% after 10 hours.

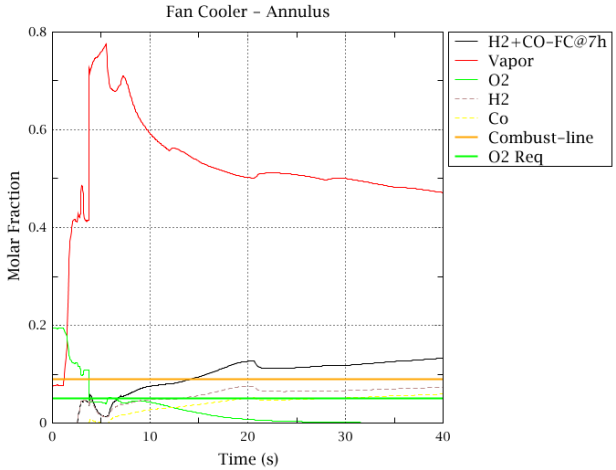

Figure 15 – FC Molar Fraction in Annulus

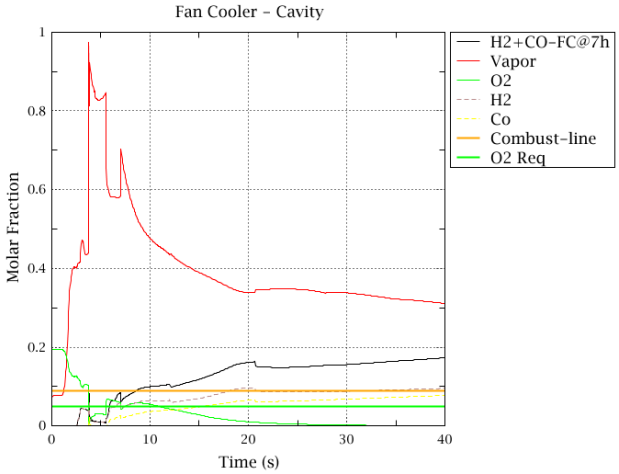

Figure 16 – FC Molar Fraction in Cavity

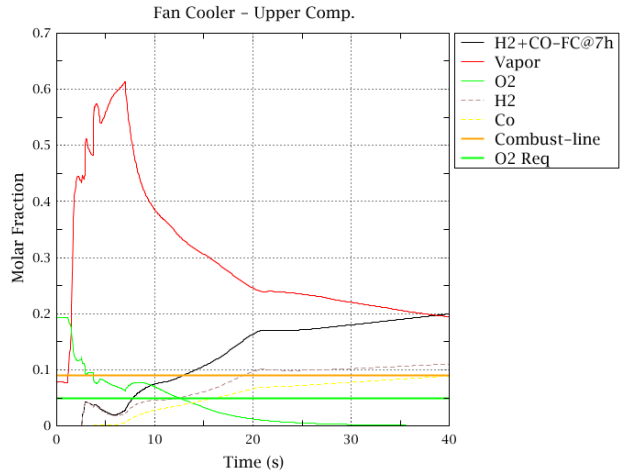

Figure 17 – FC Molar Fraction in Upper Comp.

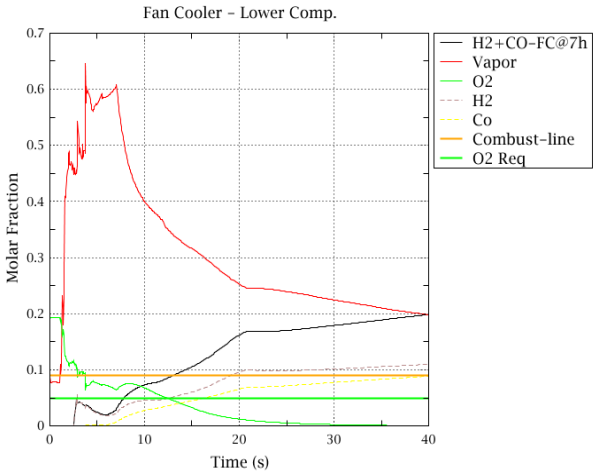

Figure 18 – FC Molar Fraction in Lower Comp.

Towards the end, after 15 hours, the environment can be considered inert due to the lack of oxygen. As seen in the figures above by the bottom green line, the molar mass fraction is below 5% which prohibits any combustions.

Fan Cooler activation at 8 hours

A very similar trend is seen with fan coolers activating at 8 hours. The vapor fraction drops off quickly and is at or less than 50% in all compartments after 10 hours. There is still a small window for combustion between 11 and 15 hours. After 15 hours, the oxygen mass fraction is well below the 5% required for H_2+CO combustion so no deflagrations are to be expected.

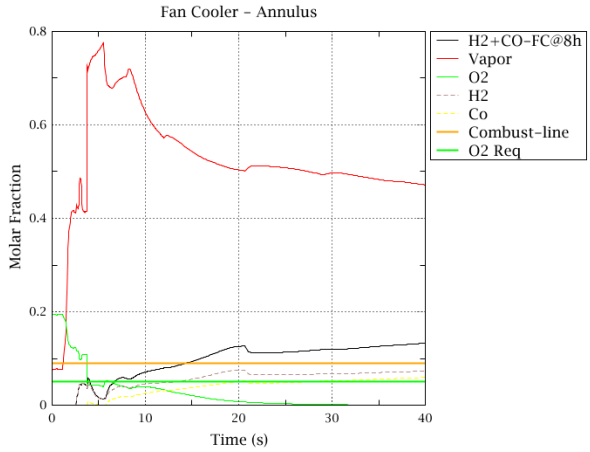

Figure 19 – FC Molar Fraction in Annulus

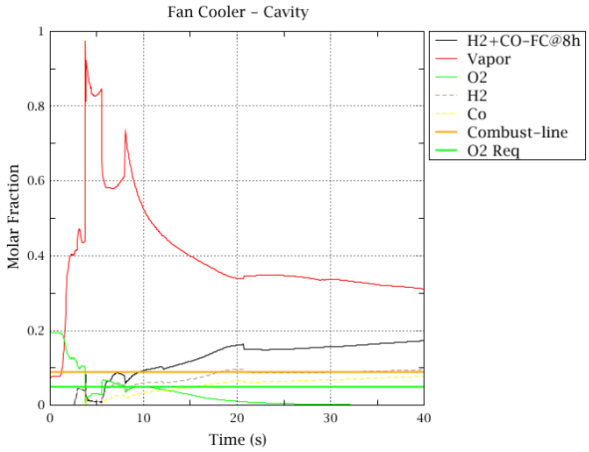

Figure 20 – FC Molar Fraction in Cavity

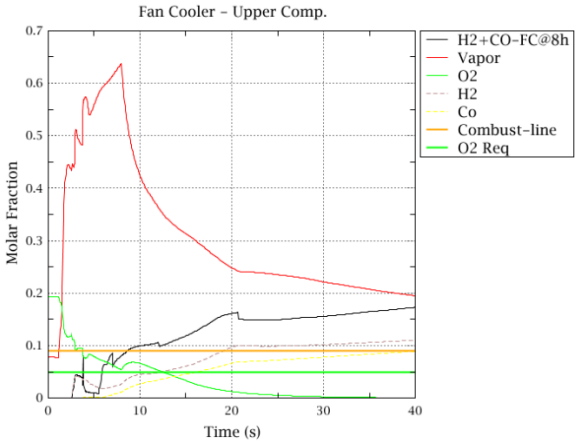

Figure 21 – FC Molar Fraction in Lower Comp.

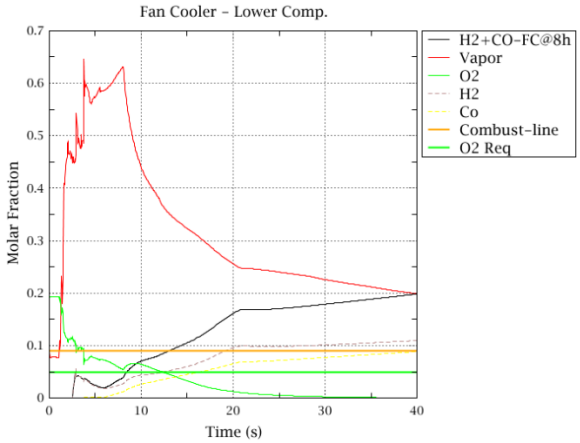

Figure 22 – FC Molar Fraction in Upper Comp

Fan Cooler activation at 9 hours

With fan cooler activation at 9 hours, there is little change in the molar mass fractions from the earlier activation times. In the upper and lower compartments, the vapor fraction is at 50% right at 10 hours compared to below 50% for the other fan cooler activation times caused by the later start time. Deflagrations are still expected but with a much smaller window in the upper and lower compartments. At 13 hours, the conditions are present for deflagrations to take place with oxygen molar mass fractions just above 5% and the combined H_2+CO molar mass fraction just reaching 9%. The oxygen mass fraction drops below 5% before t=15 hours so no combustions are expected after that time.

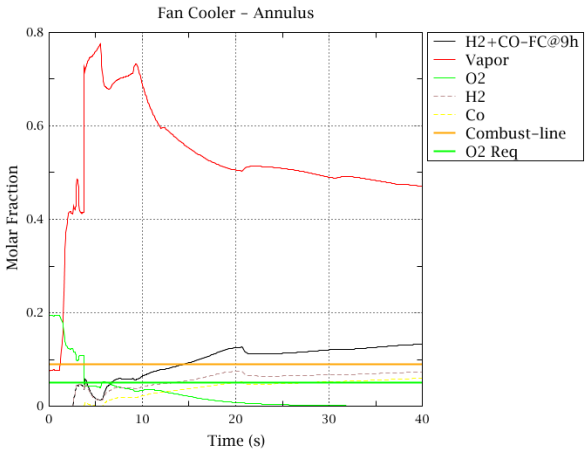

Figure 24 – FC Molar Fraction in Annulus

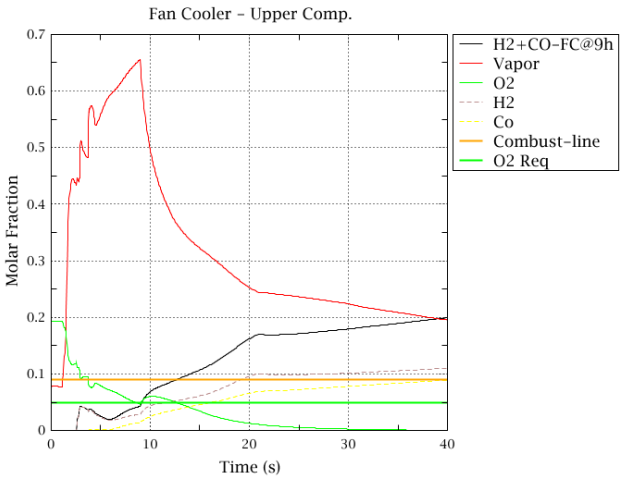

Figure 25 – FC Molar Fraction in Upper Comp

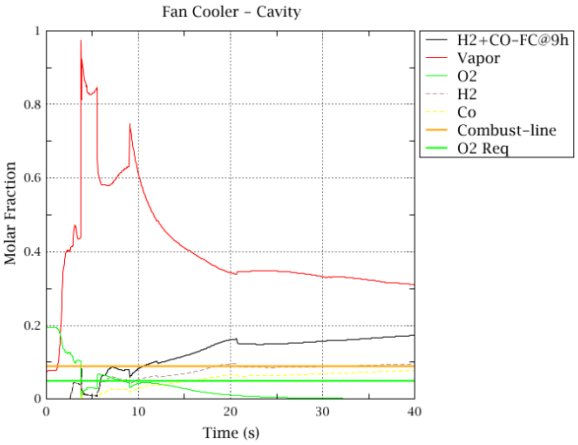

Figure 26 – FC Molar Fraction in Cavity

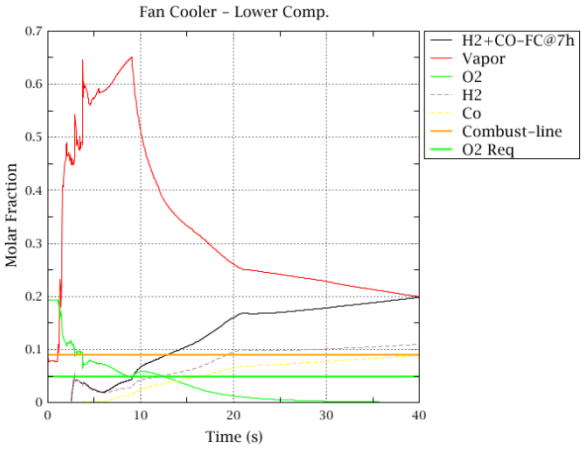

Figure 27 – FC Molar Fraction in Lower Comp

In the annulus, no combustions are expected as criteria are not met. Once the hydrogen and CO mass fractions reaches 9%, oxygen is already below 5%. Furthermore, the vapor mass fraction is above 55% until 15 hours which maintains the atmosphere in this compartment inert.

The cavity does have a window of combustion between 11 and 13 hours once the vapor fraction drops below 55%. Figure 26 shows this.

Fan Cooler activation at 10 hours

The outcome of activating the fan coolers 10 hours after the start of the accident results in a minimal window of just minutes for combustion to occur. The annulus and cavity will not experience any deflagrations. The vapor fraction maintains the annular compartment inert for the first 15 hours and the cavity is deficient in oxygen for combustions to take place; therefore, the criteria are never met as shown in the figures below.

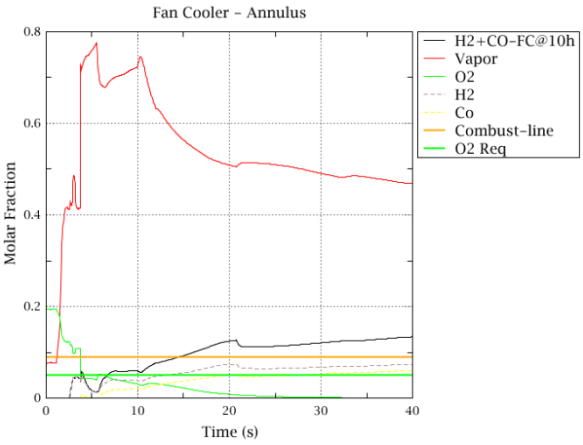

Figure 28 - Molar Fraction in Annulus

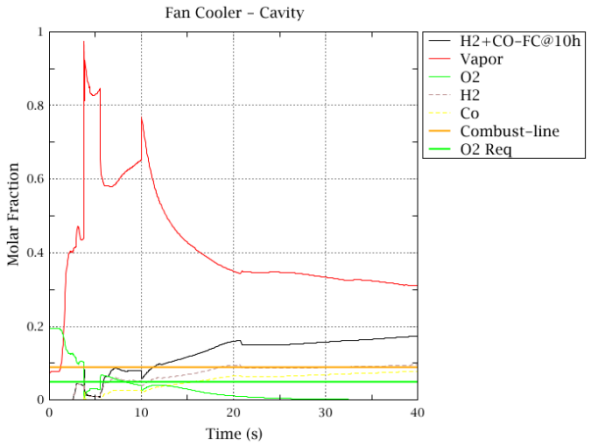

Figure 2923 - Molar Fraction in Cavity

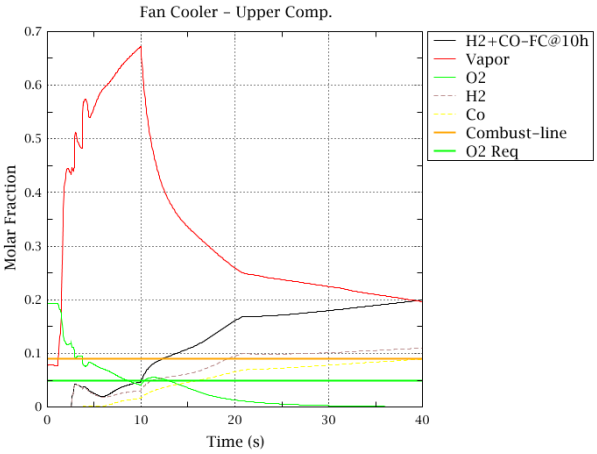

Figure 30 - Molar Fraction in Upper Comp.

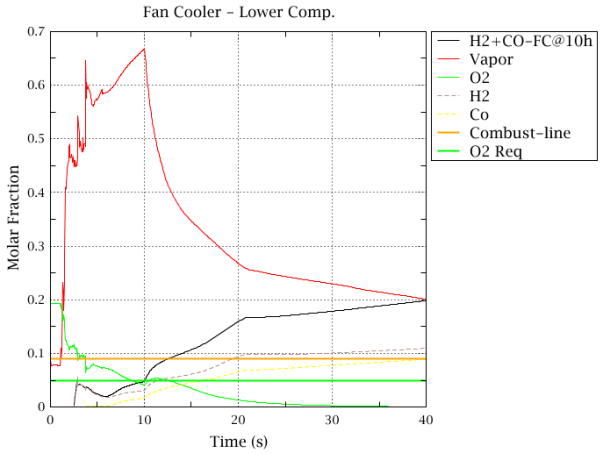

Figure 3124 - Molar Fraction in Lower Comp

For the lower compartment, no deflagrations are expected either. At 13 hours, H_2+CO reaches 9% molar mass fraction needed for deflagrations to occur but the atmosphere does not contain the 5% oxygen needed to sustain the reaction. The same cannot be said for the upper compartment where. H_2+CO molar mass fraction reaches 9% at 12.3 hours. There are 25 minutes where deflagrations may occur as oxygen molar fraction does not decrease below 5% until 12.75 hours. This may cause a small pressure spike depending on the combustion completeness and if a source of ignition is present.

CONCLUSIONS

The start-up of fan coolers during what is considered a critical time of the accident (7-10 hours) has a considerable effect. Their initiation causes the molar mass fraction of vapor to precipitously drop creating a situation ripe for combustion events to occur. The decrease in the vapor fraction causes the increase of the H_2+CO fraction to unsafe levels, close to or above the 9% threshold requirement for deflagrations to take place while the oxygen fraction remains close to the 5% level which maintains the criteria for combustion events of these flammable gases.

The analysis of the results for the fan cooler situation led the team to activate the burn package and perform further simulations to analyze how possible combustion events would develop and the impact they would have in the containment atmosphere. Some parameters were changes which are mentioned in the BURN analysis section further below. The continuation of the study is with the effect of the containment spray system in the containment pressure and atmosphere. Results for this part are resumed below.

Containment Spray Study

The impact of spray systems was also studied to determine their feasibility in containment recovery. Since the critical time for an SBO accident scenario fell around 7 to 10 hours, several simulations were performed with spray actuation times of 7,8,9 and 10 hours under different spray conditions to determine the impact of the spray system in containment pressure and atmospheric conditions (molar mass fractions). Like the fan cooler simulations, PARS were implemented into the containment compartments. The burn package for this section was OFF.

A total of 16 cases were executed under different scenarios with the containment spray system. The table below shows the cases performed.

Table 10 - Spray System Settings

CASE NAME	CASE NO.	TIME ON (HRS)	INITIAL SPRAY TEMP (K)	SOURCE	FLOW RATE (M^3/S)
INFINITE COLD SPRAY	1/2/3/4	7/8/9/10	295.0	Infinite	0.122
INFINITE COLD SPRAY – 20% NOMINAL FLOW RATE	5/6/7/8	7/8/9/10	295.0	Infinite	0.0244
SPRAY W/ RECIRCULATION	9/10/11/12	7/8/9/10	295.0 – Sump temp.	RWST - Sumps	0.122
SPRAY W/ RECIRC – 20% NOMINAL FLOW RATE	13/14/15/16	7/8/9/10	295.0 – Sump temp.	RWST - Sumps	0.0244

Table 10 above shows the 4 types of cases performed: An infinite cold source, an infinite cold source with reduced flow rate, spray injection from the reactor water storage tank (RWST) with recirculation from the sumps, and the same type of case but with a reduced flow rate. 20% of nominal flow rate to be exact.

As mentioned, an infinite cold source was assumed for the first 8 cases. This is plausible due to the new implementation of flex systems in a lot of NPP after the events in Fukushima. Flex systems can use any nearby water reservoirs such as lakes or rivers to insert cold water into the containment or spent fuel pools via the containment spray systems. The 20% nominal flow rate cases were inserted to see with further detail the impact a lower water insertion rate had in the containment building based on a study performed by CIEMAT.

A small improvement that was made in this section of the code was the addition of control functions that will actuate based on time instead of pressure. Therefore, the containment spray system could be actuated at different times as required. Also, the droplet distribution through the different control volumes was refined. There were some missing flow path connections using the spray system which were inserted into the input.

Infinite Cold Spray Analysis

The first analysis performed involved cases 1,2,3,4 which looked at the effects of having an infinite cold source for the spray system. The figures below show the effect on pressure and temperature compared to the reference. The pressure drops from the different initiation times can be seen in Figure 32 with all pressures settling to around 1 bar after 17 hours. As time goes on, the pressure remains stable and then after 30 hours increases slightly due to the increase in temperature as seen in figure 33. The same trend can be observed on containment temperature once the spray system actuates with temperatures dropping from 390 K to 300 in about 8 hours. The temperature spike seen in around 30 hours is due to an increase in the amount of vapor in the upper compartment will be seen in the figures demonstrating the molar mass fractions for the atmosphere at the different control volumes compartments.

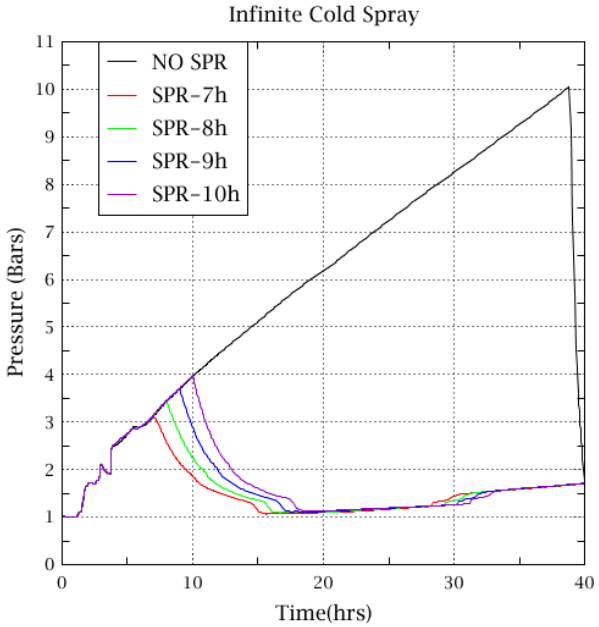

Figure 3225 - Pressure at Activation of Inf. Cold Spray

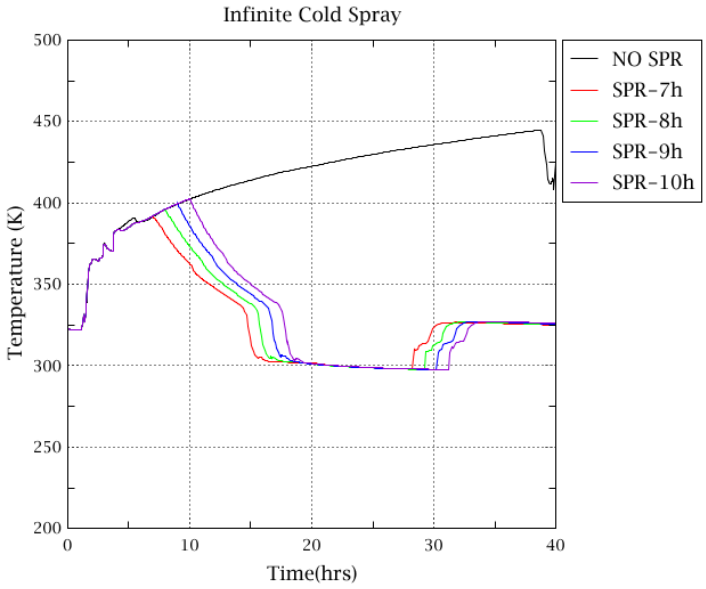

Figure 263 - Temperature at Activation of Inf. Cold Spray

Activation at 7 hours

The figures below represent the molar fractions of oxygen, vapor, hydrogen and carbon monoxide. As seen by the figures, all volumes remain inert because the oxygen molar mass fractions are below 5% when the H_2+CO levels are above 9%. Without oxygen, the combustion cannot take place and the containment building will not undergo any drastic changes in pressure.

The figures below also show the decrease in the vapor fractions once the spray system actuates due to the condensation caused by the water droplets, lowering pressure and temperature.

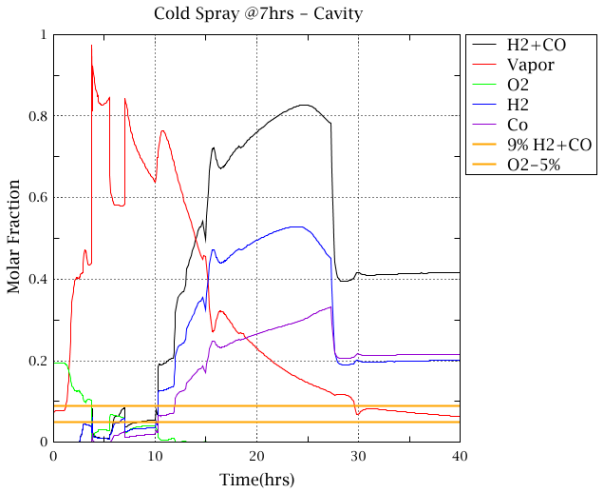

Figure 274 - Molar Fraction Cavity

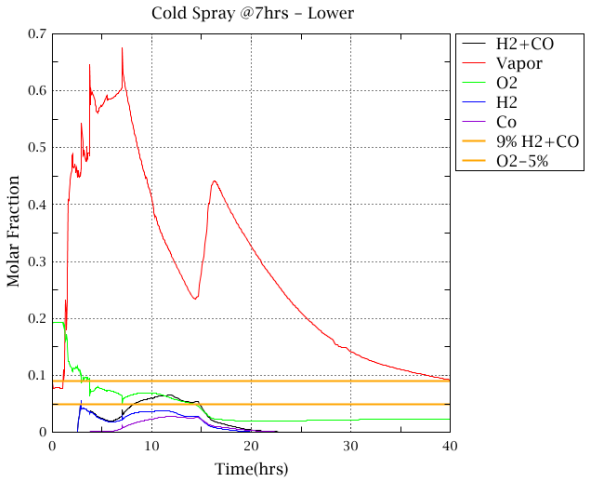

Figure 295 - Molar Fraction in Lower Comp.

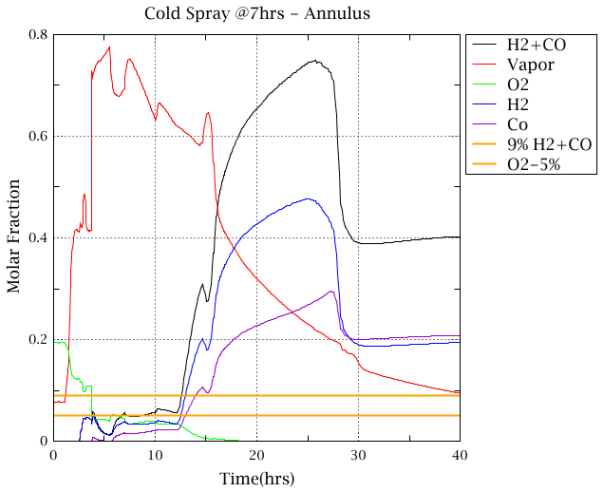

Figure 286 - Molar Fraction in Annulus

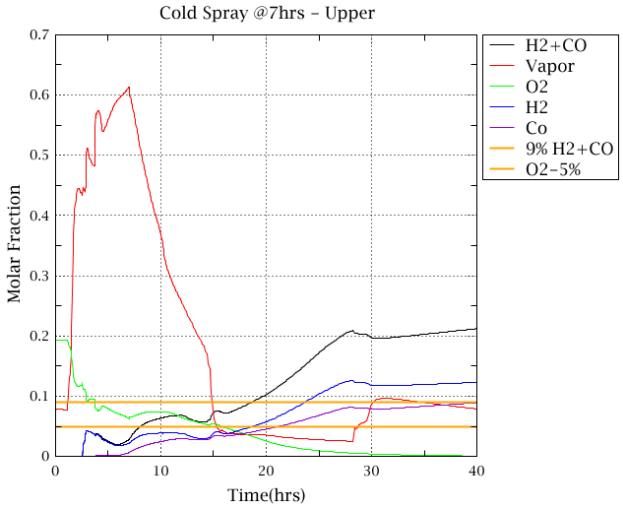

Figure 37 - Molar Fraction in Upper Comp.

Activation at 8 hours

The figures below show the molar fractions for the different compartments.

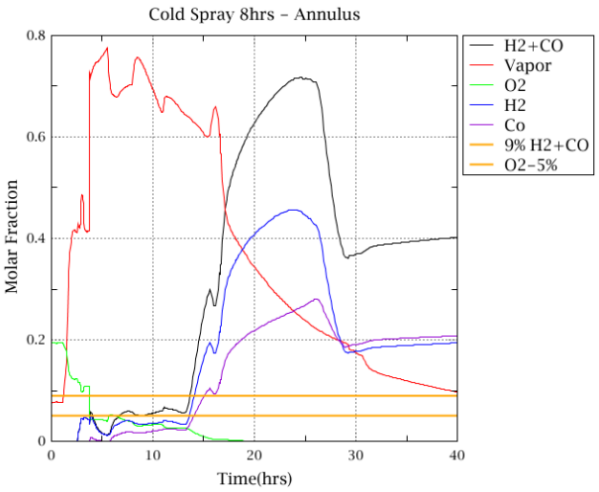

Figure 308 - Molar Fraction in Annulus

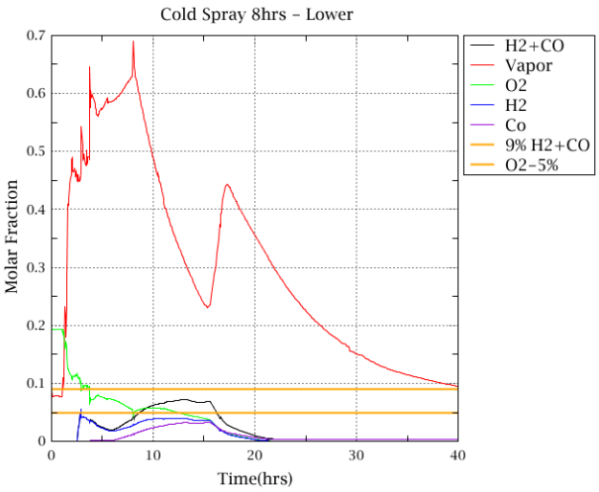

Figure 319 - Molar Fraction in Lower Comp.

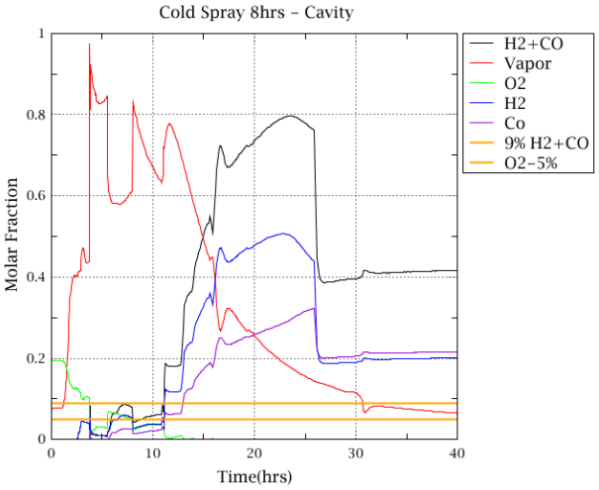

Figure 40 - Molar Fraction in Cavity

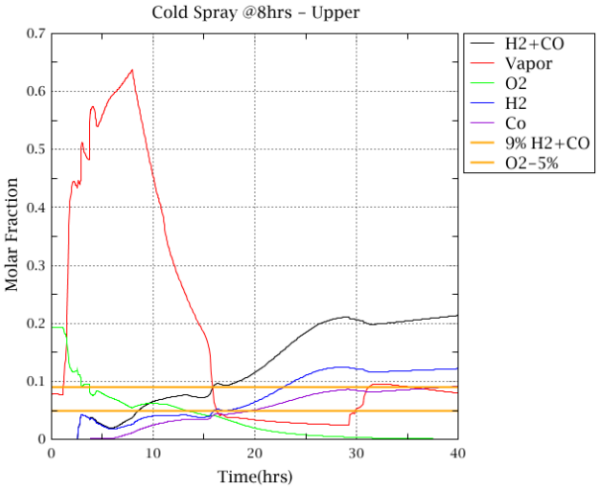

Figure 41 - Molar Fraction in Upper Comp.

A very similar trend is seen with spray activation at 8 hours compared to activation at 7 hours. However, there is a slightly higher risk of hydrogen combustion. Analyzing figure 41, it can be seen that at 16 hours, the H_2+CO fraction nears the 9% limit with the oxygen molar mass fraction hovering above the 5% limit. This may result in a combustion event.

Activation at 9 hours

Activation of the sprays at 9 hours still avoids any H_2+CO combustions but the limit is much closer. Both lower and upper compartments experience a faster increase in the H_2+CO levels. However, the oxygen level dips right below 5% for there to be any combustions. The annulus and cavity compartments are maintained inert by the high vapor molar mass fraction in the first 15 hours and by then, the oxygen molar mass fraction decreases below the required amount needed for combustions to take place.

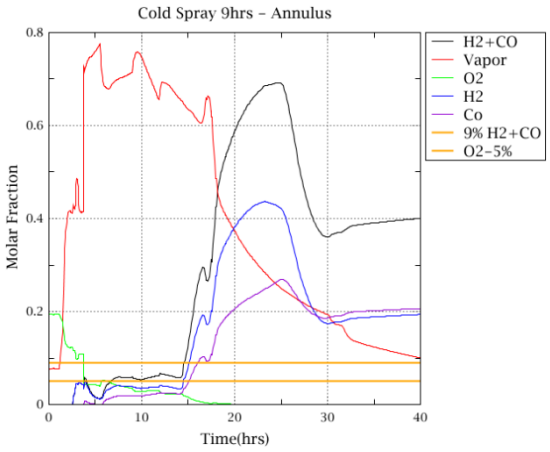

Figure 42 - Molar Fraction in Annulus

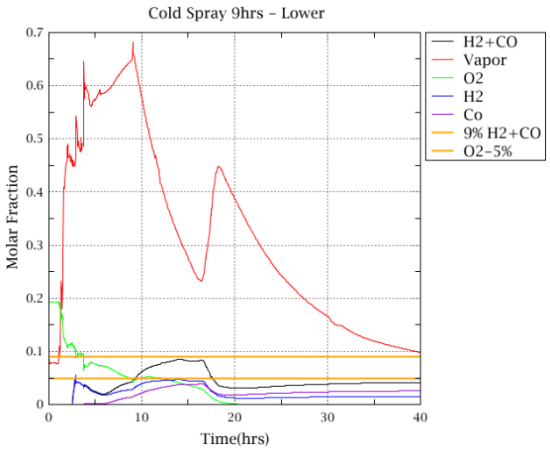

Figure 43 - Molar Fraction in Lower Comp.

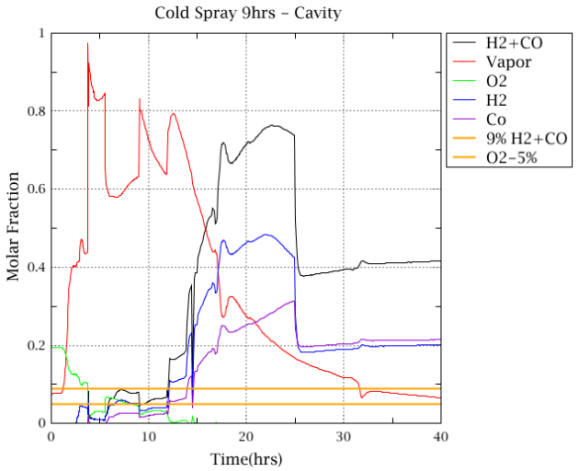

Figure 44 - Molar Fraction in Cavity

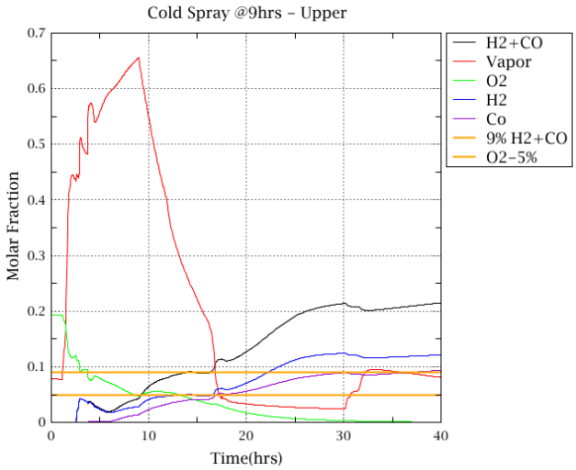

Figure 44 - Molar Fraction in Upper Comp.

Activation at 10 hours

Spray activation at 10 hours also leads to no deflagrations. The oxygen percent in the upper compartment reaches 5% at 11.3 hours and then decreases below this limit one hour later at 12.4 hours. The combustible gases molar mass fraction is not high enough during this period to set off a combustion event.

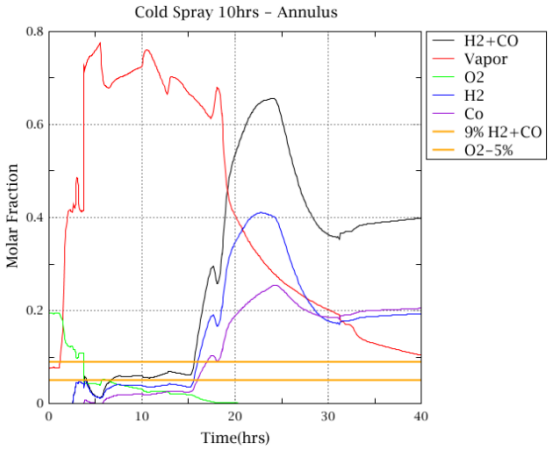

Figure 45 - Molar Fraction in Annulus

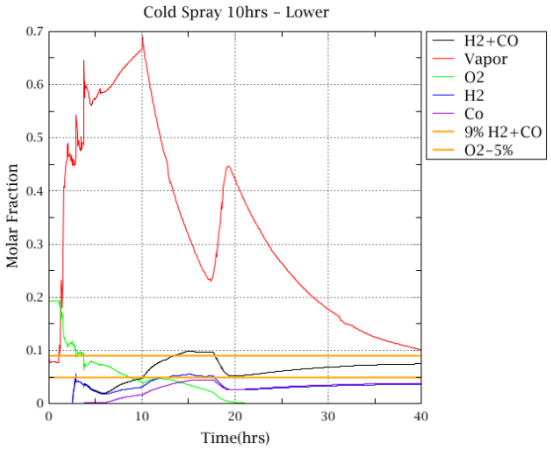

Figure 46 - Molar Fraction in Lower Comp.

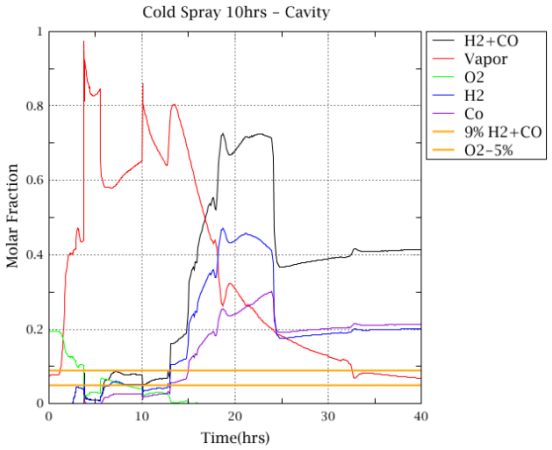

Figure 47 - Molar Fraction in Cavity

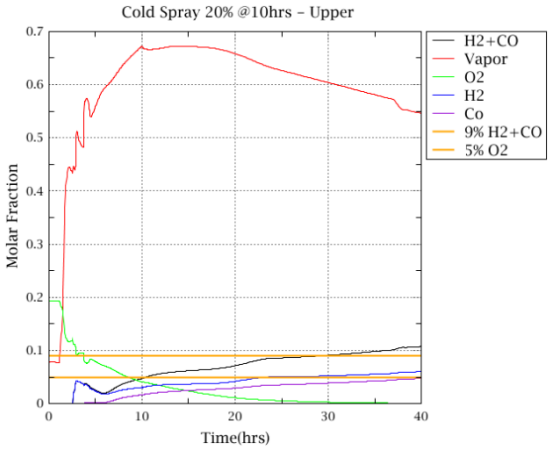

Figure 48 - Molar Fraction in Upper Comp.

In the annulus and cavity, the high vapor molar fraction keeps the compartments inert. After 18 hours, the vapor has condensed due to the heat removal provided by the spray system. However, by this point, the oxygen mass fraction is too low and the combustion criteria are not met.

Conclusions

After reviewing the data, activating the containment spray system with an infinite cold source ensures the safety in the integrity of the containment building. The earlier the sprays can be actuated, the lower the chance for a combustion to take place as seen in the cases where the sprays were activated at 7 and 8 hours. With the cases where activation occurs at 9 and 10 hours, the molar masses are much closer to the flammability limits for combustions. Furthermore, earlier spray initiation prevents pressure build-up inside the containment although as seen in figure 32, initiation time has little impact on final pressure measurements.

Infinite Cold Spray at 20% Nominal Flow Rate

It was of interest to study containment behavior if the nominal flow rate was reduced to 20% and see what impact it would have in the containment. The reduced flow rate of 0.0244 m^3/s is a relevant reproduction of the effect a flex system would have on the containment's atmosphere since the pumps used to run the flex system are of lower power compared to the pumps used to run the containment spray system during other scenarios. In the figures below, pressures and temperatures are shown for spray activations at 7, 8, 9, and 10 hours.

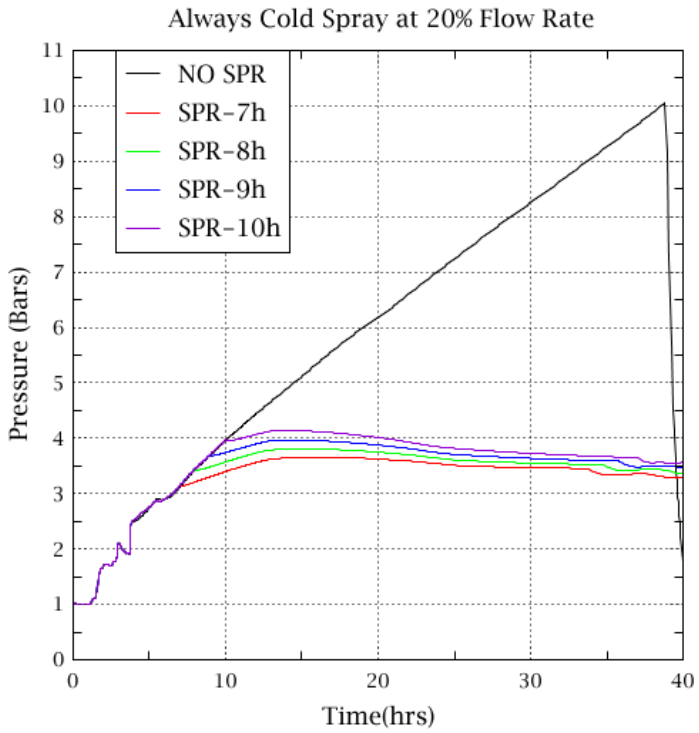

Figure 49 - Containment Pressure with Infinite Cold Source at 20% Nominal Flow rate

A few obvious differences are present with 20% nominal flow compared to the previous case with 100% flow. First, the pressure drop is not drastic and extends for a much lower time compared to the results obtained with nominal flow rates. In the previous cases, pressure dropped to 1 bar (100 kPa) a short while after the initiation of the spray system. Meanwhile in this case, the pressure drop is only to about 3.5 bars. The lower flow rate results in a minor but constant pressure decrease.

This is also evident by the temperatures seen in the containment atmosphere. Once the sprays are activated, the containment temperature undergoes a very slow and gradual decline from approximately 400 K to 385 K. The lower injection rate leads to slower cooling. This is shown in figure 50 below.

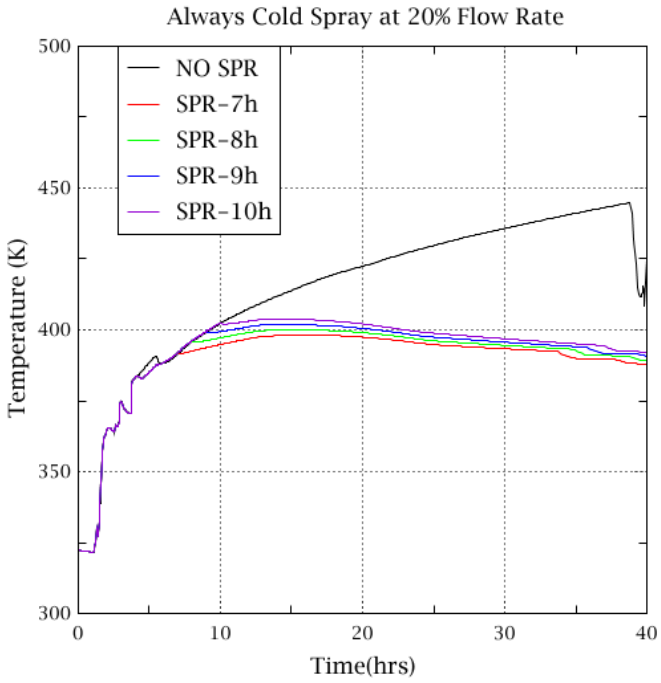

Figure 50 - Containment Temperature with Infinite Cold Source at 20% Nominal Flow rate

The next step in determining the safety of the containment is analyzing the molar mass fractions for possible combustion events.

Activation at 7 hours

Activation of the spray system with a reduced mass flow rate at 7 hours maintains the vapor fraction in all compartments well above 55% except for the upper containment after 35 hours. This follows the higher overall temperatures in these compartments compared to the previous case where full nominal flow was in effect. The decreased flow rate of the spray containment system maintains the atmosphere at a higher vapor fraction due to the decreased condensation occurring in the compartments.

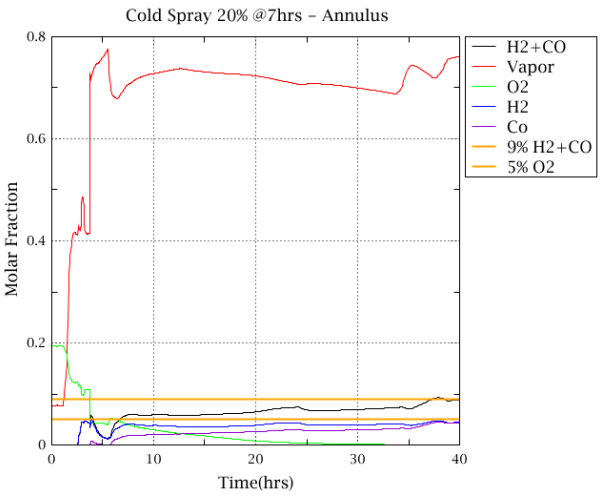

Figure 51 – Molar Fraction in Annulus

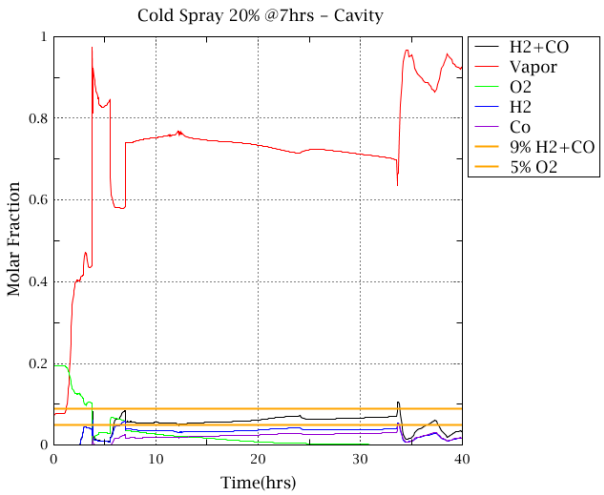

Figure 53 – Molar Fraction in Cavity

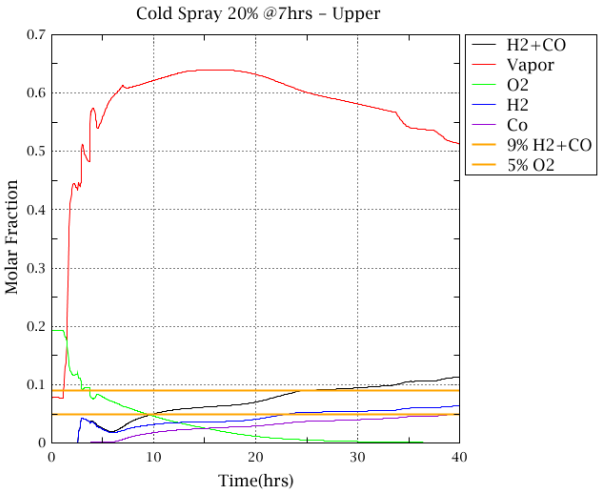

Figure 52 – Molar Fraction in Upper Comp.

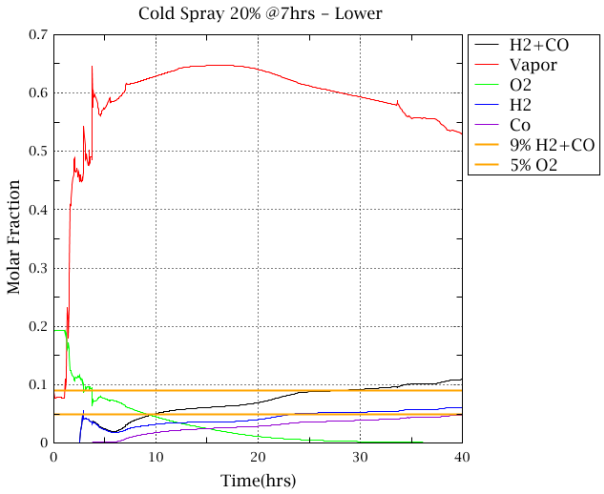

Figure 54 – Molar Fraction in Lower Comp.

In the upper and lower compartments, the H_2+CO combined molar fraction does pass the 9% threshold limit with vapor fractions dropping below 55% after 35 hours. However, the oxygen molar fraction is well below 5% in these compartments so they are inert.

Activation at 8 hours

No deflagrations are expected with spray activation at 8 hours either. The lower injection rate of water from the spray system maintains the vapor fraction of all compartments high rendering them vapor-inert for the first 35 hours. After that, the lack of oxygen keeps the containment safe from combustion events. There are no other striking features worth mentioning from the figures below.

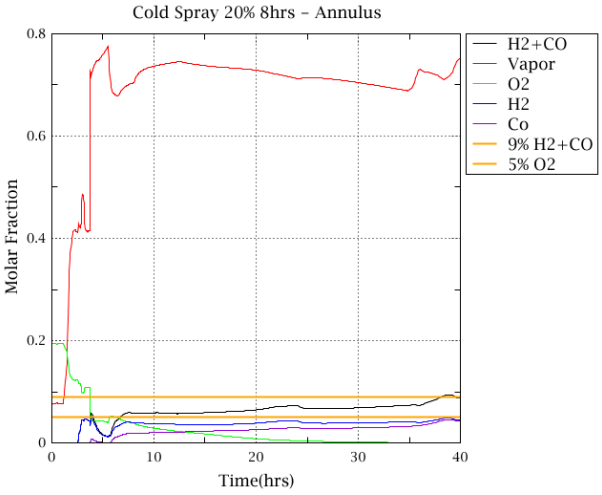

Figure 55 – Molar Fraction in Annulus

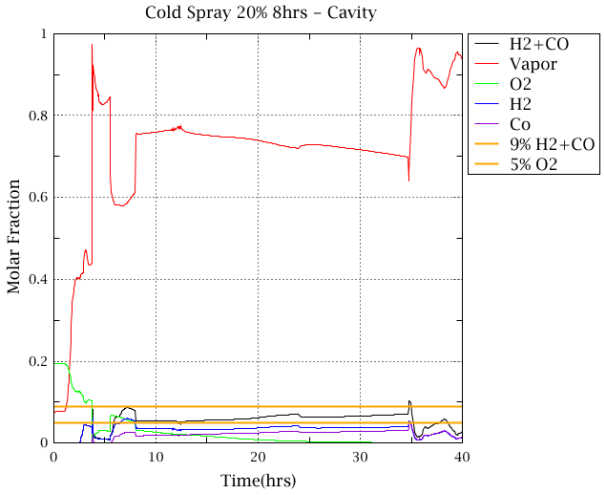

Figure 57 – Molar Fraction in Cavity

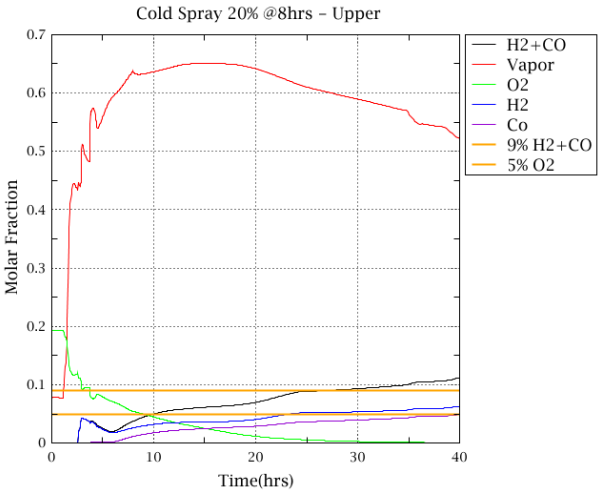

Figure 56 – Molar Fraction in Upper Comp.

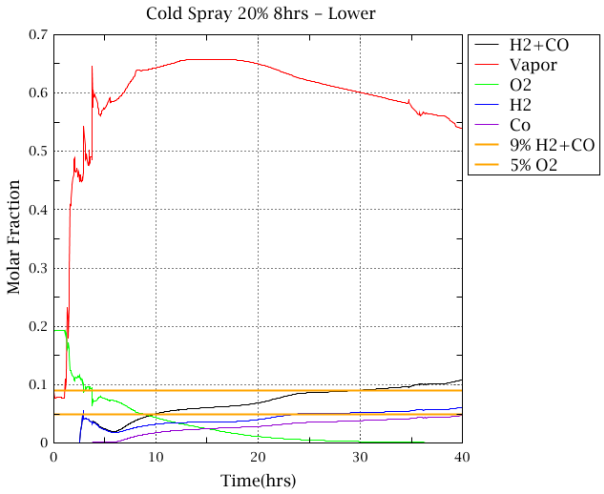

Figure 58 – Molar Fraction in Lower Comp.

Activation at 9 hours

The same results occur with later activation of the spray system at 9 hours. The vapor fraction remains high due to the higher temperatures and the compartments remain inert. Furthermore, the very low oxygen molar mass fractions prevent deflagrations from occurring even when the H_2+CO levels are above the required 9% molar mass fraction threshold.

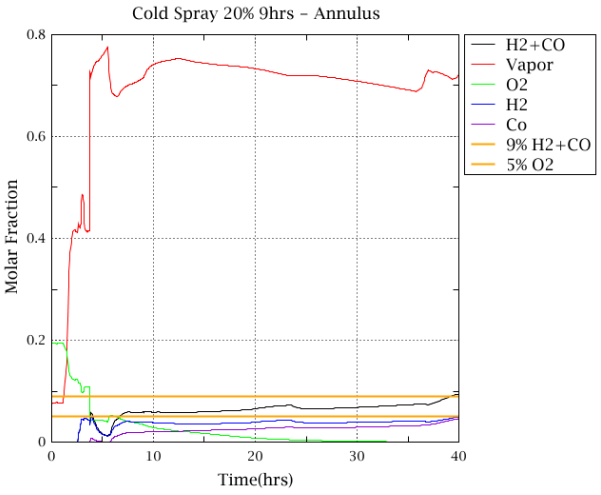

Figure 59 – Molar Fraction in Annulus

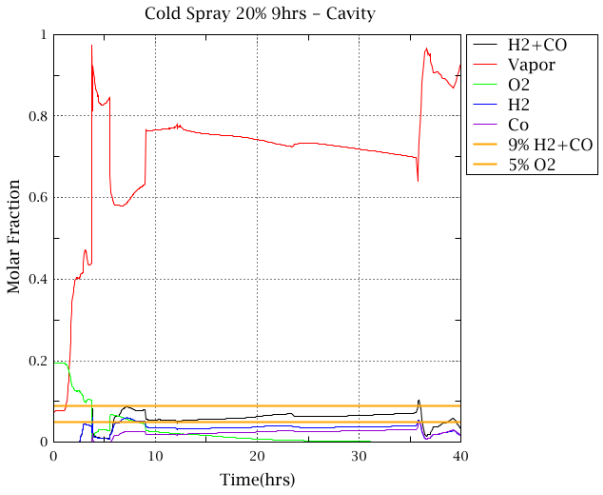

Figure 61 – Molar Fraction in Cavity

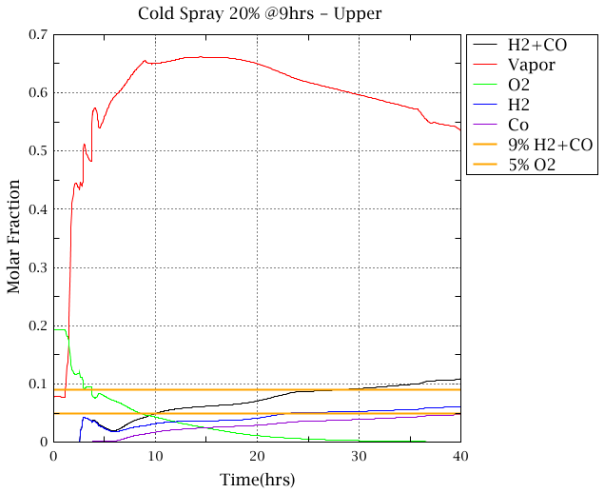

Figure 60 – Molar Fraction in Upper Comp.

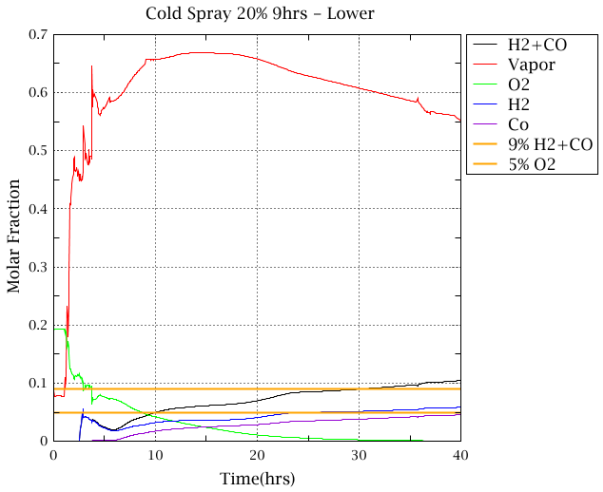

Figure 62 – Molar Fraction in Lower Comp.

Activation at 10 hours

The trend continues with activation of the spray system at 10 hours. The high vapor molar fraction and low oxygen and H_2+CO molar mass fractions amounts prevent any combustion events from occurring.

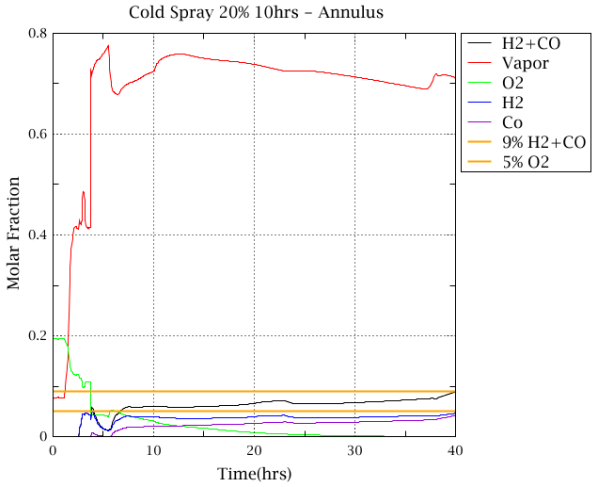

Figure 63 – Molar Fraction in Annulus

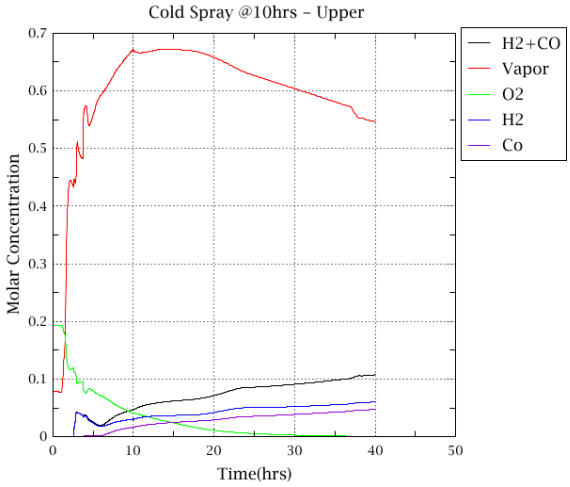

Figure 64 – Molar Fraction in Upper Comp.

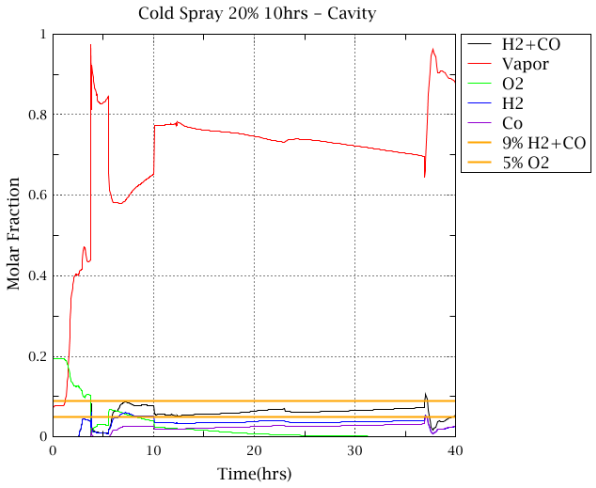

Figure 65 – Molar Fraction in Cavity

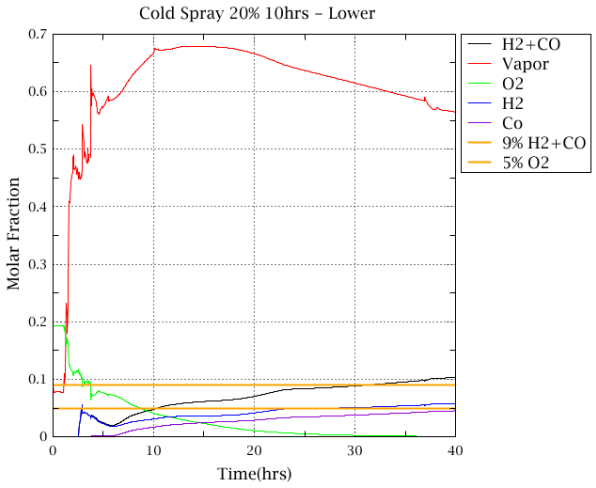

Figure 66 – Molar Fraction in Lower Comp.

Conclusions

Although containment pressure does not drop significantly with a lower flow rate in the injection system, hovering around 3.5 bars, the containment and its compartments seem to be significantly safer from combustion events due to a much higher molar mass fraction of vapor. This causes the compartments and containment to be vapor-inert.

With these results, it can be concluded that water injection into the containment via the spray system at a reduced rate is a viable option for maintaining integrity of the containment building for a short-to-intermediate time period. Pressures in the 3-4 bar range for prolonged time (days/weeks) in the containment building require closer inspection and simulation to determine the effect on the integrity of the containment building and is beyond the scope of this study.

Spray with Recirculation from Sumps

The next set of conditions involved examining containment recovery and depressurization using water from the reactor water storage tank (RWST) and then using recirculation by taking water from the sumps. The figures below show the pressure and temperature for the different cases.

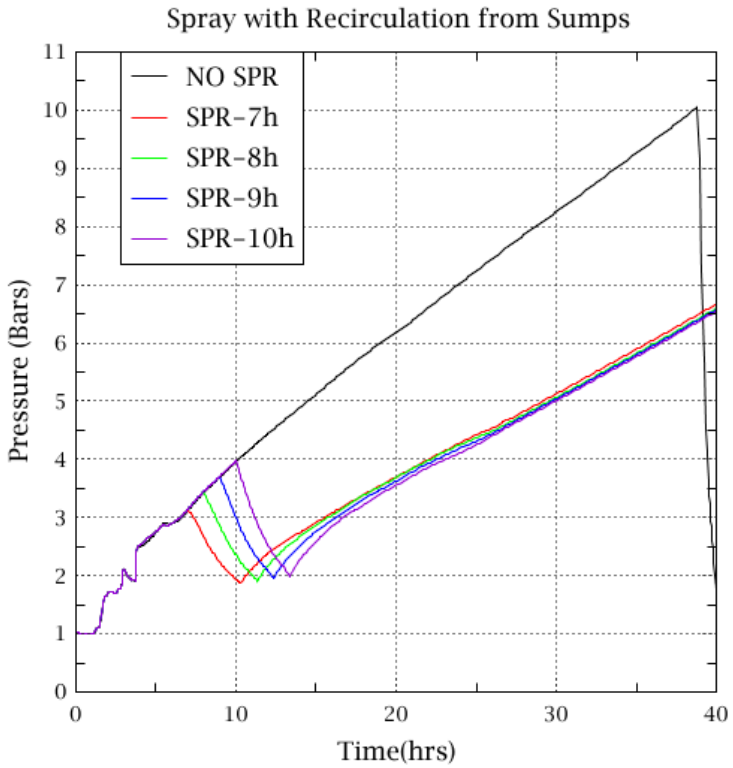

Figure 67 – Containment Pressure from Spray Activation with RWST as Source

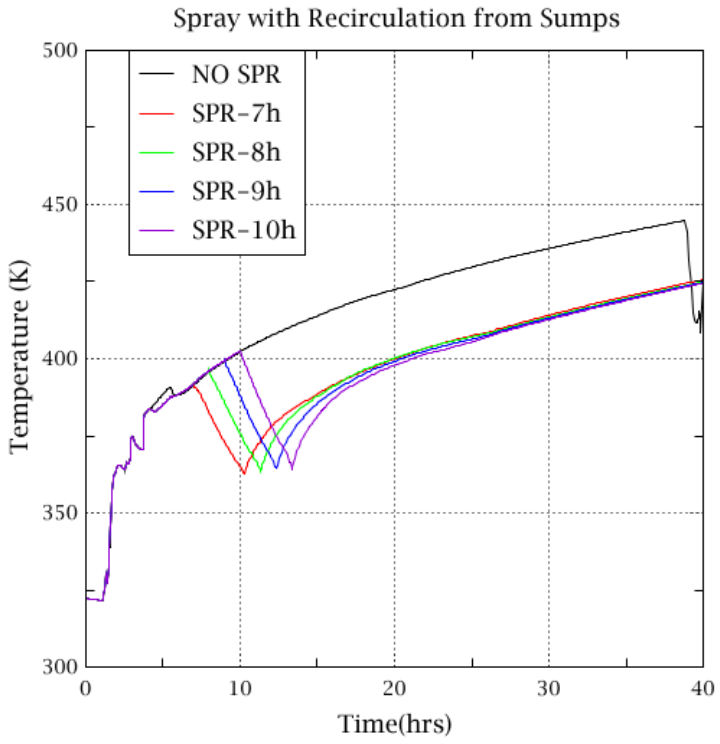

Figure 68 – Containment Temperature from Spray Activation with RWST as Source

Figures 67 and 68 show the immediate effect the initiation of the spray system has in the containment pressure and temperature. Both properties drop for the duration of the capacity of the RWST to deliver water to the spray system. From the figures, it can also be shown that the RWST has a capacity to power the spray system for roughly 3 hours before it starts taking water from the sumps as the pressure and temperature decreases only last 3 hours.

Activation at 7 hours

The figures below show the effect of activation of the spray system at 7 hours. The first striking distinction in these graphs is the steep drop in the water vapor molar mass fraction. This comes from the activation of the spray system which condenses the vapor back to liquid water. The temperature starts to rise again as the water that is being sucked from the sumps is being slowly heated by the decay heat of radioactive products in the containment building and the corium in the cavity. This causes the water vapor molar mass fraction to increase again and make the compartments vapor-inert as the mass fractions are greater than 70%.

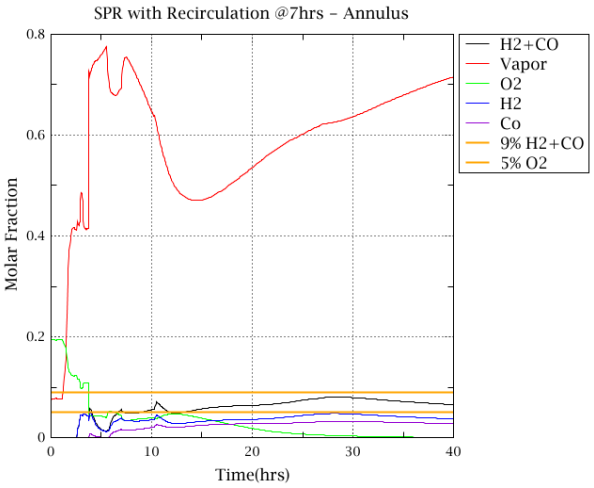

Figure 69 – Molar Fraction in Annulus

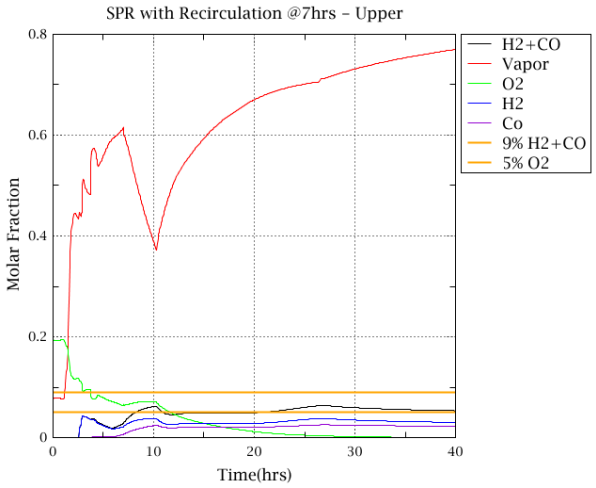

Figure 70 – Molar Fraction in Upper Comp.

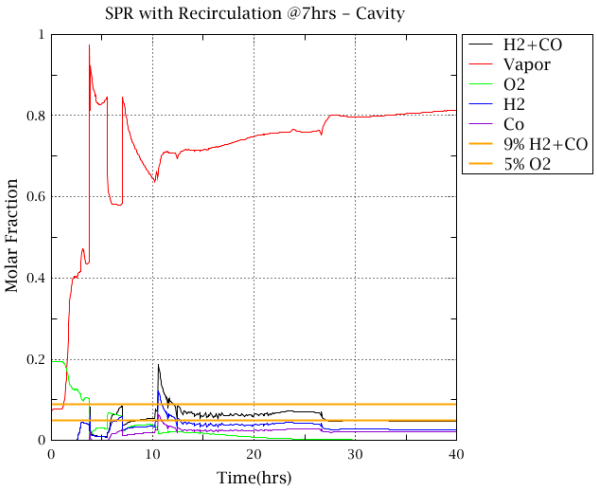

Figure 71 – Molar Fraction in Cavity

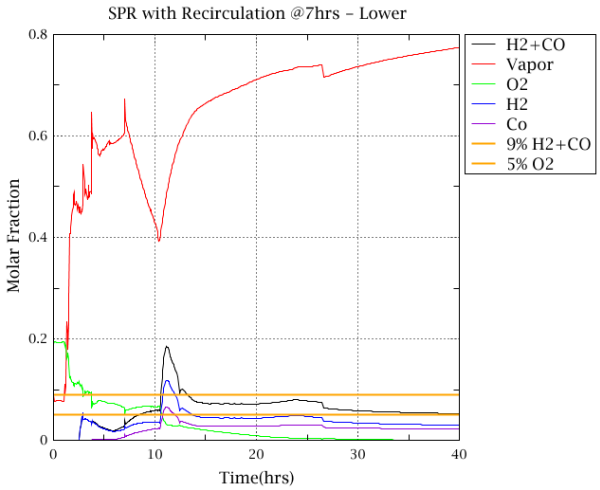

Figure 72 – Molar Fraction in Lower Comp.

There are no moments where deflagrations can occur in any of the compartments. The peaks in H_2+CO seen in figures 72 and 71 corresponding to the lower compartment and the cavity respectively reach the 9% molar mass fraction level required for combustion but the compartments are maintained inert by a high vapor fraction in the cavity and a lack of oxygen in the lower compartment.

Activation at 8 hours

Initiating the spray system at 8 hours has very similar results as those in the previous section. If there is one distinction to make, is that the H_2+CO mass fraction remains lower and never reaches the combustion threshold in the lower compartment. No combustions are to be expected in these compartments as conditions are not met as shown by the figures below.

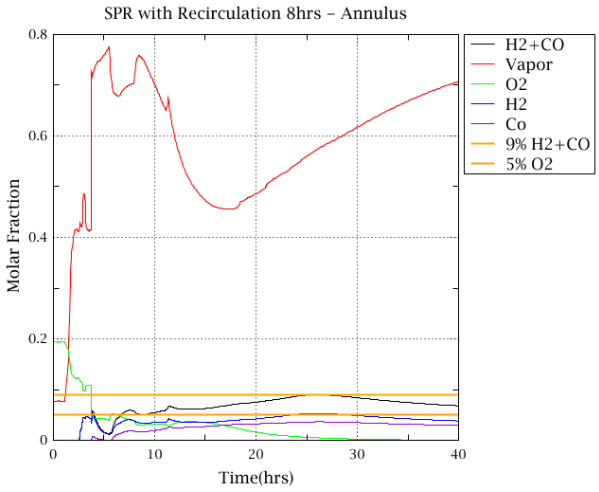

Figure 73 – Molar Fraction in Annulus

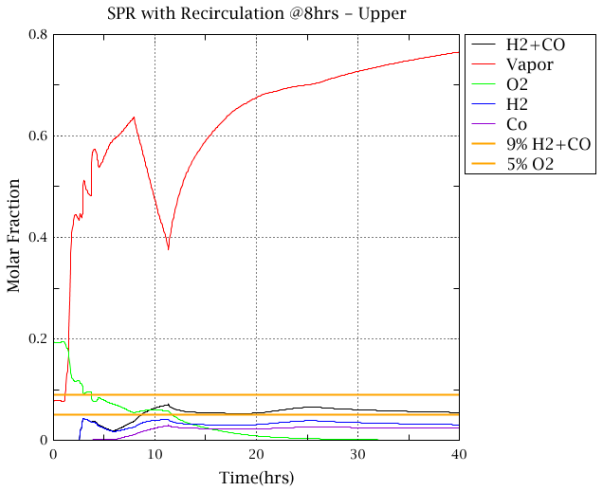

Figure 74 – Molar Fraction in Upper Comp.

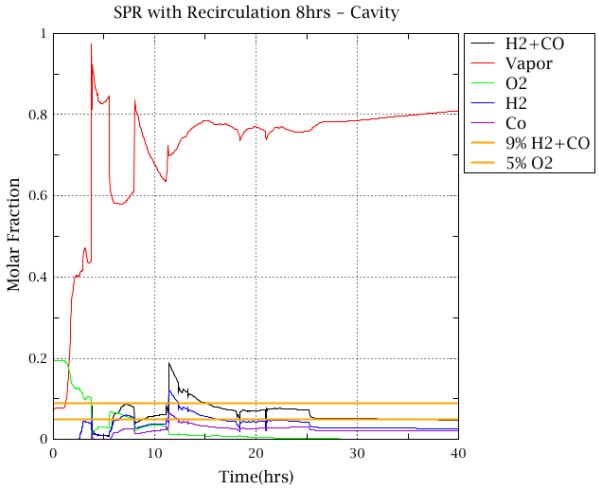

Figure 75 – Molar Fraction in Cavity

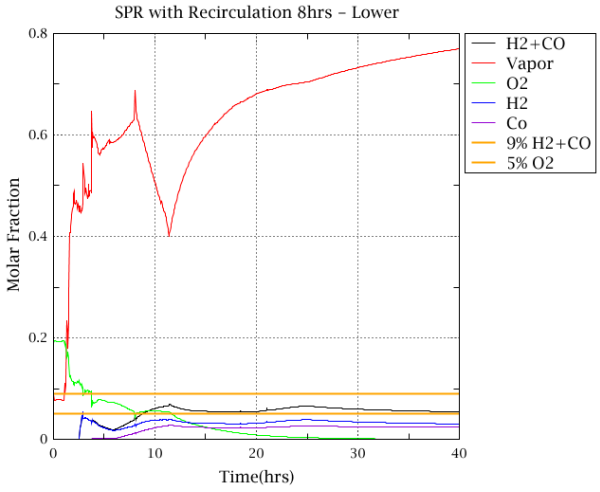

Figure 76 – Molar Fraction in Lower Comp.

Activation at 9 hours

Combustion events are also not expected at initiation of the spray system at 9 hours. The low oxygen and H_2+CO molar mass fractions maintain the compartments inert through the first 40 hours.

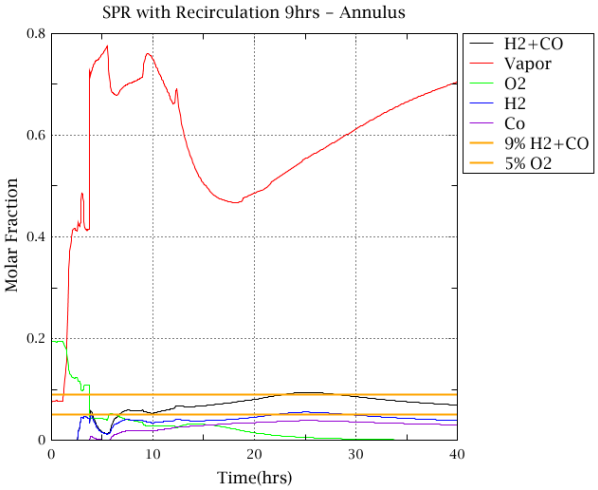

Figure 77 – Molar Fraction in Annulus

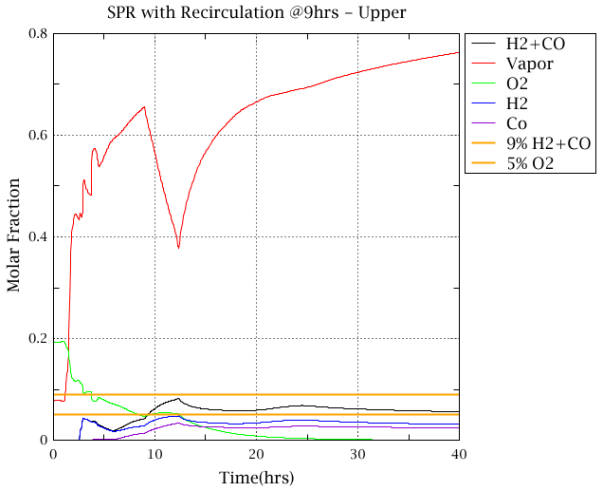

Figure 78 – Molar Fraction in Upper Comp.

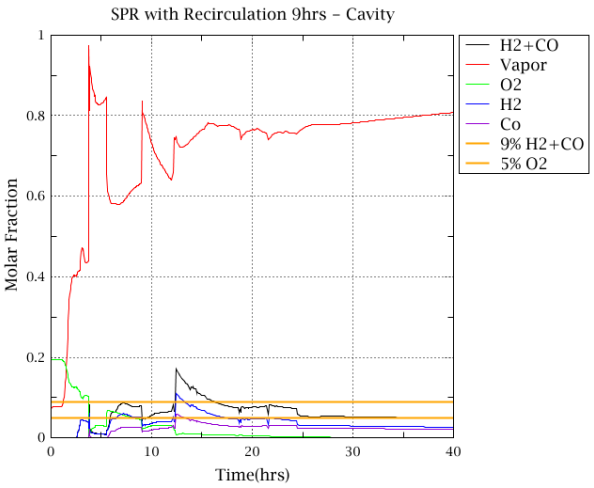

Figure 79 – Molar Fraction in Cavity

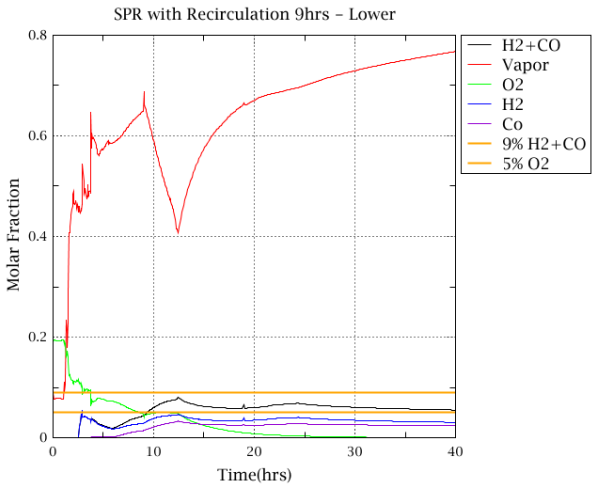

Figure 80 – Molar Fraction in Lower Comp.

Activation at 10 hours

Combustion events are also prevented with the initiation of the spray system at 10 hours.

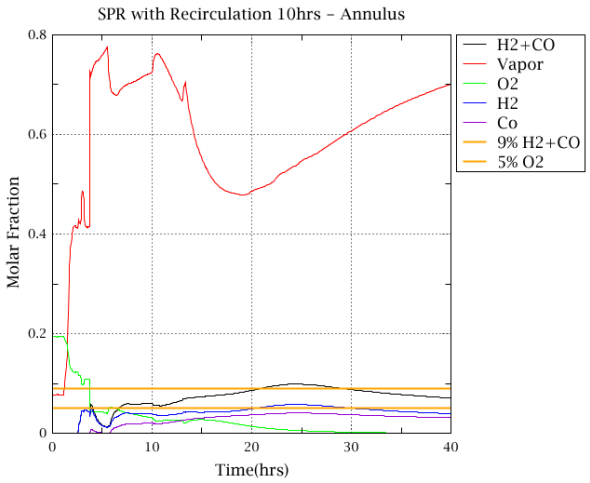

Figure 81 – Molar Fraction in Annulus

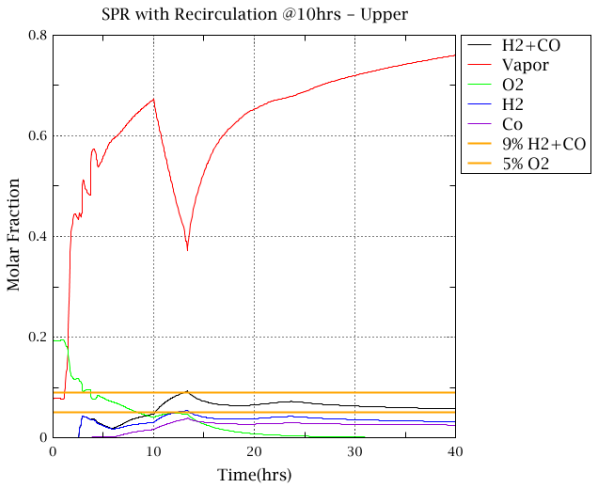

Figure 82 – Molar Fraction in Upper Comp.

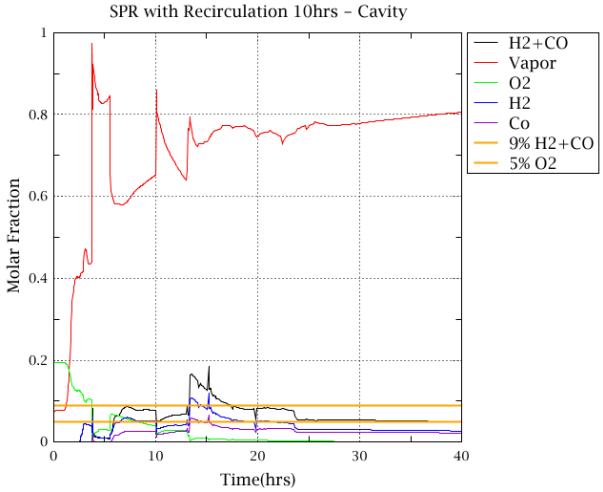

Figure 83 – Molar Fraction in Cavity

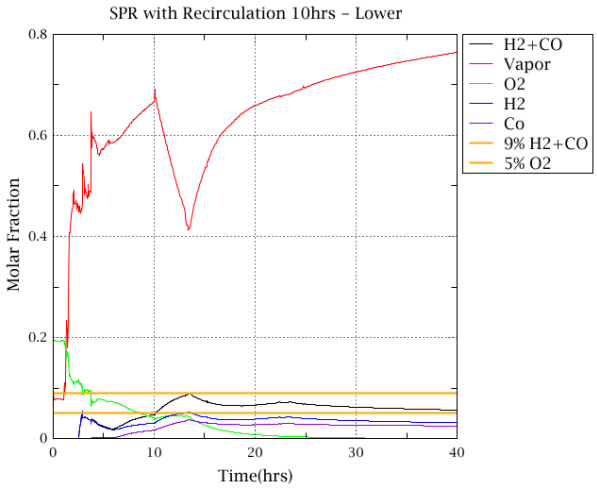

Figure 84 – Molar Fraction in Lower Comp.

Looking at figure 82, there is a very small window of time that prevents combustion around the 13.5-hour mark. The oxygen molar mass fraction drops below 5% just before the H_2+CO peak. A further delay in spray injection could push the decrease in oxygen to a later time coinciding with a high molar mass fraction of hydrogen and CO which could initiate a combustion event.

Conclusions

The spray system proves to be a very useful system in initially lowering containment pressure and preventing combustion events from taking place. With the systems actuation, the water vapor fraction which maintains the compartments inert decreases below the 55% threshold required to prevent deflagrations; however, the oxygen and H_2+CO levels remain low enough where these events cannot take place. Afterwards, the vapor molar mass fraction increases due to the increase in containment temperature which continues to prevent combustion events from initiating.

Spray at 20% Nominal Flow Rate with Recirculation from Sumps

Like the cases that were executed with cold water at 20%, it was of interest to examine the effects that lowering the flow rate in the sprays would have on the containment. The source remained the same, the RWST with recirculation from the sumps once it is empty. The figures below show the pressure and temperatures for the cases performed at different times of activation of the spray system.

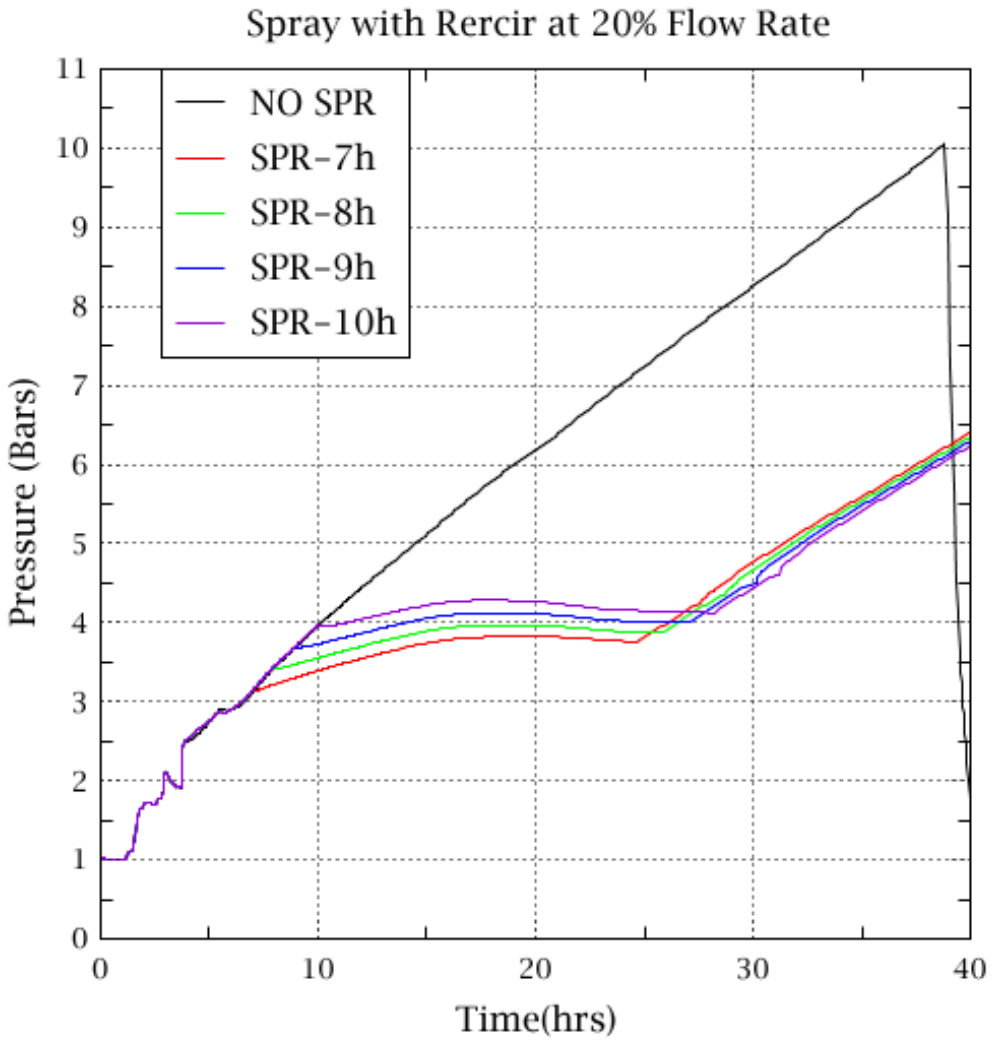

Figure 85 – Containment Pressure with Cont. Sprays at 20% NFR with RWST as Source

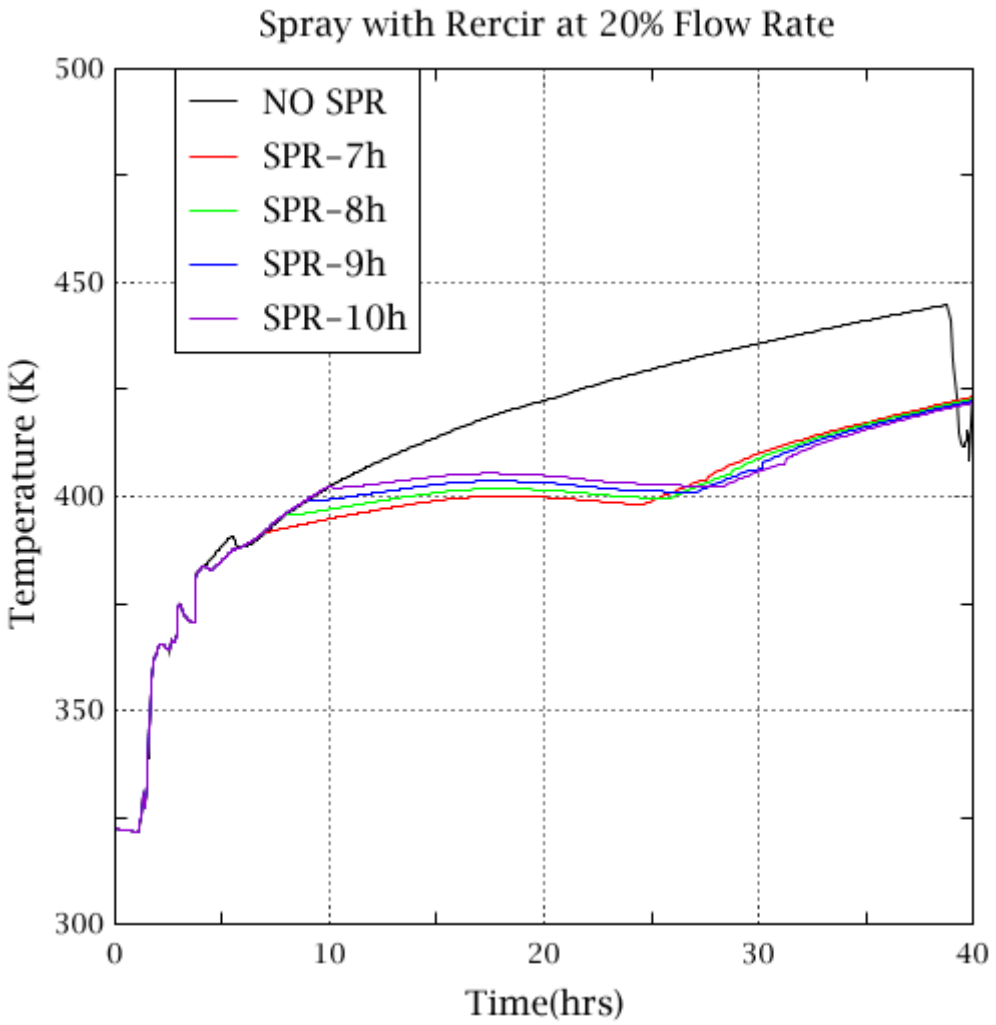

Figure 86 – Containment Temperature with Cont. Sprays at 20% NFR with RWST as Source

Due to the reduced flow rate in the sprays, there is less cooling of the atmosphere as seen in figure 86; therefore, the pressure decrease is minimal. However, the longer rate of injection maintains the pressure and temperature stable for a much longer period of time. It can be seen that once the spray system is activated, the containment pressure along with the temperature remain steady for the next 15 hours or so before pressure starts to increase again.

Having this time frame of containment stability gives a good window of opportunity to implement other methods for containment recovery and minimize the risk of damage to the structure.

Activation at 7 hours

There are no deflagrations expected in these compartments due to the amount of steam. As we can see in the figure below, the molar fraction of steam remains well above 60% in all compartments. This prevents any combustions events from happening.

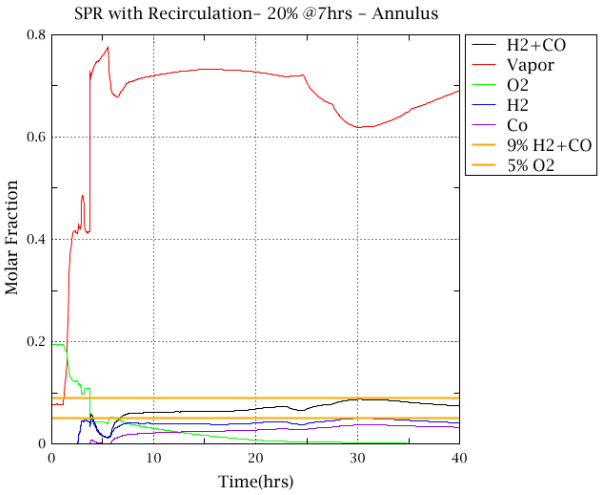

Figure 87 – Molar Fraction in Annulus

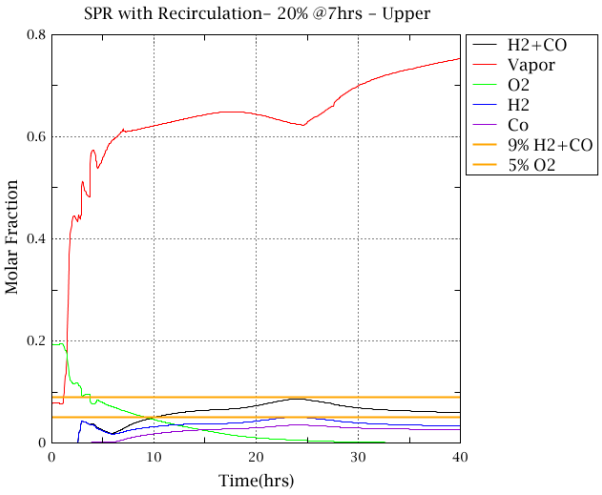

Figure 88 – Molar Fraction in Upper Comp.

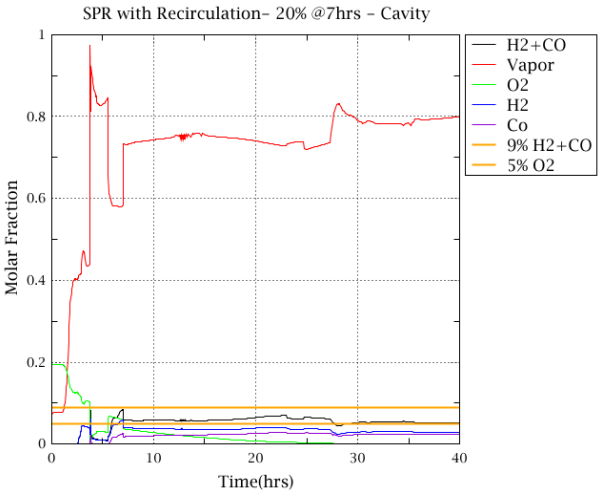

Figure 89 – Molar Fraction in Cavity

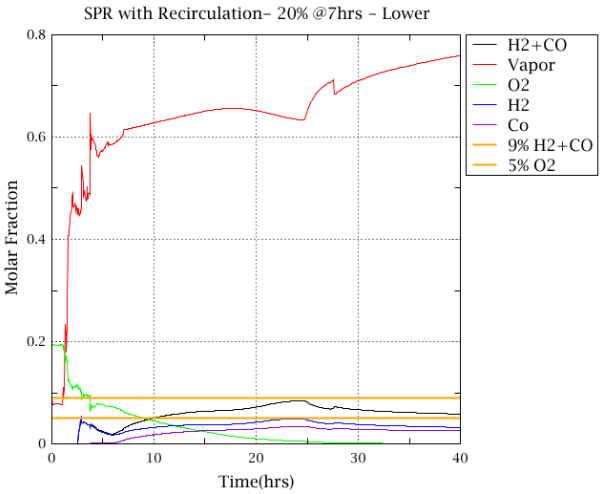

Figure 90 – Molar Fraction in Lower Comp.

Activation at 8 hours

Molar mass fractions for H_2+CO remain below the combustion limit when sprays are activated at 8 hours. The high temperature in the containment keeps water vapor molar fractions high, always above 60% except for the cavity at initiation of the spray system. This sustains the vapor-inert environment in the compartments preventing hydrogen combustions from occurring.

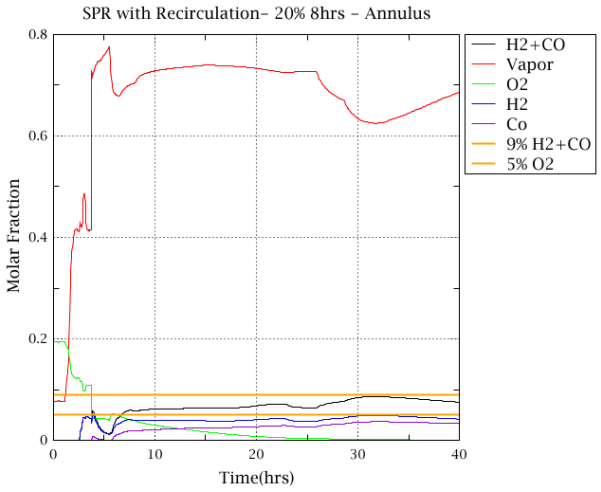

Figure 91 – Molar Fraction in Annulus

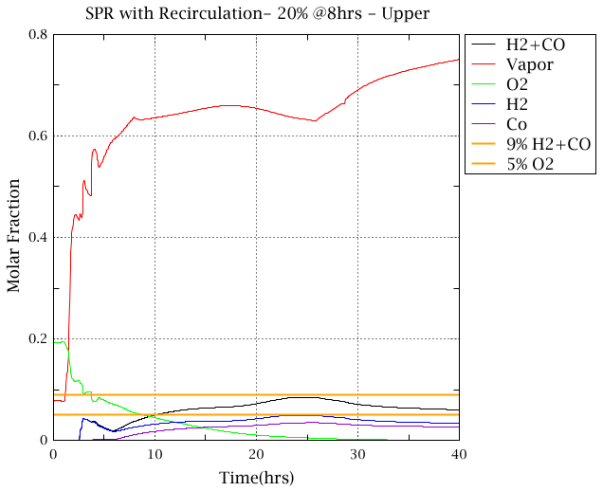

Figure 92 – Molar Fraction in Upper Comp.

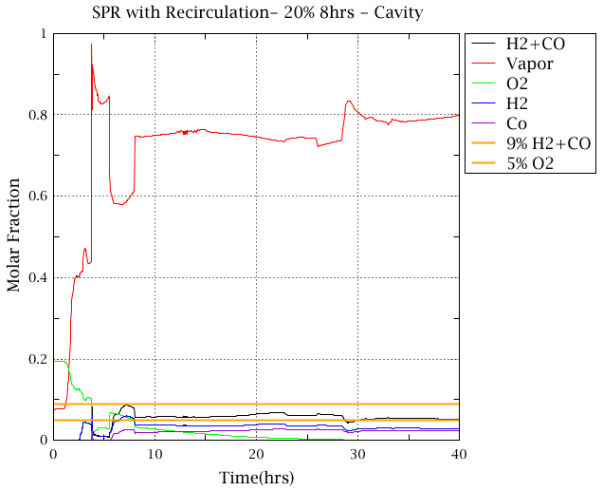

Figure 93 – Molar Fraction in Cavity

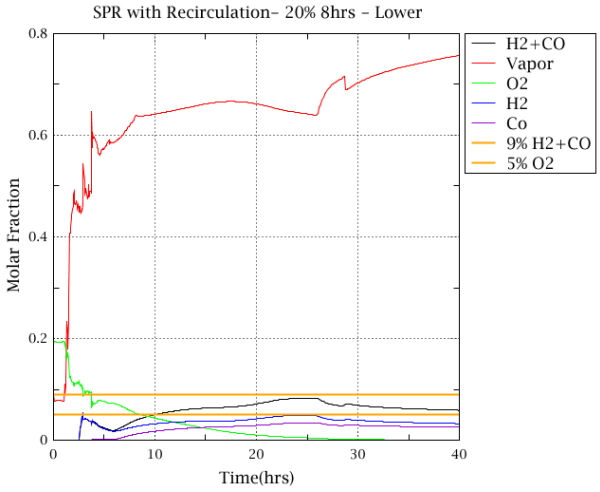

Figure 94 – Molar Fraction in Lower Comp.

Oxygen levels decrease below 5% 10 hours into the accident while the H_2+CO molar fractions never reach 9%. These are favorable conditions for the containment building.

Activation at 9 hours

The conditions for combustion are also not present in any of the compartments as shown in the figures below. The diminished flow rate of water into the containment from the spray system maintains the water vapor fraction above 60% preventing any combustion events.

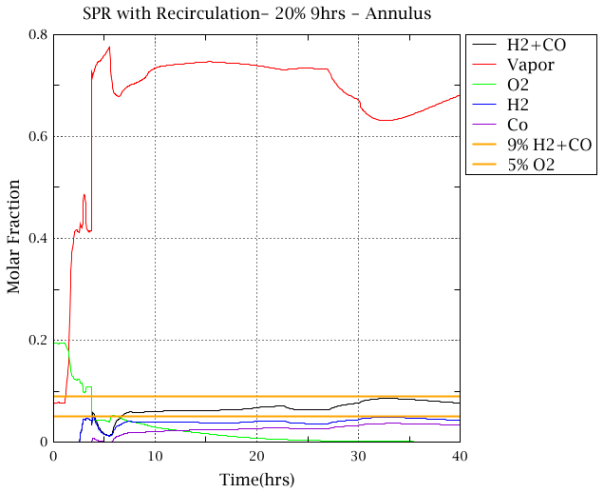

Figure 95 – Molar Fraction in Annulus

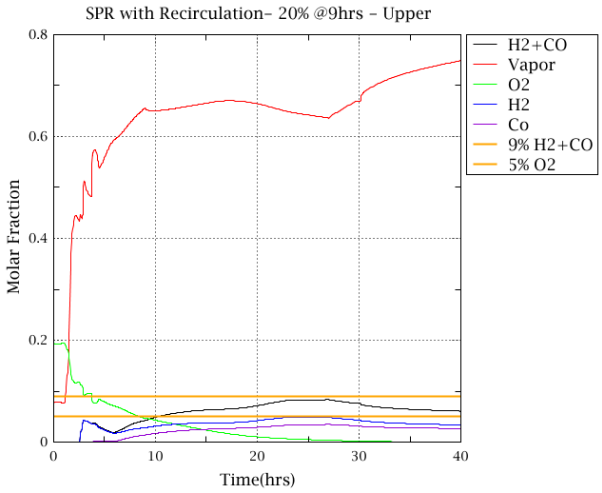

Figure 96 – Molar Fraction in Upper Comp.

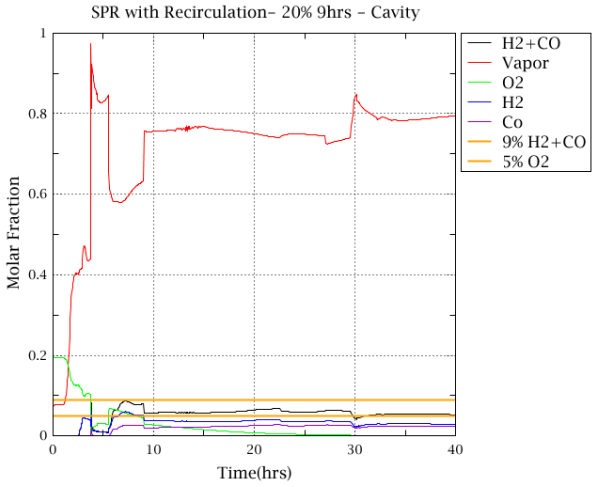

Figure 97 – Molar Fraction in Cavity

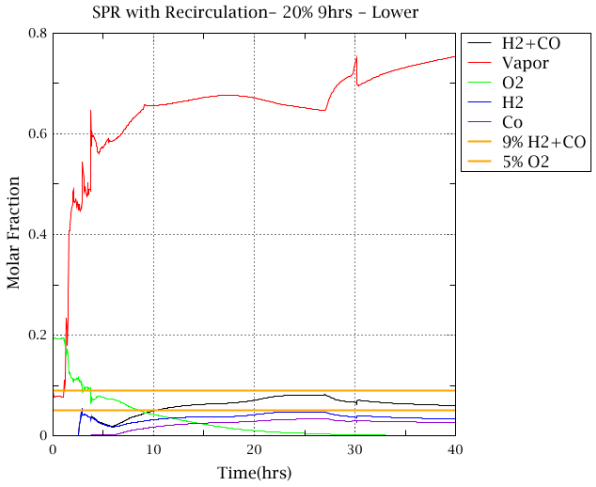

Figure 98 – Molar Fraction in Lower Comp

Activation at 10 hours

A very similar result is seen like in the previous cases with activation of the spray systems at 10 hours. The figures below show the molar mass fractions for the compartments.

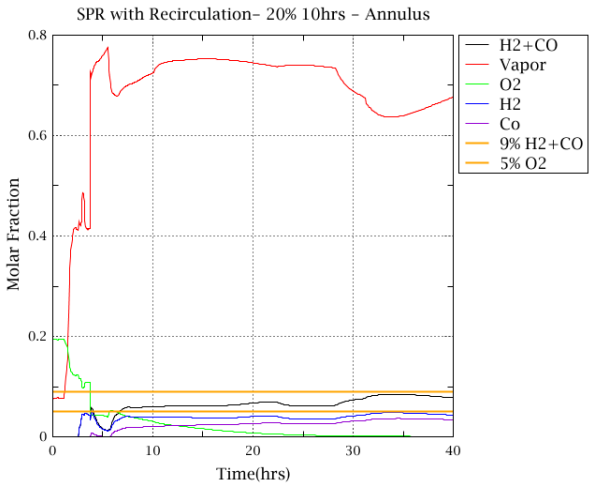

Figure 98 – Molar Fraction in Annulus

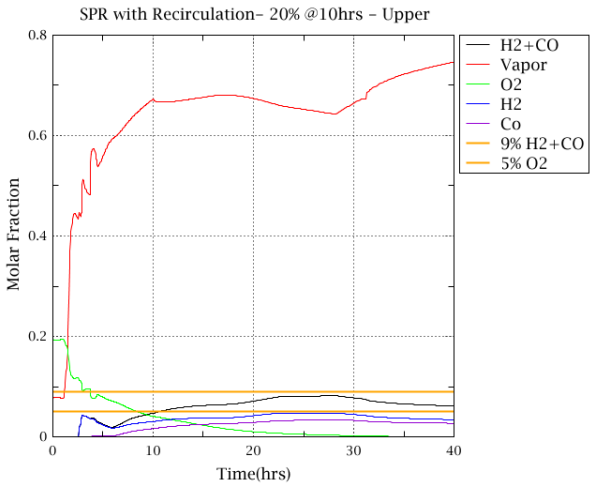

Figure 99 – Molar Fraction in Upper Comp.

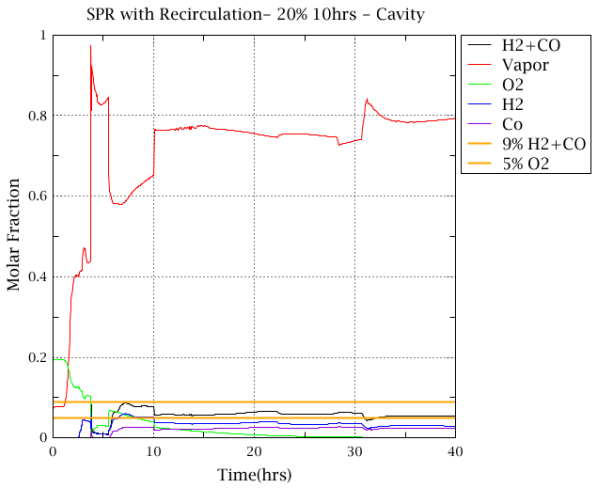

Figure 100 – Molar Fraction in Cavity

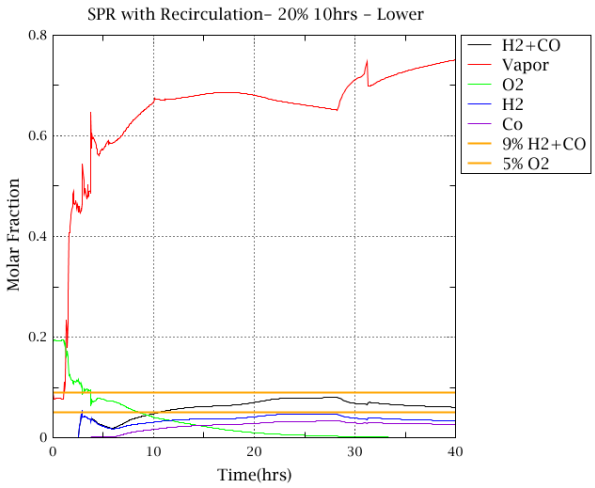

Figure 101 – Molar Fraction in Lower Comp.

The high vapor molar mass fraction in the compartments maintains the atmospheres inert. H_2+CO molar mass fractions reach their peak 25 hours into the accident for lower and upper compartments but are still below the combustion threshold limit.

Conclusions

The spray injection system is effectively able to maintain the containment under safe conditions for the first 30 hours. Combustion events are disabled due to the high vapor fraction in all the compartments. The pressure build-up in the long term needs to be analyzed however. Once the containment cannot be cooled anymore, the increasing temperature and pressure can push the containment building to its structural limits.

As seen in figure 84, after 40 hours, the pressure inside the containment passes the 6 bars mark (600 kPa). At this pressure, the containment fragility curve comes into play where the risk of a breach becomes possible. If conditions remain with no changes, then the pressure would continue to increase, increasing the possibility of containment failure according to the containment's specific fragility curve.

Effectiveness of PARs in H_2 Reduction

The study also involved in seeing how effective the particles autocatalytic recombiners (PARS) were in removing combustible gases from the containment atmosphere. To study this, 22 PARS were placed in total in the containment building in different compartments. The number of PARS placed in compartments is mentioned in the plant modeling section.

The figures below show the effect of the PARS. Values are compared to a reference case without PARS for the different compartments in the containment building: Annulus, Dome, Lower and Upper compartments.

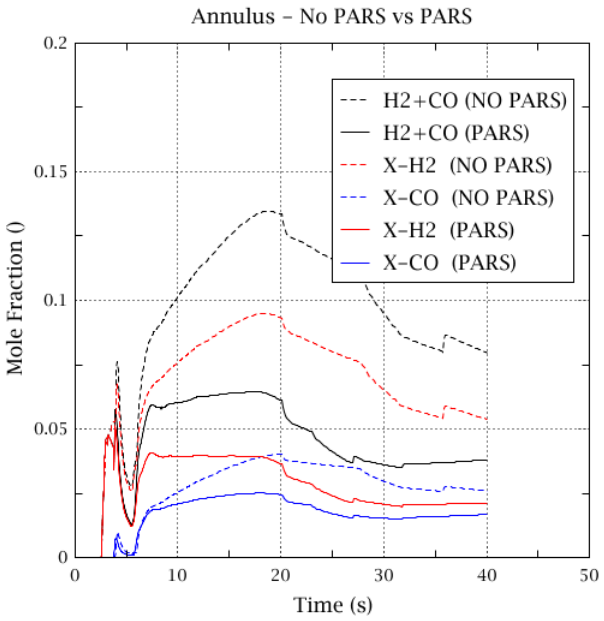

Figure 102 – H2 and CO in Annulus

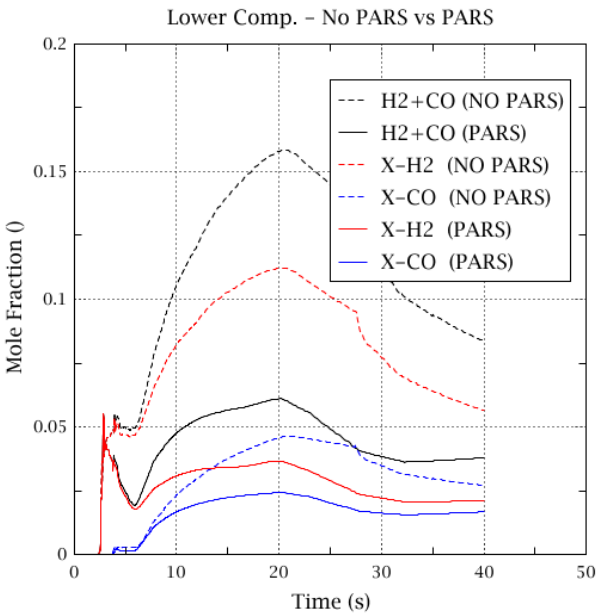

Figure 103 – H2 and CO in Lower Comp.

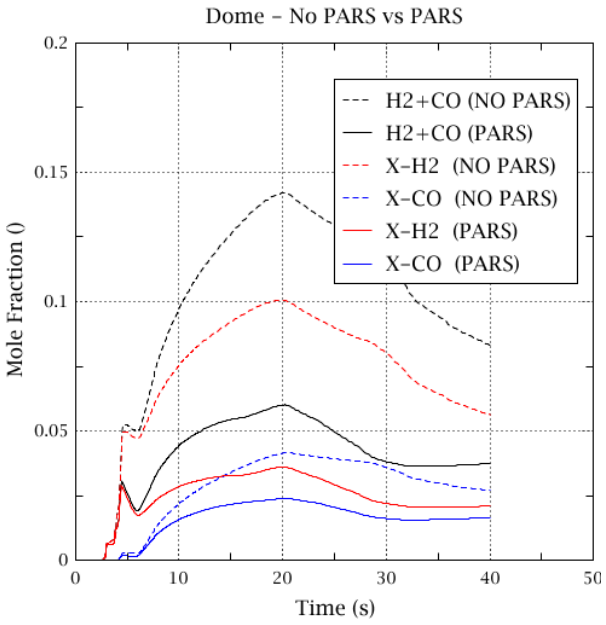

Figure 104 – H2 and CO in Dome

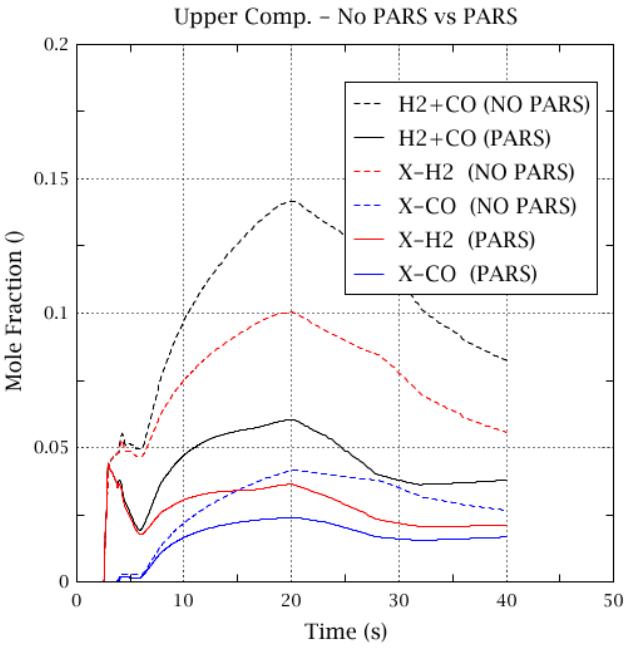

Figure 105 – H2 and CO in Upper Comp.

In the figures above, the dotted lines represent the base case simulation that had no PARS; the solid lines represent the case with PARS in the compartments. The effect of the PARS is very noticeable. The combined H_2 + CO limits without PARS is nearly 15%, well past the non-combustion limit of 9%. By comparison, PARS are effective removing CO and H_2 as seen by the solid black line. The combined molar mass fractions of H_2 + CO peak at around 6%.

The initial spike in the molar mass fraction of H_2 is attributed to the failure of the reactor vessel, which releases the contained hydrogen produced from the oxidation of Zirconium and stainless steel. CO does not start to be produced until a few hours later due to MCCI.

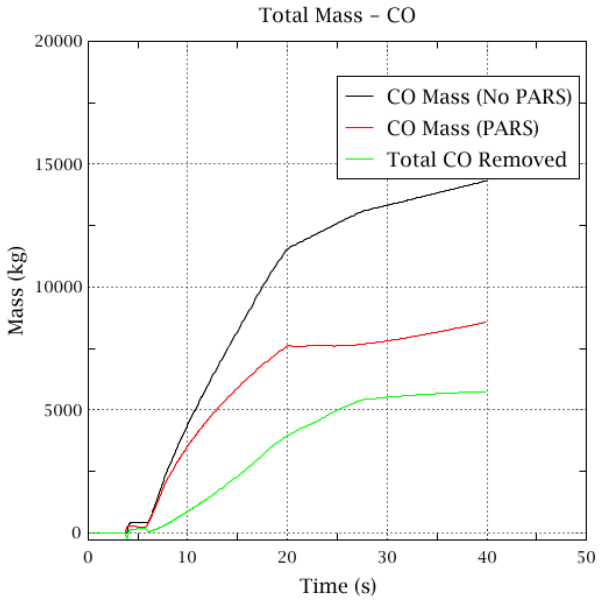

Figure 106 – CO Mass

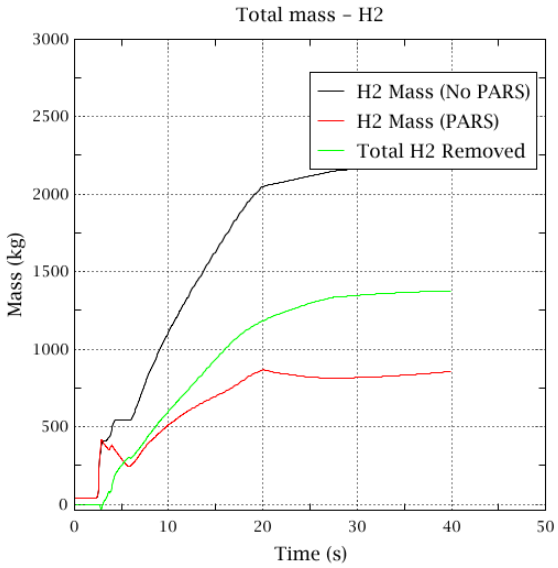

Figure 107 – H2 Mass

The figures above show the H_2 and CO masses. The green line shows the amount of gas removed by the PARS after 40 hours.

Table 11 - Mass of Gases Removed by PARS

GAS	TOTAL MASS GENERATED (KG)	MASS REMOVED (KG)	PERCENT REMOVED	TOTAL MASS IN CONTAINMENT (KG)
H_2	2192.4	1376.5	62.7%	815.9
CO	14320.3	5745	40.1%	8573.3

The final results show that PARS have a significant impact by preventing the combustion of hydrogen and carbon monoxide through their removal. The PARS remove 62.7% of hydrogen mass and 40% of carbon monoxide mass in the containment. The removal of these masses ensures that there will be no deflagrations inside the containment since the combined molar fractions in the volumes is below 9%.

PARS Package vs. Control Function Modeling Comparison

It was also of interest to test and examine the difference between the PARS created using the control functions and the PARS package included in MELCOR. The PARS created using control functions apply a proprietary correlation for the NIS PARS for the removal of H_2 and CO.

On the other hand, The MELCOR PAR model is based on the Fischer model which is a parametric model developed for the most common PAR design. The user input provides correlation coefficients for the general mathematical form of the model. These coefficients are used by the code to calculate the total gas flow rate through a PAR unit. From the PAR gas flow rate together with user-provided PAR efficiencies, transient relaxation times, delay times, and the internally calculated hydrogen mole fractions, a per-PAR-unit hydrogen reaction rate is calculated. This rate is then multiplied by the current timestep and the user-provided number of active PAR units to determine the change in hydrogen, oxygen, and steam masses. These differential masses are then passed to the Control Volume Hydrodynamics (CVH) package as source/sink terms. The PARS package however does not calculate CO removal rates from PARS, only H_2; therefore, only hydrogen comparisons are examined in this section.

The figures below show the molar mass fractions and hydrogen masses comparison for the two PARS implementations.

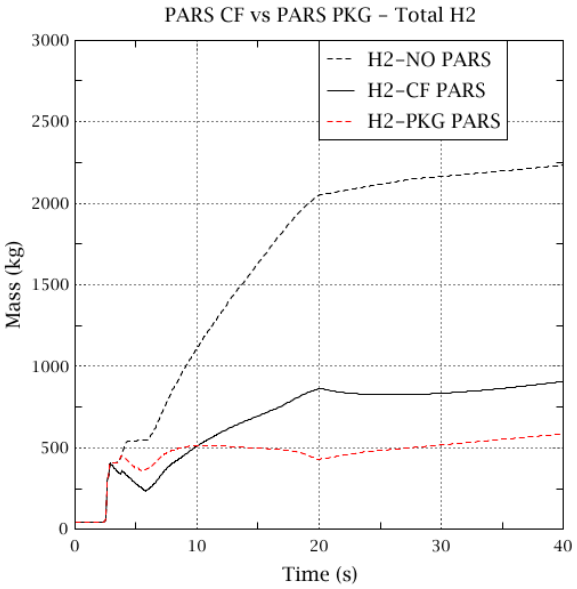

Figure 108 – Total H2 Mass

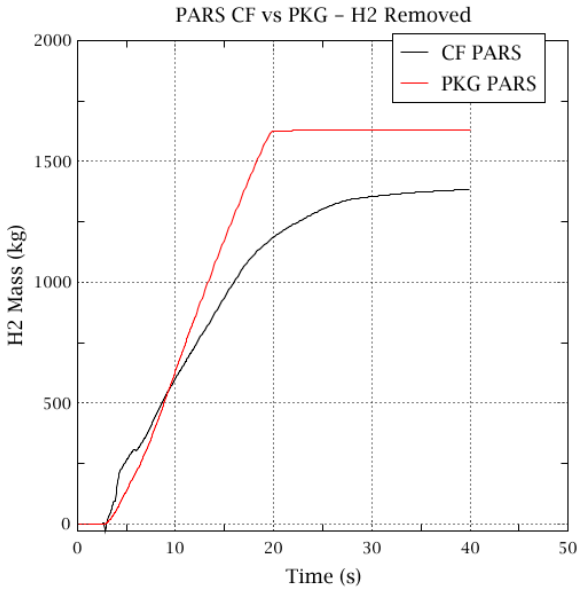

Figure 109 – Total H2 Removed

The figures above show the total mass of hydrogen and the total amount removed by PARS using the package and control functions. The effect of the PARS is clear as the total hydrogen mass is much lower than with no PARS as shown in figure 108. Furthermore, it is shown that the total mass of hydrogen is lower using the MELCORS PARS package compared to modeling PARS with control functions. The difference in removal can be seen in Figure 109 and table 12.

Table 12 – H_2 PARS Comparison

PARS MODEL	H_2 MASS REMOVED (KG)	H_2 MASS LEFT IN CONTAINMENT (KG)	PERCENT REMOVED
CF	1376.5	815.9	62.7%
PKG	1627.3	565.1	74.2%
DIFFENCE IN H_2 REMOVAL		250.8 kg	

The following figures show the molar mass fractions for all compartments using the different methods for PARS removal.

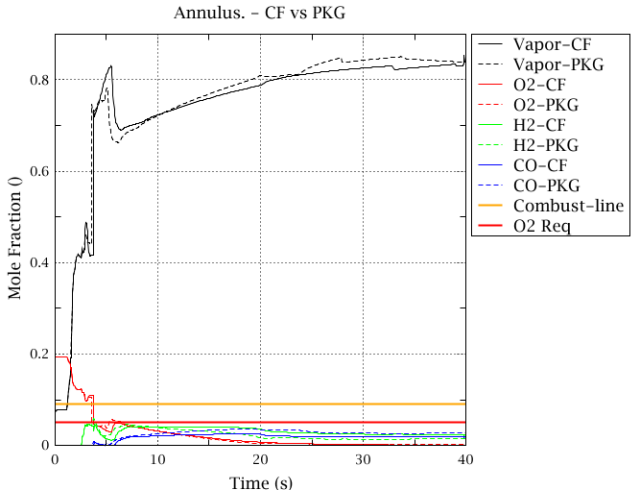

Figure 110 – Annulus Comparison

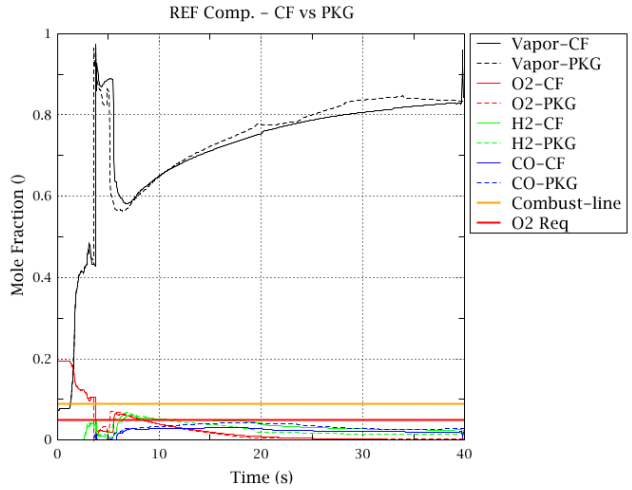

Figure 112 – Chamber Comparison

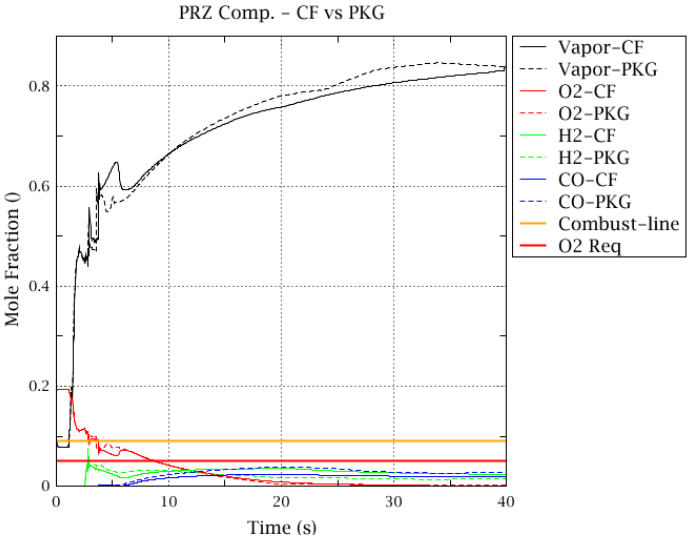

Figure 111 – Pressurizer Comparison

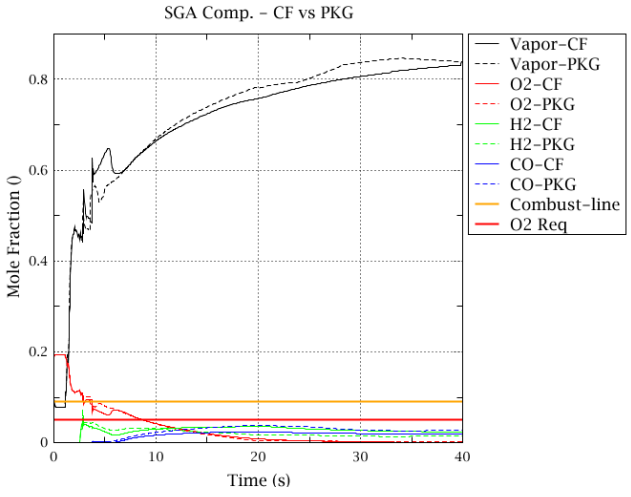

Figure 113 – SGA Comparison

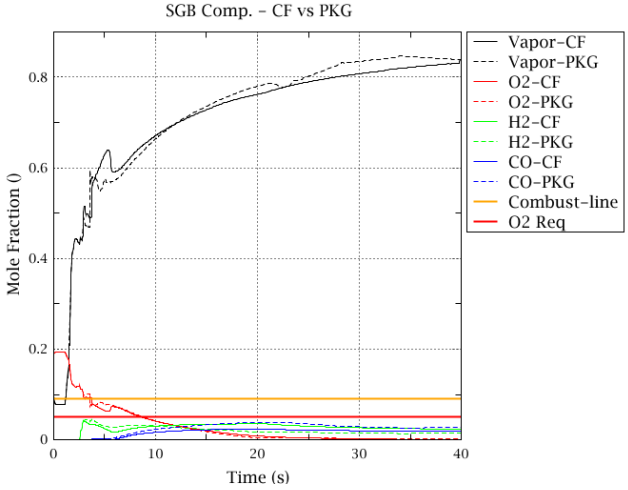

Figure 114 – SGB Comparison

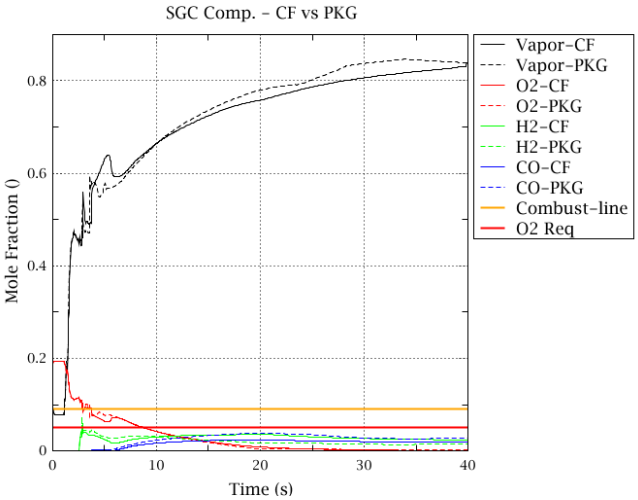

Figure 116 – SGC Comparison

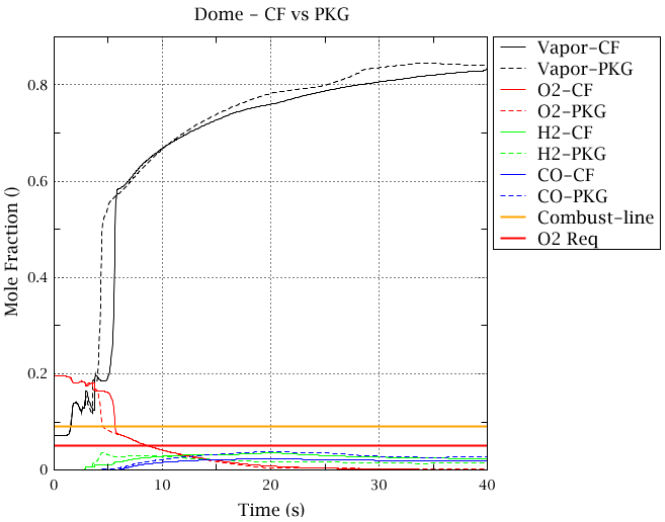

Figure 118 – Dome Comparison

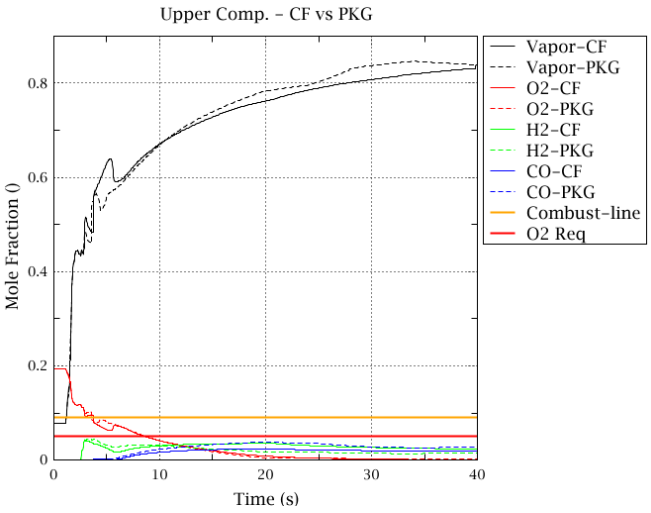

Figure 117 – Upper Comp. Comparison

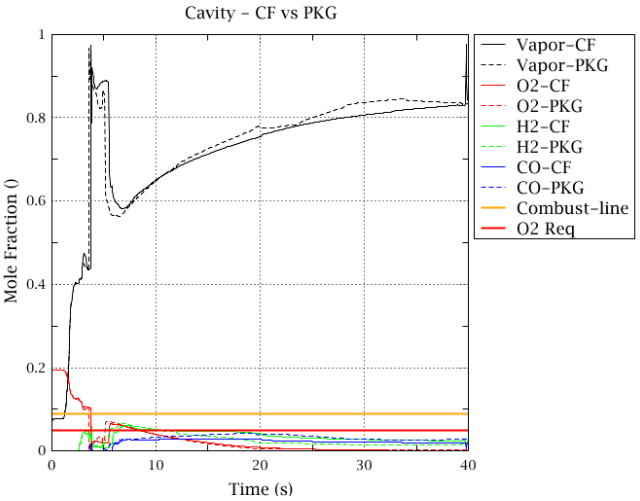

Figure 115 – Cavity Comparison

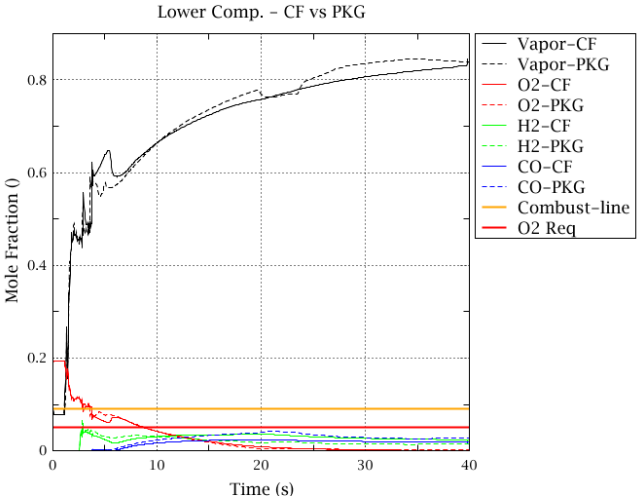

Figure 119 – Lower Comp. Comparison

There are some comparisons of the molar fractions among the compartments worth making between the two methods of H_2 removal.

- CO molar mass fractions will be higher using the PARS package because the CF have some removal of CO.
- Water vapor molar mass fraction behavior is very similar between the two. However, after 11 hours, the PARS PKG method tends to have slightly higher values than that for CF.
- The behavior of the molar mass of oxygen is almost equal between the PARS methods except for some very minor differences once the vessel ruptures.

In conclusion, the control function method for modeling PARS is very effective in simulating the effect of PARS in the containment compared to the build in MELCOR option. The differences come from the proprietary correlations of the PARS model used which cause discrepancies in the values and calculation rates.

Other PARS models should be tested and/or input into the simulation for further confirmation. The several amounts of options within the PARS package may also provide results much closer to the actual performance of the modeled PAR.

BURN package

Based on the objectives of this project, to provide safety insights about the feasibility to forego the opening of the FCV by activating the Containment Heat Removal System of 3-loop PWR with large dry containment after a SBO, and the results obtained, it turned into a topic of interest how a combustion scenario would develop inside the containment building and its implications. Therefore, it was decided to activate the burn package and execute some cases based on the probability of a combustion event.

Some changes were imposed on the default burn settings for a more bounding approach. This involved assuming a higher combustion completion in the most important compartments and changing the ignition limits so that a hydrogen burning would occur. Changing these settings ensured a more containment straining combustion scenario.

Note the following flammability limits imposed:

1. **$X(H_2) + (5/3)\ X(CO) > 0.05$**
2. **Containment inerting by X(steam) > 0.55**
3. **Containment inert when $X(O_2) < 0.05$**

A few sensitivity cases were run with a different flammability limit, requiring the concentrations to be:

$X(H_2) + X(CO) > 0.08$

The input for the burn package is shown below:

```
!!!!!!!!!!!!!!!!!!!!!!!!!!!!!!!!!!!!!!!!!!!!
!                 BURN              !
!!!!!!!!!!!!!!!!!!!!!!!!!!!!!!!!!!!!!!!!!!!!
!                 iactv
BUR_INPUT         ACTIVE
!
!                 XH2IGN          XCOIGN          XH2IGY          XCOIGY     XO2IG          XMSCIG
BUR_IGN           0.05            0.03            0.04            0.02       0.05           0.55
!BUR_IGN          0.08            0.04            0.07            0.03       0.05           0.55
!
BUR_CC  5       !N      CVNAM           key             cc              iccdch
                  1       -1              const           0.7             sc
                  2       'LOW-COMP'      const           0.95            sc
                  3       'UP-COMP'       const           0.95            sc
                  4       'DOM-COMP'      const           0.95            sc
                  5       'ANN-COMP'      const           0.8             sc
!
```

The input lines above show the activation of the burn package along with the settings that were set for the simulations for combustion completeness and the ignition criteria. There were two ignition criteria set as shown in the BUR_IGN line: 5% concentration and 8% concentration for ignition to start. These limits were decided to ensure combustion events and as a way for the solution to be conservative.

The BUR_CC line sets the combustion completion parameters for the simulation. Each line represents a compartment and how “complete” the combustion in that compartment is denoted by a value from 0 to 1 representing 0% to 100%. The line with a -1 for compartment name represents all other

compartments not named. There were other many options in the burn package for more control of the combustion phenomenon but they were deemed not necessary.

Fan Cooler Analysis with BURN package

When a subsystem of the CHR is activated (in our case the fan-coolers because they provide containment cooling whenever they are actuating) the containment pressure is drastically reduced by condensing steam. The steam condensation leads to a de-inertization of the containment atmosphere and from a lack of combustible control systems, H2 and CO combustion occurs. The presence of PARS also has a significant effect on the gas concentrations in the atmosphere. Therefore, 2 types of cases were simulated using MELCOR: with and without PARS. Fan coolers were activated at different times in both types of cases with the BURN package on and results were analyzed.

Fan Cooler activation without PARS in Containment Building

The activation of fan coolers without PARS in the containment building leads to extremely dangerous conditions, especially if these systems are actuated late after the beginning of the accident. The built-up hydrogen and CO in the atmosphere over time is maintained inert in the containment by the amount of water vapor. The activation of fan coolers causes massive deflagrations that quickly cause pressure to spike. The figure below shows the evolution of pressure through the accident when fan coolers are activated at different times.

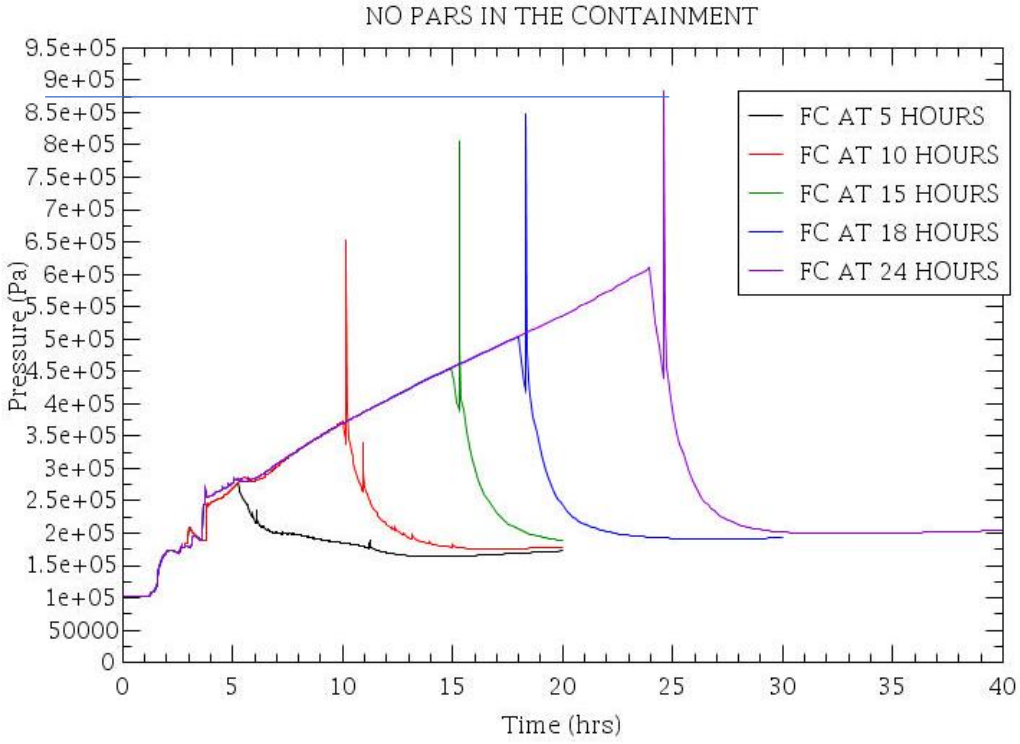

Figure 120 – Pressure with Fan Activation at different times during SBO with BUR package ON

As we can see from Figure 120, the fan coolers cause significant pressure spikes in the containment building shortly after they are activated. To avoid damage to the containment building, it is seen that earlier activation of the fan coolers leads to lower pressure spikes. When they are activated at 5 hours, pressure decreases and minor combustion events happen but there are no major pressure spikes. If fan coolers are activated 5 hours later, then the pressure spike from the combustion event reaches 6.5 bars. This pressure remains below the initial values of the containment fragility curve but it should still be considered a dangerous deflagration.

Activation of the fan coolers at 15, 18 and 24 hours lead to deflagrations events that cause subsequently higher pressure spikes: 8.1, 8.5, and 8.8 bars respectively. Deflagrations causing these pressures pose a severe risk for the containment building. The containment fragility curve shows that at 8 bars there is a 20% chance of containment failure while pressures reaching 8.8 bars show a 75% chance of failure.

The figure below shows the water vapor and oxygen molar fractions. It can be seen from the figure that when fan coolers are activated, the water vapor starts to be removed which is what is keeping the containment building inert. This causes hydrogen and CO deflagrations as seen in figure 122. The combustion events deplete most of the oxygen in the containment building which prevents any further burn events. Figure 121 shows this as most values are below the purple line which denotes the 5% Oxygen limit. Meanwhile, hydrogen and CO molar fractions increase above the combustion threshold after the burn event but these gases cannot burn due to the lack of oxygen in the containment atmosphere.

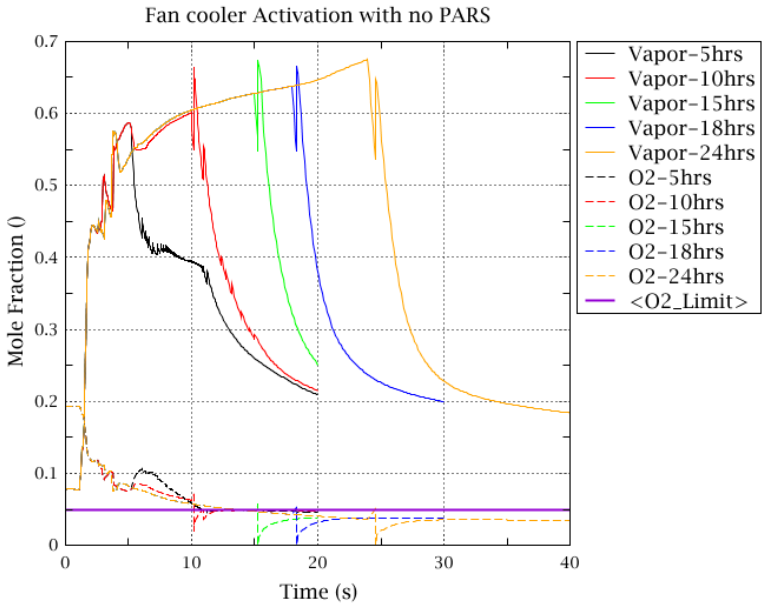

Figure 121- Water Vapor and Oxygen molar fraction values in Containment

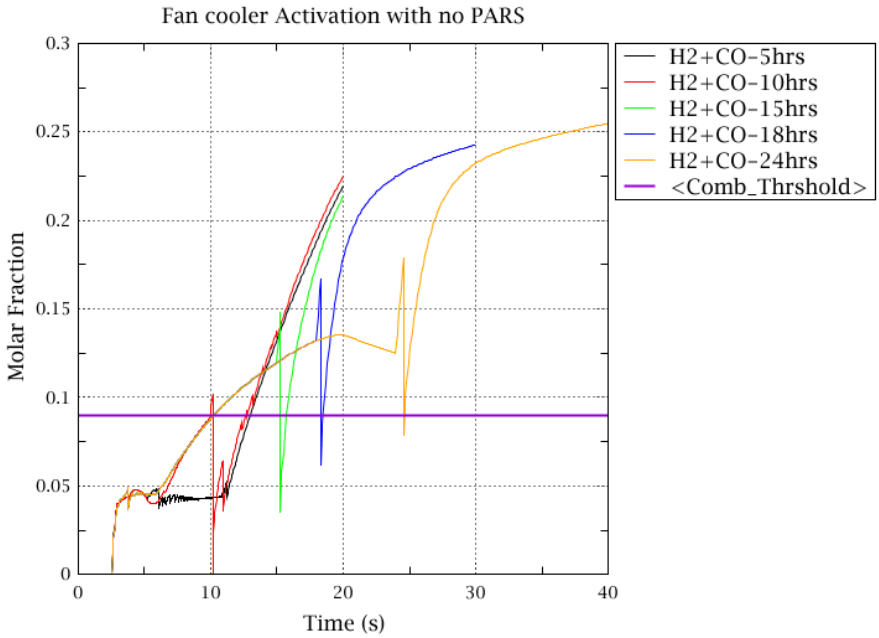

Figure 122 – H2+CO Molar Fraction in Containment

Fan Cooler activation with PARS in Containment Building

Fan Cooler Activation with PARS at 5% Flammability Limit

This section shows the results obtained with MELCOR for our reference PWR plant equipped with PARs and FCVS in case of SBO with subsequent activation of the CHR. The figure below shows the pressure evolution through the accident transient when fan coolers are activated at different times during an SBO.

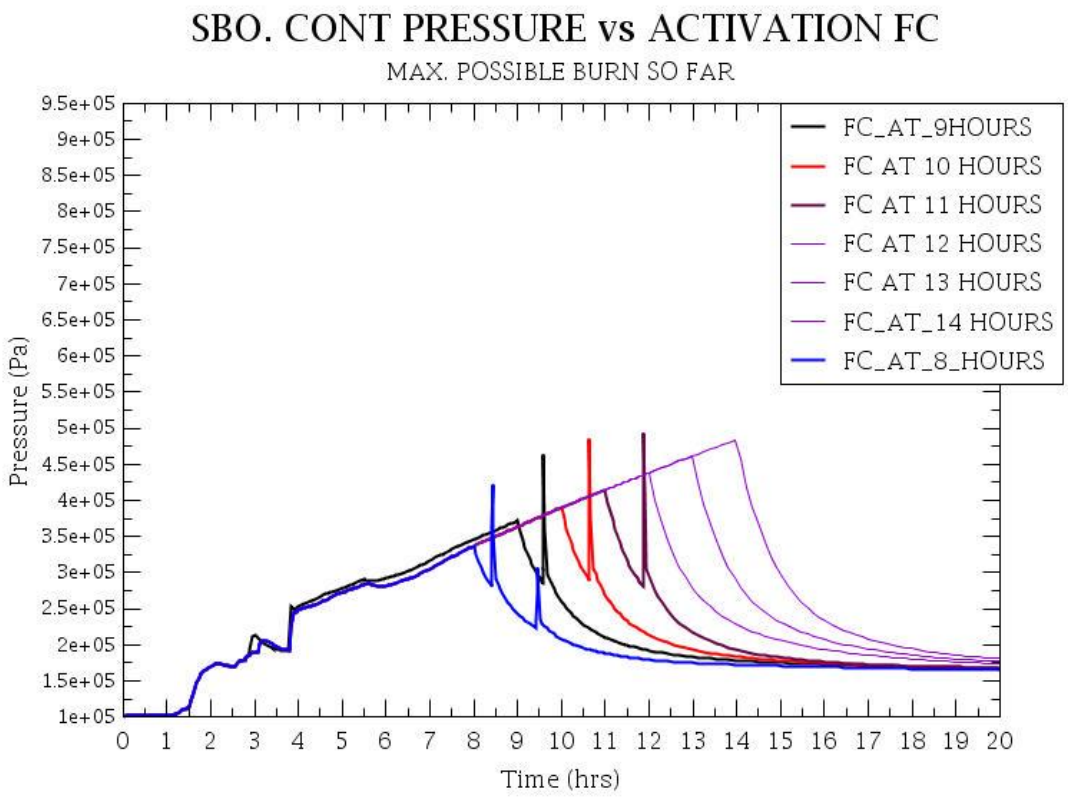

Figure 123 – Pressures for FC activation at different times with BURN Package ON

It can be seen from figure 123 that the containment pressures are suppressed when the fan-coolers are activated. Also, the atmosphere becomes de-intertied with the activation leading to combustion scenarios that cause pressure peaks. When the fan coolers are activated at 8 hours, there are 2 combustion events as seen by the two peaks. The peaks do not pose a threat to containment integrity however as the pressures remain below 4.5 bars. However, later activation times lead to deflagrations that conclude in higher pressure spikes. This is due to the higher amount of hydrogen and CO in the containment atmosphere which means that more gases are being burnt. However, the containment peak pressure resulting from gas combustion is well below the FCVS set point and the cumulative probability for the containment failure is well below the 10%.

When the fan-coolers are activated 12 hours after the onset of the SBO, there is no combustion of burnable gases because of oxygen depletion. As seen in figure 124 in the next page, the molar fraction of oxygen in the containment building drops below 5% before H_2+CO can reach the required molar mass fraction for combustion.

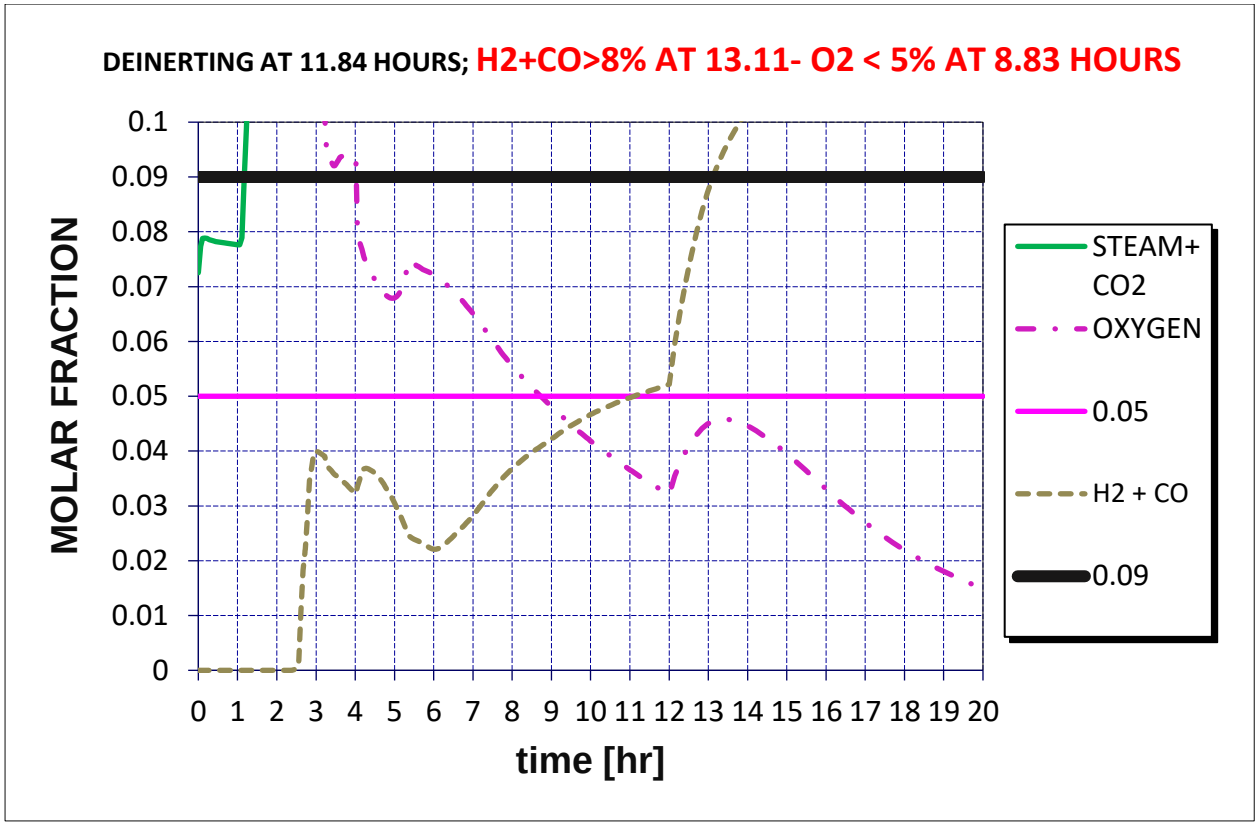

Figure 124 – Molar Fractions with FC activation at 12 hours

Fan Cooler Activation with PARS at 8% Flammability Limit

To approach a more realistic scenario, the flammability limits were increased to 8%. The figure below shows the pressure evolution with activation of fan coolers at different

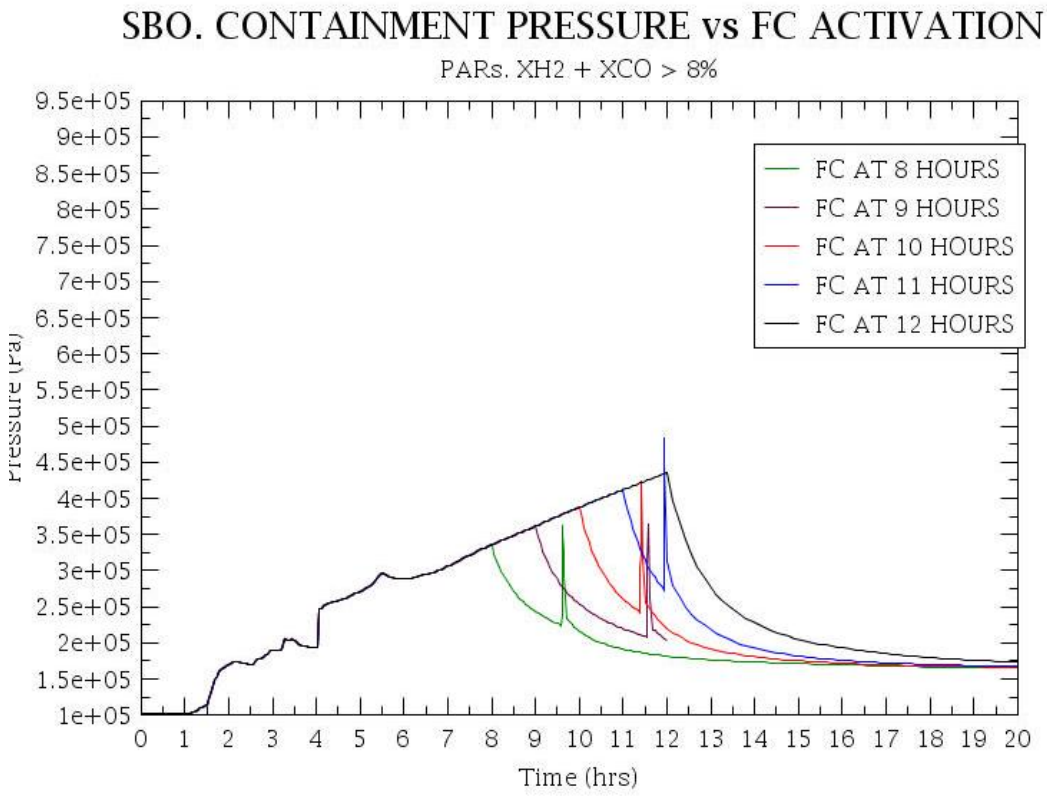

Figure 125 – Pressures with 8% flammability limit using FC

Combustion events still occur when the flammability limit is raised to 8%. A comparison between figures 123 and 125 show a counterintuitive fact, containment peak pressure is slightly higher when the flammability limit is lower; in our case when flammability limit is lower than 5%. This is another effect of the PARs: the earlier the combustion occurs, more burnable gases are available for combustion and, as a result, the peak pressure is higher as the flammability limit is lower.

The pressure peaks resulting from the combustions with the higher flammability limit however do not pose a threat to containment integrity. The peak pressure occurs when fan coolers are activated at 11 hours causing hydrogen deflagrations that increase the pressure to 5 bars. This is still well below the limits of the containment fragility curve. The tables below show detailed values for flammability limits for 5% and 8%.

Table 13 – Summary of values for simulations with BURN PACKAGE

	FC Activated at 8 hrs		FC Activated at 10 hrs		FC Activated at 11 hrs	
Concentrations	5%	8%	5%	8%	5%	8%
P_postburn (bars)	2.8	2.24	2.89	2.42	2.8	2.73
P_preburn (bars)	4.21	3.57	4.85	4.24	4.94	4.84
ΔP_burn (bars)	***1.41***	***1.33***	***1.96***	***1.82***	***2.14***	***2.11***
Time of Ignition (hrs)	8.41	9.59	10.62	11.39	11.85	11.92
Total H2 (kg)	362	367	470	451	514	510
H2 Burned (kg)	245 (68%)	219 (60%)	310 (66%)	290 (64%)	336 (65.4%)	309 (60.6%)

Conclusion

The activation of the burn package in the simulations where fan coolers are used for containment heat removal lead to combustion events that require careful evaluation. Turning on the fan coolers between 8 and 11 hours lead to combustion events that while they do not necessarily threaten the integrity of the containment building, should still be completely avoided as combustion events can cause damage to useful instrumentation inside the containment and may aggravate local instabilities of the containment building and/or other systems nearby.

Final Remarks

Overall, it can be said that the project was a success. The main objectives were met and very valuable insights were obtained from the results of the project.

First of all, MELCOR simulations were finally able to be executed without errors. This was the first objective of the project. Some MELCOR expertise was lost due to disuse and through this project it was greatly regained along with a variety of new skills. The changes in the input structure of MELCOR from the code overhaul that updated the code from version 1.8 to 2.1 required some relearning of EXEC and PLOT packages and their corresponding functions. Many of the MELCOR packages also underwent major improvements in the simulation of the phenomenology corresponding to each package. This introduced many new settings and options to adjust the sensitivity coefficients of the equations governing the phenomenology.

The changes in the packages required learning new options which took time and testing to see the effect on the simulation. Enabling and applying many of these options improved the model and allowed for different approaches to the simulation. An example of this would be changing the combustion completeness in different compartments closer to 1 to simulate the total burning of hydrogen, thus, creating a more limiting situation.

Creating and using these options also required tedious troubleshooting as a lot of times MELCOR would terminate due to fatal errors. When this occurred, the input had to be examined and based on the type of error and suggestion from MELCOR and tweaked to be able to execute properly but many times, this would either create errors in other places or would not fix the problem. However, MELCOR simulations were in the end able to be executed while adjusting many options and parameters in the input.

The second objective was tightly integrated with the first one as I worked alongside with the severe accident expert of CSN, Fernando Robledo Sanchez. A lot of discussion and learning was shared as both of us were continually learning how to use different MELCOR packages and troubleshooting errors when the simulations would fail. This process was mutually very beneficial as both of us gained a good level of expertise using the code.

The third and final objective was also satisfactorily accomplished as valuable insights for heat removal strategies using the containment heat removal systems and the effects of PARs were obtained. As a reminder, the goal was to utilize the CHR systems to lower pressure and prevent opening the FCV system to depressurize the containment.

The analysis performed using the CHR systems showed that, while the initiation of these systems is effective in reducing pressure inside the containment building, the possibility for a combustion scenario is also created due to the de-inertization of the containment atmosphere. This is particularly true when the fan coolers are activated based on the results. The cooling and condensing of the air by the fan coolers in the containment compartments lowers the vapor molar mass fraction in the air. The vapor is the main agent in maintaining inert atmospheric conditions. When the vapor fraction is lowered, the combined hydrogen and carbon monoxide molar mass fractions can reach the percentage required for combustion events to take place.

However, in these scenarios, the most limiting factor for combustion events is how much oxygen is there in the atmosphere. The PARs present in the compartments react the hydrogen and carbon monoxide with oxygen which lowers the amount of oxygen in the atmosphere, lowering the amount of combustible gases and oxygen. These two events caused by the PARs effectively lower the risk of deflagrations but activation of the fan coolers must be done with caution as there are time intervals

where hydrogen and carbon monoxide burn events can occur as seen in the results in the burn section thereby causing dangerous conditions for the integrity of the containment building.

Performing the containment analysis using the burn package demonstrated this need as there are combustion events that test the integrity of the containment when fan coolers are activated anytime between 7 and 11 hours into the accident. The burning of these combustible gases spikes the pressure inside the containment. These pressure peaks (strongest combustion event leads to a peak of 5 bar) however are within the limits of the containment stress curve and do not seemingly pose a challenge to the containment building. Regardless, these types of events are not preferable as damages to other systems and measuring instruments can occur which may lead to problems later down the road.

Activation of the containment spray system yields better temporary results, especially when flow rates are reduced to 20% of the nominal value. The cases performed with the lowered spray flow rates showed that conditions remain stable for a longer period of time while maintaining the containment atmosphere inert. The vapor molar mass fraction does not precipitously drop as it does when the spray injection flow rate is nominal which maintains it above the 55% molar mass fraction and thereby in the safe zone according to the Shapiro diagram shown in figure 2.

This insight can be especially helpful when there is no infinite water source nearby to continue feeding the containment spray system and only the RWST is available. Lowering the injection rate maintains conditions inside the containment in a safe zone for a longer period of time delaying the opening of the FCV. This allows time for other containment strategies to be applied.

The analysis of PARs demonstrated how effective they are in removing combustible gases in the containment. This tremendously decreases the chances for combustion events and ensures that the containment building will not fail due to a hydrogen combustion event. However, they do not prevent the failure of the containment building due to over-pressurization. The activation of CHR systems is required to prevent this.

The limited time frame of the project restricted the scope. The analyses performed can be expanded to analyze other strategies to prevent the opening of the FCV. Combining the activation of the containment heat removal systems would be a start and examining which combinations would yield the best results in lowering containment pressure while preventing combustion events. Improvements in the containment model could also be performed by dividing the large compartments such as the upper compartment into smaller ones. This would provide greater insight into the hydrogen concentrations at different levels of the containment. The options in the BURN package could also be tuned to represent different combustion scenarios through the compartments.

Overall, the project was considered a success as all three objectives were fulfilled.

Acknowledgements

The completion of this project as a culmination of the master program in nuclear engineering was able to be carried out thanks to the support of many parties.

Foremost, I would like to thank the Spanish Consejo de Seguridad Nuclear for sponsoring this project and providing the aid and tools needed. Without their help and sponsorship, this project would not have been possible. The Catedra Argos enabled this project and I am very grateful for that.

Secondly, I would like to thank CIEMAT for their technical help with MELCOR when errors executing MELCOR would arise. Their help was instrumental and being able to change and manipulate the MELCOR input code and be able to perform simulations.

I would also like to greatly thank Fernando Robledo Sanz for his support and mentorship in this project. He was instrumental in the development of the project topic and also taught me with much detail phenomenology of severe accidents.

An honorable mention to Miguel Sanchez Perea as overseer of the project.

Lastly, all of my friends and family for their support in many little ways that make a big difference.

References

1. Yang, J.W. *PWR dry containment issue characterization*. United States: N. p., 1990. Web.

2. IAEA Safety Standard Series, *Design of Reactor Containment Systems for Nuclear Power Plants. Austria* 2004,

3. Unites States NRC. L.L Humpries. *MELCOR Computer Code Manual Vol.1: Primer and Users' Guide.* United States. 2017.

4. Unites States NRC. L.L Humpries. *MELCOR Computer Code Manual Vol.2: Reference Manual.* United States. 2017.

5. J.Fontanet and L.E. Herranz (CIEMAT). *Impact of New Safety Systems on Severe accidents.* Spain. 2017.

6. W. Herring, CH. Homann, J. Stuckert (Karlsruhe Institute of Technology) *Integration of New Experiments into the Reflood Map.* Germany, 2015

7. Didier Jacquemain (IRSN – Institut de Radioprotection et de Surete Nucleares). *Nuclear Power Reactor Core Melt Accidents – Current State of Knowledge. 2015.*

8. Journeau, Christophe & Brayer, Claude & Piluso, P. (2002). Uncertainties on Thermodynamic and Physical Property DataBases for Severe Accidents and their Consequences on Safety Calculations.